Transition to synchrony in finite Kuramoto ensembles

Promovendin:
Dipl.-phys. Franziska Peter

Hauptbetreuer:
Prof. Dr. Arkady Pikovsky

Universitäts-Dissertation

zur Erlangung des akademischen Grades
"doctor rerum naturalium" (Dr. rer. nat.)
in der Wissenschaftsdisziplin Theoretische Physik
eingereicht an der Mathematisch-Naturwissenschaftlichen Fakultät

in der Arbeitsgruppe

Statistische Physik und Chaostheorie

am

Institut für Physik und Astronomie
Universität Potsdam

Hauptbetreuer und Erstgutachter:	Prof. Dr. Arkady Pikovsky, Universität Potsdam
Externer Gutachter:	Prof. Dr. Ralph G. Andrzejak, Dpt. of Information and Communication Technologies, Universitat Pompeu Fabra, Barcelona
Zweiter externer Gutachter:	Dr. habil. Michael Zaks, Institut für Physik, Humboldt Universität zu Berlin
Datum der Disputation:	1. April 2019

Zusammenfassung

Synchronisation – die Annäherung der Rhythmen gekoppelter selbst oszillierender Systeme – ist ein faszinierendes dynamisches Phänomen, das in vielen biologischen, sozialen und technischen Systemen auftritt.

Die vorliegende Arbeit befasst sich mit Synchronisation in endlichen Ensembles schwach gekoppelter selbst-erhaltender Oszillatoren mit unterschiedlichen natürlichen Frequenzen.

Das Standardmodell für dieses kollektive Phänomen ist das Kuramoto-Modell – unter anderem aufgrund seiner Lösbarkeit im thermodynamischen Limes unendlich vieler Oszillatoren. Ähnlich einem thermodynamischen Phasenübergang zeigt im Fall unendlich vieler Oszillatoren ein Ordnungsparameter den Übergang von Inkohärenz zu einem partiell synchronen Zustand an, in dem ein Teil der Oszillatoren mit einer gemeinsamen Frequenz rotiert. Im endlichen Fall treten Fluktuationen auf.

In dieser Arbeit betrachten wir den bisher wenig beachteten Fall von bis zu wenigen hundert Oszillatoren, unter denen vergleichbar starke Fluktuationen auftreten, bei denen aber ein Vergleich zu Frequenzverteilungen im unendlichen Fall möglich ist.

Zunächst definieren wir einen alternativen Ordnungsparameter zur Feststellung einer kollektiven Mode im endlichen Kuramoto-Modell. Dann prüfen wir die Abhängigkeit des Synchronisationsgrades und der mittleren Rotationsfrequenz der kollektiven Mode von Eigenschaften der natürlichen Frequenzverteilung für verschiedene Kopplungsstärken.

Wir stellen dabei zunächst numerisch fest, dass der Synchronisationsgrad stark von der Form der Verteilung (gemessen durch die Kurtosis) und die Rotationsfrequenz der kollektiven Mode stark von der Asymmetrie der Verteilung (gemessen durch die Schiefe) der natürlichen Frequenzen abhängt. Beides können wir im thermodynamischen Limes analytisch verifizieren.

Mit diesen Ergebnissen können wir Erkenntnisse anderer Autoren besser verstehen und verallgemeinern. Etwas abseits des roten Fadens dieser Arbeit finden wir außerdem einen analytischen Ausdruck für die Volumenkontraktion im Phasenraum.

Der zweite Teil der Arbeit konzentriert sich auf den ordnenden Effekt von Fluktuationen, die durch die Endlichkeit des Systems zustande kommen. Im unendlichen Modell sind die Oszillatoren eindeutig in kohärent und inkohärent und damit in geordnet und ungeordnet getrennt. Im endlichen Fall können die auftretenden Fluktuationen zusätzliche Ordnung unter den asynchronen Oszillatoren erzeugen. Das grundlegende Prinzip, die rauschinduzierte Synchronisation, ist aus einer Reihe von Publikationen bekannt. Unter den gekoppelten Oszillatoren nähern sich die Phasen aufgrund der Fluktuationen des Ordnungsparameters an, wie wir einerseits direkt numerisch zeigen und andererseits mit einem Synchronisationsmaß aus der gerichteten Statistik zwischen Paaren passiver Oszillatoren nachweisen.

Wir bestimmen die Abhängigkeit dieses Synchronisationsmaßes vom Verhältnis von paarweiser natürlicher Frequenzdifferenz zur Varianz der Fluktuationen. Dabei finden wir eine gute Übereinstimmung mit einem einfachen analytischen Modell, in welchem wir die deterministischen Fluktuationen des Ordnungsparameters durch weißes Rauschen ersetzen.

Abstract

Synchronization – the adjustment of rhythms among coupled self-oscillatory systems – is a fascinating dynamical phenomenon found in many biological, social, and technical systems.

The present thesis deals with synchronization in finite ensembles of weakly coupled self-sustained oscillators with distributed frequencies.

The standard model for the description of this collective phenomenon is the Kuramoto model – partly due to its analytical tractability in the thermodynamic limit of infinitely many oscillators. Similar to a phase transition in the thermodynamic limit, an order parameter indicates the transition from incoherence to a partially synchronized state. In the latter, a part of the oscillators rotates at a common frequency. In the finite case, fluctuations occur, originating from the quenched noise of the finite natural frequency sample.

We study intermediate ensembles of a few hundred oscillators in which fluctuations are comparably strong but which also allow for a comparison to frequency distributions in the infinite limit.

First, we define an alternative order parameter for the indication of a collective mode in the finite case. Then we test the dependence of the degree of synchronization and the mean rotation frequency of the collective mode on different characteristics for different coupling strengths.

We find, first numerically, that the degree of synchronization depends strongly on the form (quantified by kurtosis) of the natural frequency sample and the rotation frequency of the collective mode depends on the asymmetry (quantified by skewness) of the sample. Both findings are verified in the infinite limit.

With these findings, we better understand and generalize observations of other authors. A bit aside of the general line of thoughts, we find an analytical expression for the volume contraction in phase space.

The second part of this thesis concentrates on an ordering effect of the finite-size fluctuations. In the infinite limit, the oscillators are separated into coherent and incoherent thus ordered and disordered oscillators. In finite ensembles, finite-size fluctuations can generate additional order among the asynchronous oscillators. The basic principle – noise-induced synchronization – is known from several recent papers. Among coupled oscillators, phases are pushed together by the order parameter fluctuations, as we on the one hand show directly and on the other hand quantify with a synchronization measure from directed statistics between pairs of passive oscillators.

We determine the dependence of this synchronization measure from the ratio of pairwise natural frequency difference and variance of the order parameter fluctuations. We find a good agreement with a simple analytical model, in which we replace the deterministic fluctuations of the order parameter by white noise.

Published online at the
Institutional Repository of the University of Potsdam:
https://doi.org/10.25932/publishup-42916
https://nbn-resolving.org/urn:nbn:de:kobv:517-opus4-429168

Contents

Chapter 1

Introduction

How do the billions of heart muscle cells in our chest know when to contract? Why do hipsters all look the same when they are so deliberately wanting to be different? Are school girls that jointly refuse to partake in the swimming course conspiring liars? Why is shift work unhealthy? And what brings about the vigorous shaking of epileptic patients?

These questions are all subject to current research[1]. Although the scope of the effects is broad, they share the same basic mechanism: Synchronization, the adjustment of rhythms among self-sustained oscillators[2] due to their weak coupling. Much like the first half of the 20th century is seen as the heyday of quantum mechanics today, later generations might connect our time with the onset of an understanding of biological organisms in physical and mathematical terms. Biological rhythms and their mutual adjustment form a central part of this new discipline. Apart from the life sciences, also social sciences benefit from the theoretical framework of synchronization. Precise experiments and inspirations are in large part derived from electrical engineering, and applications in this field are innumerable. Sophisticated molecular- and cell-biological, gene-technological methods, diverse methods of neuroscience, but also the fast advances in data science feed the development of a theoretical framework.

Some systems, e.g. heart pacemakers that swear the heart muscle cells to a common beat frequency, have a clear driver-follower relation. Other systems, such as firefly colonies in the Great Smokey Mountains [Fau10], reach unison in their flashing by democratic means. This striving for consensus is the key mechanism discussed in this thesis. It can be thought of as a group of musicians that, without conductor, manages to find a common rhythm simply by listening to what all others play – and adapting to it.

The phenomenon already fascinated Arthur T. Winfree and he developed a model for large populations of weakly coupled rhythmic units with different natural frequencies [Win67]. Yoshiki Kuramoto further simplified this model to a self-consistent mean field model he could solve analytically [Kur75]. Like spins align below the critical Curie temperature, oscillators adapt their speed of rotation above a critical coupling strength. In both the Curie-Weiss model for ferromagnets [KPW13] and the Kuramoto model for self-sustained oscillators, all microscopic units contribute to the macroscopic mean field, and the mean fields acts back on all units. In the thermodynamic limit of infinitely many microscopic units, both mean fields assume constant values, whereby the microscopic units effectively decouple. This allows for a self-consistent solution of the model in terms of the

[1] See e.g. [NDL+16, Tou14, CHB12, GRD12, WHS+10].

[2] Systems that keep an inner rhythm or periodic cycle by balancing between energy loss (due to dissipation) and energy consumption (e.g. in organisms: ATP) – in the theory of dynamical systems those are limit-cycle oscillators. Each oscillator has its own preferred "natural" frequency, but as we see, willingly adapts to a sufficiently strong periodic forcing.

mean field.

This thesis is dedicated to weakening this strong model assumption: Kuramoto's populations consist of infinitely many oscillators – but which population of fireflies or which clapping audience actually meets this assumption? In particular, the combination of all-to-all coupling and thermodynamic limit are realized in few examples only. Typically the physical interaction between cells, insects, laser beams, or humans has a finite range, so that mostly only nearest neighbors interact.

One reason for why finite-size networks occur often in nature is an effect in time-dependent networks. Let us consider an example where indeed a large number of units interacts globally: stirred yeast cells that synchronize their glycolytic cycles, see e.g. [BBW00]. Only the artificial stirring brings each cell in the cuvette into a vicinity of any other cell within seconds, while one glycolytic cycle takes roughly a minute. If every interaction between two cells is replaced by a network link that lasts as long as the interaction, then the network is constantly rewiring much faster than the dynamics in the cells evolves. Time-scale separation then allows to consider the network as static and completely connected. In the natural system, where persistent stirring is absent, the time scales of network and dynamics become comparable – the network might even evolve more slowly. Depending on the density of cells in the solution, the network might temporarily disconnect into smaller networks. As many natural networks are separated into strongly connected hubs with few inter-connecting links, the typical intermediate sub-network is likely comparable to an all-to-all coupled finite-size network.

Apart from this network effect, many systems are a priori finite.

In contrast to the infinite case, the finite-size Kuramoto model is of both experimental and mathematical interest. In experiments, small ensemble sizes are often either inevitable for practical reasons or conceptually necessary. To study cell cycle kinetics, it is desirable to reach synchronization in these cycles, preferentially among few cells [SS07]. A Kuramoto-type transition to synchrony with cell density as bifurcation parameter was detected by limiting to a few hundred cells [WPZH12]. Many technical experiments work with a small number of units, for instance experiments with electro-chemical oscillators [KKJ$^+$14], with metronomes [BUTN13], or on power grids [FNP08].

From the mathematical side, the link between finite and infinite systems is still not fully understood. In [Str00], Steven H. Strogatz assesses finite ensemble fluctuations as one of two major open questions in the field. Also [ABV$^+$05] and [PR15] include the topic into their reviews. Most efforts directed towards this issue studied the scaling of fluctuations, considering the model from a thermodynamic perspective for thousands or more oscillators. The finite-size Kuramoto model is therefore our central object of study. We want to find out how much of the theory for the thermodynamic limit holds also in finite ensembles, and which additional effects occur. The "rigorous convergence results" that Strogatz called for are still pending, but as a first step this thesis considerably refines the dynamical picture of finite populations of self-sustained oscillators.

We take a different perspective from the scaling-of-fluctuations community, and discuss the model for only few (20-200) oscillators, where the quenched noise from finite frequency sampling is most prominent. Fluctuations are comparably strong and therefore also the its effects in the ensemble are more pronounced. The samples are large enough, though, to allow for a comparison to natural frequency distributions in the infinite limit.

First, we want to see if a collective dynamics is still well defined for such small samples, albeit the finite-size fluctuations.

Further, we know from recent literature that the Kuramoto phase transition is a first or second order phase transition for a uniform or a Lorentz distribution of natural frequencies,

respectively. The variability between different finite samples of the natural frequency distribution can therefore be expected to reflect in the mean field dynamics.

As a last question, recent findings on noise-induced synchronization suggest that the finite-size fluctuations in the Kuramoto model should generate a similar effect.

The thesis starts in Chap. 2 with a short overview over the necessary concepts for understanding this thesis. As the main focus of this work is on the finite-size Kuramoto model, we also give a brief literature review of recent findings in the topic.

Chap. 3 relates properties of the natural frequency distribution of a finite ensemble of oscillators to the resulting dynamics. The synchronization transition resembles a thermodynamic phase transition. In the thermodynamic limit, the Kuramoto order parameter equals zero below critical coupling; at the transition, a synchronous solution with finite order parameter bifurcates and indicates the partially synchronous state where oscillators are separated into synchronous and asynchronous ones.

In finite ensembles, the order parameter fluctuates and the mean of the order parameter changes smoothly with coupling strength, and can therefore not indicate the transition point. We therefore define an alternative indicator for the transition to a collective mode in finite ensembles.

One important feature of finite populations is the sampling distribution of their natural frequencies. We find that the coupling strength at which the collective mode or a specific degree of synchrony is achieved depends strongly on the shape of the frequency sample: In peaked samples with few strong outliers, oscillators form a collective mode at comparably weak coupling – a central synchronized cluster forms, unimpressed by the far away fast rotating outliers – but then much stronger coupling is needed to synchronize also these outliers. In flatter distributions, in contrast, comparably strong coupling is necessary to lock the first oscillators, but a slightly stronger coupling already suffices to synchronize all of them. Quantifying the shape by the fourth moment, or kurtosis, of the distribution, we prove the observed shape dependence in infinite ensembles by evaluating the self-consistency equation for the order parameter for a family of distributions that has kurtosis as a parameter.

A similar reasoning reveals the effect of asymmetry in natural frequency samples. We find that in both finite and infinite ensembles, sign and value of the skewness of the frequency sample or distribution determine direction and velocity, respectively, of the global mean field rotation for a given coupling strength. Again, the self-consistency equation of the order parameter for a family of distributions with variable skewness shows this relation in the thermodynamic limit.

As an additional result, we are able to analytically express the total volume contraction in phase space for arbitrary coupling strengths.

In Chap. 4, we discover a synchronizing effect of the thermodynamic mean field fluctuations. The theory in the thermodynamic limit suggests to think synchronous oscillators as locked thus ordered and asynchronous oscillators as incoherent thus disordered. This picture does not hold for finite ensembles. As is known from other systems, weak noise can have a synchronizing effect (even on non-identical oscillators). On the other hand, several authors report on positive Lyapunov exponents for both sub- and super-critical coupling strengths, indicating weak chaos that should have a similar effect as noise.

We investigate two different Kuramoto ensembles with a) Gaussian distributed natural frequencies at super-critical coupling and b) equidistant natural frequencies at sub-critical coupling. In a), fluctuations are weak compared to the typical difference of natural frequencies among the asynchronous oscillators. Therefore, we need to let the mean field act on (uncoupled) oscillators with smaller frequency difference to detect the synchronizing effect. We quantify synchronization by pairwise correlation among these oscillators. Last, we model the mean field fluctuations as Gaussian white noise and find an analytical expression for the same pairwise correlation measure as in the numerical experiments as a function of noise intensity and frequency difference.

Two Appendices close the thesis: App. A contains auxiliary analytical calculations; App. B is a protocol of some of the numerical experiments – both for Chapters 3 and 4.

Chapter 2

Background and State of the Art

In this chapter, we recall the theoretical foundations for this thesis and give a brief review on relevant literature regarding the finite Kuramoto model.

Sect. 2.1 is concerned with the basic theory. We keep this section short and present only the most necessary theoretical background, namely the Adler equation Sect. 2.1.1, the Winfree model Sect. 2.1.2, and the Kuramoto model Sect. 2.1.3. We refrain from repeating the derivations of the model equations in all detail. The Adler equation is discussed in all detail in [Str15] Chap. 4.3 and [PRK03] Chaps. 3 and 7. For a derivation of the Winfree model, or "phase model" turn to [Izh07], Chap. 10. An elegant and accurate deduction of the Kuramoto model can be found in [PRK03], Chap. 12, and in [Tön08], Sect. 2.1.

In Sect. 2.2, we list and shortly review literature on the scaling of fluctuations and on chaoticity in the finite size Kuramoto model.

2.1 Theoretical prerequisites

In the following, we discuss the basic models that build the theoretical foundation of this thesis. The Adler equation can be seen as the backbone of the Kuramoto equation. The Kuramoto model was derived from the Winfree equation with few additional assumptions. The Winfree- and the Kuramoto model describe ensembles of weakly coupled oscillators that adapt their self-sustained rhythms to each other. We start by discussing such self-sustained oscillators.

All biological oscillators fuel their activity by consumption of energy. They balance energy losses and keep their inner cycles and rhythms (e.g. the Krebs cycle, heart beat, neural firing, gene expression, etc.) running at an approximately fixed level. Mathematically, this can be described by attractive limit-cycle oscillators – dynamical systems with an isolated periodic orbit that is, at least in a vicinity, attractive (= basin of attraction). The motion on a limit cycle with period T can be parameterized by a single variable that can be mapped to a uniformly rotating variable called phase. The motion on the limit cycle corresponds to a zero Lyapunov exponent, and perturbations along the limit cycle neither grow nor decay. In contrast, any perturbation in transverse direction returns exponentially fast to the limit cycle.

The basin of attraction of the limit cycle can be parametrized by the phase on the limit cycle (and an amplitude): A stroboscopic map with period T maps an arbitrary point in phase space forward in time, asymptotically reaching a point on the limit cycle. All points in the basin of attraction that map to the same point on the limit cycle form a submanifold called isochrone. This parametrization persists under weak perturbations that are merely strong enough to bring the oscillator slightly off the limit cycle. Three theories of Winfree, Kuramoto, and Malkin describe the action of weak periodic perturbation on the phase dynamics of a limit cycle oscillator – for a short review see [IK06], for deeper insights into the theory turn to [PRK03, Izh07]. Oscillators whose dynamics can be reduced in this way to the (phase-) dynamics on the limit cycle are called phase oscillators.

2.1.1 Adler equation, 1946

The Adler equation is a standard example in the theory of low-dimensional nonlinear dynamics that is key to the understanding of the Kuramoto model. It describes a weakly periodically driven self-sustained oscillator with some natural frequency that adjusts its frequency to a sufficiently close driving frequency. Adler's key modeling assumptions were the similarity between the frequency of the driving and the natural frequency of the oscillator (i.e. small frequency detuning μ), a rapid decay of amplitude perturbations as compared to the inverse frequency detuning, and weak external driving.

These three assumptions allow to reduce the mathematical description to the phase difference Ψ between driver and oscillator. With some geometrical considerations and linearization around small frequency differences, the original article [Adl46] motivates the following Adler equation

$$\frac{\mathrm{d}\Psi}{\mathrm{d}t} = -\mu + a\sin(\Psi). \qquad (2.1)$$

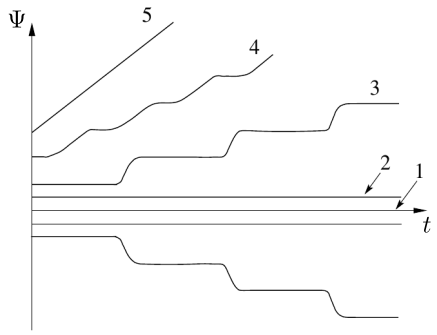

Fig. 2.1: Solutions $\Psi(t)$ of Eq. (2.1) for different frequency detunings μ. 1: $\mu = 0$; 2: $\mu < 0, |\mu| < a$ (inside Arnold tongue); 3,4,5: $\mu < 0, |\mu| > a$ (outside Arnold tongue) with increasing detuning. Figure adapted from [PRK03].

The parameter a (for definiteness $a > 0$) quantifies the coupling strength between the driver and follower.

Let us discuss the different solutions of the Adler equation. Ratio μ/a is the bifurcation parameter of a saddle node bifurcations at $\mu/a = \pm 1$. For $|\mu/a| > 1$, the equation has no fix points and the phase difference Ψ rotates freely. Is is slowed down around the bottleneck at $\Psi = \pm\pi/2$ and performs quick phase slips (see smooth jumps in Fig. (2.1)) inbetween. An analytic expression of $\Psi(t)$ is given in the original article. Decreasing $|\mu/a|$ to below 1, a pair of a stable and an unstable fix points is born, corresponding to a constant phase difference Ψ. Driver and driven oscillator rotate at the same speed, called $1:1$ locking. Averaging $\dot{\Psi}$ over time gives the so called observed frequency. Inside $|\mu/a| < 1$ it vanishes, outside it can be approximated as $\langle\dot{\psi}\rangle_t \sim \sqrt{\mu - a}$, converging to linear growth as μ increases. The condition $|\mu/a| < 1$ forms a triangle in the a-μ plane, called Arnold tongue.

The discretized phase equation exhibits much richer behavior. A stroboscopic mapping of the Adler equation at each period of the driving results in a circle map. The map has additional Arnold tongues of rational locking ratios other than $1:1$ that are thinner (and not triangular) and thus experimentally harder to access. A more detailed picture of the ordering of the widths of the tongues depending on the locking ratio is given by the Farey tree, [GP85]. The "devils staircase" of observed frequency against ratio of driving and oscillator frequency illustrates the same fractal structure. Above a critical coupling, the mapping becomes non-invertible and may exhibit chaos. Where the Arnold tongues of different rotation numbers overlap, chaos can be reached over a cascade of period-doublings.

Generalizing the Adler equation to higher modes in the coupling function, i.e. adding terms with $\sin(n\Psi)$, the system displays higher order locking as well.

As we saw, the Adler equation is a basic equation in nonlinear dynamics that is fully soluble and understood. It can help to understand other systems like the Kuramoto model better. The Kuramoto model is a simplification of the Winfree model:

2.1.2 Winfree model, 1967

The ingenuity of Arthur T. Winfree, a theoretical biologist from Florida, manifests in a generalization of the plentiful and diverse types of oscillations in biology to few mathematical models and concepts. His most prominent model, thus decorated with his name, describes the synchronization of a population of self-sustained relaxation oscillators by weak mutual coupling, [Win67]. He realized that such seemingly fundamentally different phenomena as primordial cells of pacemaker nodes, rhythmically and collectively flashing fireflies, and all sorts of circadian rhythms are all fingerprints of the same nonlinear mechanism.

In Winfree's model, weak coupling of limit cycle oscillators acts as mutual weak perturbation [GMP17]. The phase oscillators with distributed frequencies interact via a product of the "sensitivity function" and the "intensity function". The sensitivity function $Q(\theta)$, or phase response curve of an oscillator, describes in which phase of its inner cycle it reacts how strongly on a perturbation. The intensity function is a sum over the so called pulse functions $P(\theta)$ of all other oscillators that describe how strongly these oscillators perturb the other oscillators in which phase of their own cycles.

$$\text{Winfree model} \qquad \dot{\theta}_i = \omega_i + Q(\theta_i)\frac{\epsilon}{N}\sum_{j=1}^{N} P(\theta_j). \tag{2.2}$$

Although Winfree already observed synchronization among this type of oscillators, the product form of the interaction complicated an analytical treatment of the problem.

2.1.3 Kuramoto model, 1975

In 1975, Kuramoto proposed to substitute the product coupling in the Winfree model by a form that allowed him to solve the model analytically [Kur75]. His derivation starts from Stuart-Landau oscillators coupled over the sum of complex amplitudes. He formulates three assumptions

i) global coupling, i.e. all oscillators are coupled to all others with the same coupling strength,

ii) infinite growth and decay rate of the amplitude (all dynamics happens on the limit cycle) with constant ratio, but finite frequency and coupling strength, and

iii) the thermodynamic limit of infinitely many oscillators.

In this case, the Stuart-Landau oscillators reduce to phase oscillators. Their coupling depends only on the phase difference between the oscillators and is of sinusoidal form. Condition ii) can be alleviated to the condition of sufficiently weak coupling and small frequency dispersion as well as sufficiently strong attraction of the limit cycles. The small frequency dispersion rules out higher locking orders than $1:1$ by separation of time scales. The weak coupling leaves the limit-cycles undeformed.

The resulting Kuramoto model describes N phase oscillators with natural frequencies ω_i distributed according to a distribution $g(\omega)$:

$$\text{Kuramoto model} \qquad \dot{\theta}_i = \omega_i + \frac{\epsilon}{N}\sum_{j=1}^{N} \sin(\theta_j - \theta_i). \tag{2.3}$$

We restrict our analysis to positive coupling strengths ϵ. To reduce the system to the necessary number of parameters it is convenient to change to a rotational reference frame for which the distribution $g(\omega)$ is centered around zero and normalize the distribution to unit

standard-deviation. The coupling of phases θ_i is sinusoidal such that the ensemble strives for a minimization of the phase differences. The system achieves partial (and eventually complete) frequency locking at sufficiently large coupling strength ϵ. The model can be written in a simpler form via the Kuramoto order parameter

$$Z := R\mathrm{e}^{\imath\varphi} := \frac{1}{N}\sum_{j=1}^{N}\mathrm{e}^{\imath\theta_j}. \tag{2.4}$$

The Kuramoto mean field Z is the centroid of the polygon connecting the phases θ_j on the unit circle. Phase φ shows the direction in which this centroid lies from the center of the circle. Only when all phases are equal, amplitude R is exactly one. In contrast many configurations are compatible with $R = 0$.

With the help of Z, model equation Eq. (2.3) can be rewritten as

$$\dot{\theta}_i = \omega_i + \epsilon R\sin(\varphi - \theta_i), \tag{2.5}$$

which reflects the structure of the system: each oscillator contributes to a complex-valued mean field which acts back on all oscillators. This mechanism is the key to the self-consistency theory that Kuramoto developed for the infinite case $N \to \infty$, where R converges to a constant, so that the oscillators effectively decouple.

In the infinite limit, the complex order parameter Z is an integral

$$Z = \int_{-\infty}^{\infty}\mathrm{d}\omega\int_{-\pi}^{\pi}\mathrm{d}\theta\, g(\omega)P(\theta|\omega,\epsilon R) \tag{2.6}$$

over the natural frequency distribution $g(\omega)$ and the density of phases $P(\theta|\omega,\epsilon R)$. Assuming that R is constant and φ rotates at constant frequency Ω, Eq. (2.5) describes Adler oscillators with the above mentioned two types of solutions (see text below Eq. (2.1)). Likewise, the density of phases separates into two densities, depending on the condition

$$|\Omega - \omega| \quad \begin{cases} \leq \epsilon R & \text{synchronous} \\ > \epsilon R & \text{asynchronous.} \end{cases} \tag{2.7}$$

Synchronous oscillators lock their frequency to the mean field, so their phase distribution is a delta distribution around the fixed point of Eq. (2.5). Asynchronous oscillators rotate with varying speed and their phase density is proportional to $1/|\dot{\theta}|$. Knowing these densities as functions of ϵR, one can insert them into the integrals in the right-hand side of Eq. (2.6). The two types of oscillators and the imaginary and real part in this equation amount to four integrals. For symmetric $g(\omega)$, the imaginary integrals cancel and the real integral of the asynchronous oscillator vanishes. In this case, after rotating into the reference frame of the global phase $\psi = \theta_i - \varphi$, Eq. (2.6) becomes

$$R = \epsilon R\int_{-\pi/2}^{\pi/2}\mathrm{d}\psi\, g(\Omega + \epsilon R\sin\psi)\cos^2\psi. \tag{2.8}$$

Assuming a Lorentzian natural frequency distribution $g(\omega) = \gamma/[\pi(\omega^2 + \gamma^2)]$, Kuramoto solved this integral by complex integration. For $\epsilon < 2\gamma$, the only solution of Eq. (2.8) is zero; above, another solution $R = \sqrt{1 - 2\gamma/\epsilon}$ appears, corresponding to partial synchrony in the sense of coexistence of synchronous and asynchronous oscillators. Complete synchrony, in which all oscillators lock to the mean field, is only possible for frequency distributions

with bounded support.

In the sub-critical coupling regime of the infinite ensemble, the phases assume a uniform distribution on the circle, corresponding $R = 0$. The super-critical density of phases is the sum of a uniform distribution of the asynchronous oscillators and a one-hump distribution that is bounded in $(-\pi/2, \pi/2)$ in the reference frame of the global phase φ. Therefore, a finite value R in the thermodynamic limit approximates only roughly the portion of locked and unlocked oscillators, but instead quantifies the alignedness of phases on the circle.

We discuss the above densities and integrals in more detail in Sect. 3.2.2. Other presentations of the derivation can be found in [Kur75, Kur84, PRK03].

The model was subsequently extended in many ways: When the sine term includes an additional phase delay β, $\sin(\theta_j - \theta_i - \beta)$, it is called Kuramoto-Sakaguchi model [SK86]. Also, higher harmonics of order n of the coupling function, $\sin[n(\theta_j - \theta_i)]$, generalize the model, e.g. [KP14]. Instead of global coupling, a network structure can be assumed [AKM$^+$08].

In 2008, a major leap in the understanding of the synchronization phenomenon in infinite ensembles was achieved by [OA08]. The authors found an attractive invariant synchronization manifold, now referenced as Ott-Antonsen manifold. The time-dependent order parameter dynamics is then described by only two variables. However, as this elegant theory finds no explicit application in this thesis, we leave its presentation and extension to [PR08, MMS09, PR15].

2.2 Recent work on the finite-size Kuramoto model

Here we briefly review a major part of former publications on the finite-size Kuramoto model that are concerned with 1. the scaling of fluctuations and with 2. chaoticity and Lyapunov exponents. The comparison to former literature reveals that we take a very different viewpoint on the Kuramoto model in the following chapters.

2.2.1 Finite-Size Fluctuations in the Kuramoto model

The scaling of fluctuations dominates the present literature on finite systems of coupled phase oscillators.

Hiroaki Daido was the first to discuss finite-size scaling laws for the Kuramoto model. In a series of papers [Dai86, Dai87, Dai90], he discusses a computation-time saving discrete-time version of the Kuramoto model that takes the form of coupled circle maps with distributed winding numbers. He calls the model Lorentzian-Dirac-sine (LDS) model to summarize the model assumptions of Lorentzian natural frequency distribution and global coupling by the sine of the phase differences. Frequency samples were generated as the tangent of equidistant points. His main interest is devoted to the scaling α of the standard deviation of the order parameter – or susceptibility in thermodynamic contexts – with distance to the critical coupling $\sigma \sim |\epsilon - \epsilon_c|^{-\alpha}/\sqrt{N}$. The quantification was quite difficult.

In [Dai86], Daido analytically predicted $\alpha_\pm = 1/2$, but then in [Dai87] obtained $\alpha_\pm \approx 1/8$ with a slight discrepancy between sub-critical α_- and super-critical α_+. He already noted a more complicated scaling function on the super-critical side that was later extensively discussed by Hong et. al.. In the meantime, though, Nishikawa and Kuramoto claimed in [KN87] that the susceptibility at the criticality is finite in the thermodynamic limit. In [Dai90], Daido gave a statistical description of the complex order parameter's behavior and uncovered a conceptual mistake in [KN87]. We extend Daido's work in many details, showing how much the dynamics can vary due to sampling of the natural frequency distribution in Chap. 3, but also how much more complicated than the classical picture of order and disorder the finite-size model is (see Chap. 4).

Similar to [Dai90], but with a version of the model with no preferred phase (gauge-invariant), [PR99] showed that the observed fluctuations in the order parameter can be described by a noisy Stuart-Landau equation for sufficiently large N. The noisy contributions to the evolution of the higher order order parameters become independent. The law of large numbers and the Furutsu-Novikov formula allow to approximate shape and mean of the noisy contributions, respectively. The hierarchy of time evolution equations for the order parameters is now a system of k coupled nonlinear stochastic differential equations with independent (individual) noise sources. Expanding around the critical point of the first order order parameter and neglecting the multiplicative noise that is comparably small close to the transition, they obtain the standard form of a noisy Hopf-Andronov bifurcation.

In the following years, a group around Hong published a series of papers [HCPT07, HPT07, SH10] that discussed scaling relations of the form $\sigma \sim N^{-\beta/\bar{\nu}} f(N^{1/\bar{\nu}}|\epsilon - \epsilon_c|/\epsilon_c)$ in the framework presented in [Dai90]. In [HCPT07] they analytically estimated the scaling function, obtaining a correlation size exponent $\bar{\nu} \sim 5/2$ that differs from typical thermodynamic equilibrium phase transitions. In [HPT07], they employed a similar analysis on scale-free networks, obtaining decisive differences only for more heterogeneous networks. In [SH10], they studied scaling relations when additional individual noise terms force the oscillators. As noise increases, the correlation size exponent is decreased to $\bar{\nu} \sim 2$. In contrast to Daido, who mostly sticked to the Lorentzian, Hong et. al. carried out all their numeric studies with a standard Gaussian natural frequency distribution.

[Tan11] reported on a different correlation size exponent of $\bar{\nu} \sim 5/4$ in the case of regularly sampled frequencies. In [NTHA12, NTA13, NIT+14], Nishikawa et. al. returned to the issue with a mostly numerical analysis of the scaling law for a diffusion coefficient of the order parameter time evolution in both the sub- and the super-critical coupling regime for general coupling functions. In comparison to the former scaling relations, they were now able to quantify long-term fluctuation correlations.

[CHK13] compared steady and dynamical scaling of fluctuations (after and before the steady state is reached), for different natural frequency sample generation methods. Also [LYK14] numerically explored the scaling with N, $(\epsilon - \epsilon_c)$, and time, here in the globally coupled Kuramoto model with or without individual noise, in a Watts-Strogatz small world network, and in a generalized version of the Ising model. [HCTP15] revisited the finite scaling problem – inspired by [Tan11] focusing on different ways of generating frequency samples.

[HS16] distributed both frequencies and coupling strengths, but in a highly symmetrical, correlated way that results in higher synchronizability and discuss the scaling of fluctuations. In [WRGB15], the authors approximated the stable solution for individual phases in the completely synchronized (FS) regime, based on the lower threshold to critical coupling for FS that was given in [VM07]. Finally, [CDJ17] discussed the scaling of the order parameter and the largest Lyapunov exponent (LLE) with $(\epsilon - \epsilon_c)$ for equidistant natural frequencies. They find a difference between mid- and endpoint rule in both scales (order parameter and LLE).

2.2.2 Chaos in the Finite-Size Kuramoto Model

We now give a short overview over publications that address chaoticity and Lyapunov exponents in the finite-size Kuramoto model.

[PMT05] discussed phase chaos as known from the Ginzburg-Landau equations in ensembles of size 4 and 20, respectively, with equidistant natural frequencies. Particularly interesting for Chap. 4 is Fig. 2 therein that shows an increase of the largest Lyapunov exponent prior to the critical coupling.

The doctoral thesis [Bar13] contains an otherwise unpublished chapter 3, in which the Lyapunov spectrum of a finite Kuramoto ensemble with Gaussian distributed frequencies is discussed. He found positive Lyapunov exponents in a wide range of super-critical coupling strengths. Some findings in the study are inconclusive, however, e.g. he found that the largest Lyapunov exponent was independent of the ensemble size.

[CGP17] performed computationally expensive studies on the largest Lyapunov exponent for different natural frequency samples that were generated either randomly or regularly (see Sect. 3.0 in this thesis) and found that the largest Lyapunov exponent scales $\sim 1/N$ or $\sim \ln N/N$ with system size N for randomly or regularly distributed frequencies, respectively. An explanation of this finding is still pending.

[PP16] dedicates a section "Global coupling: phase oscillators" to the finite Kuramoto model in which they present the sub- and super-critical Lyapunov spectrum of 400 Kuramoto oscillators.

This brief overview over the literature in the field demonstrates that in the past most works were dedicated to the scaling of fluctuations with number of oscillators, distance to the criticality, and time. The literature on Lyapunov exponents and chaoticity in the finite Kuramoto model is very limited. In what follows, we take a different approach to the here listed publications and draw our comparisons to the infinite limit in a different way, see Chap. 3. In Chap. 4, we discuss the synchronizing effect of finite-size fluctuations with a short outlook on the scaling of the effect with ensemble size.

Chapter 3

Transition to a collective mode

In 1967, Winfree created his famous model of large ensembles of coupled phase oscillators referring to "innately oscillatory devices (e.g. electronic oscillators, secretory cells, spontaneously active neurons, or individual animals)", [Win67]. From there, Kuramoto [Kur75, Kur84] derived a self-consistency mean field theory for a simplified version of the Winfree model, having in mind circadian rhythms[1] and α-rhythms in the brain, compare Sect. 2.1.3. These initial motivations represent a small part of what both theories eventually apply to. It were the radical reductions in these first publications to the very essence of synchronization in large ensembles of self-sustained oscillators that allowed for analytical tractability and understanding of the key mechanism of synchronization in large populations.

For many years now, researchers from all over the world try to weaken the rather strong model assumptions in Kuramoto's derivation to extend its applicability. Theoreticians progressed in generalizations to higher harmonics of the coupling function [KP13, PM09], network structure instead of global coupling [AKM$^+$08, RPJK16], time-varying networks [LFCP18], time delay [KSYHS98] or phase delay [SK86] in the coupling function, and common or individual noise [GPRP17].

Quite surprisingly, even identical oscillators exhibit rich behavior such as chimera states [KB02, AS04, PA15] and partial synchrony [CPR16]. Also, the stability of the synchronized solution still remains only partially understood [OA09, Chi15]. The Ott-Antonsen theory brings the two models – Winfree and Kuramoto – closer together by solving some special cases of the Winfree model in the infinite case [GMP17].

But even when limiting the discussion of Kuramoto ensembles to only the first harmonics of the coupling function, including neither Kuramoto-Sakaguchi phase delay nor network structure, many interesting aspects are still, if at all, only partly understood. Finite ensembles differ from infinite ensembles in many ways. While the phase dynamics is chaotic for intermediate-sized ensembles in a large range of coupling strengths and the order parameter fluctuates, the infinite system is fully described by merely two variables, at least in the case of a unimodal natural frequency distribution.

While in the finite Kuramoto model Eq. (2.3) the locking condition Eq. (2.7) is time-dependent, oscillators in the infinite limit strictly separate into locked and unlocked ones. In general, the finite case exhibits much richer behavior, but often evades analytical treatment. Most earlier literature on the finite-size Kuramoto model concentrated on quantifying the scaling of fluctuations around the criticality, see 2.2.1. In these publications, the smallest sample sizes already exceed 10^3. Therefore, we focus our analysis on intermediate system sizes of 25-200 oscillators, where finite-size effects are strongly pronounced, yet the infinite limit is close at hand to explain certain observations.

The two central questions we address in this chapter are:

[1] Quote from the video speech Kuramoto gave on a conference dedicated to the 40th birthday of his model, [KK15].

- What is a suitable indicator for the onset of a collective mode in finite Kuramoto ensembles?
- How does the sample-to-sample variability of the natural frequencies affect the global dynamics?

The chapter opens with an overview, Sect. 3.0, over the different types of distributions and samples used in our analysis. In Sect. 3.1, we introduce an indicator for the onset of a collective mode. As discussed in Chap. 2, the critical coupling strength in the infinite case in the case of a unimodal natural frequency distribution is unambiguous. Below, the order parameter vanishes exactly. Above, an additional non-zero solution exists. Fluctuations of the order parameter rule out such distinction in the finite case. As in [TZT$^+$12], where a similar property was used, it is the minimum of the order parameter that detects collective behavior.

When discussing the effects of sample-to-sample variability, some of them vanish with system size and others extend into the infinite limit. Therefore, in Sect. 3.2.2, we present a more general parametric approach to the solution of the self-consistency integrals. The method was used by other authors before; we extend it here to also asymmetric distributions. Sect. 3.3 and Sect. 3.4 reveal the connection between the shape of the natural frequency sample and the absolute value of the order parameter on the one hand and the effect of the symmetry of the natural frequency sample on the global phase dynamics on the other hand. In both cases, we first employ extensive numerical calculations to uncover the connections in finite populations and then juxtapose them with solutions from the infinite limit. In the latter case, families of distributions with either shape or asymmetry as parameters allow for such an analysis.

After gaining intuition for the system, Sect. 3.5 discusses the rather problematic finite-size Lorentzian case. Chaoticity in the finite Kurmamoto model is briefly discussed in Sect. 3.6.

In summary, this chapter takes a novel viewpoint on the finite Kuramoto model and clarifies several aspects of the model in general, particularly concerning different natural frequency distributions. The predominant part of the work presented in this chapter was previously condensed into [PP18]. Figures and their captions created for that publication are copied to this chapter. The discussion in this chapter often goes more into detail than in the paper, and Sect. 3.5 and Sect. 3.6 are completely additional.

3.0 Natural frequency distribution and samples

The review article [ABV$^+$05] draws a link between the dynamics of the order parameter and the underlying frequency distribution, yet collects mere hints into different directions. A central question in this chapter is therefore the following: How do the synchronization transition and the collective dynamics in the finite Kuramoto model (Eq. (2.3)) depend on the natural frequency distribution?

In the thermodynamic limit, the assumption of a Lorentz (or Cauchy) distribution dominates the literature on the Kuramoto model and its descendants, see [Kur84, OA08, MBS$^+$09a, HBH$^+$14, BPM18], because the poles of this distribution allow to solve the emerging self-consistent integrals. From a modeling perspective, the fat tails of the distribution actually contradict the assumption of small frequency dispersion. As we discussed in Sect. 2.1.3, a large dispersion allows for higher resonances, and higher harmonics of the coupling function should be taken into account in the derivation of the model. Also, several motivations – many of them from biology – point to the more natural choice of a Gaussian frequency distribution. Details of the mathematical problems related to applying our numerical method to the Lorentz distribution are discussed in Sect. 3.5.

Finite-size nonlinear models of intermediate size, as we address them here (25-200 oscillators), are often analytically intractable. Therefore, by employing numerical analysis we are quite free in the choice of the model parameters and concentrate on the more natural Gaussian distribution.

For the comparison of different system sizes it seems reasonable to generate frequency samples in a deterministic way. Inverse transform sampling of frequencies from equidistant points $x_i \in (0, 1)$ produces frequency samples that resemble the underlying distribution even for rather small sample sizes. The required quantile function is the inverse of the cumulative distribution function – in the Gaussian case: $\omega_i = \sqrt{2}\,\mathrm{erf}^{-1}(2x_i - 1)$, where erf^{-1} is the inverse error function. Frequency differences are minimal in the center and increase monotonically to both sides. The samples are symmetric, i.e., for all i there exists exactly one j such that $\omega_j = -\omega_i$. In the following, we refer to this sample as being *regular*.

Random samples, in contrast, almost surely do not possess this perfect symmetry. Small samples are compatible with a large variety of underlying distributions. The moments of a sample follow the sampling distribution that depends on both, the sample size and the underlying distribution. For Gaussian samples for instance, the variance of the mean scales as $1/N$. Also pairwise frequency differences vary between samples and – again in the case of a Gaussian sample – the smallest frequency differences are not necessarily central. This variability is reflected in the dynamics, as we see in the following sections: As the samples are compatible with different underlying frequency distributions, their different infinite limits might imply different behavior. We elaborate this idea further in Sect. 3.3.2 and 3.4.2, where we analytically show how certain links between features of a natural frequency sample and resulting dynamics persist in the infinite limit.

Finally, we stress that finite samples cannot equal their corresponding infinite-limit distribution in all moments. In the Kuramoto model Eq. (2.3), a finite mean of the natural frequency distribution $\bar{\omega} \neq 0$ can be compensated for by rotating to the corresponding reference frame $\varphi_i \to \varphi_i - \bar{\omega}$ and has no effect on the dynamics. Likewise, any standard deviation $\sigma \neq 1$ merely changes the relation between time scale and coupling strength; we divide our samples by the measured standard deviation to increase comparability between samples, and set variance to one in all distributions $g(\omega)$. Higher moments, i.e. skewness and kurtosis, in contrast, are relevant parameters.

3.1 The minimal value of the order parameter as an indicator for the transition to a collective mode

The central quantity in the Kuramoto model Eq. (2.3) is the complex Kuramoto order parameter Z, especially its absolute value R. Sect. 2 already gave us an overview over the different regimes in the infinite case: Starting from a fully incoherent state with $R = 0$, with increasing coupling strength the ensemble undergoes a critical transition to partial frequency locking. Eventually, in case of frequency distributions with bounded support, all oscillators lock to the common frequency at sufficiently strong coupling. The phase distribution of the locked oscillators narrows with increasing coupling strength. In the infinite case, R therefore clearly indicates sub- and super-critical regime.

In the finite case, though, R fluctuates (at least below the critical coupling strength of complete locking[2]), and incoherence in the sense of uncorrelated dynamics of individual oscillators is not indicated by $R = 0$.

[2] Above the critical value of complete locking, where all oscillators rotate uniformly with the frequency of the mean field, the order parameter becomes stationary. For a discussion of this type of critical coupling strength see [VM07].

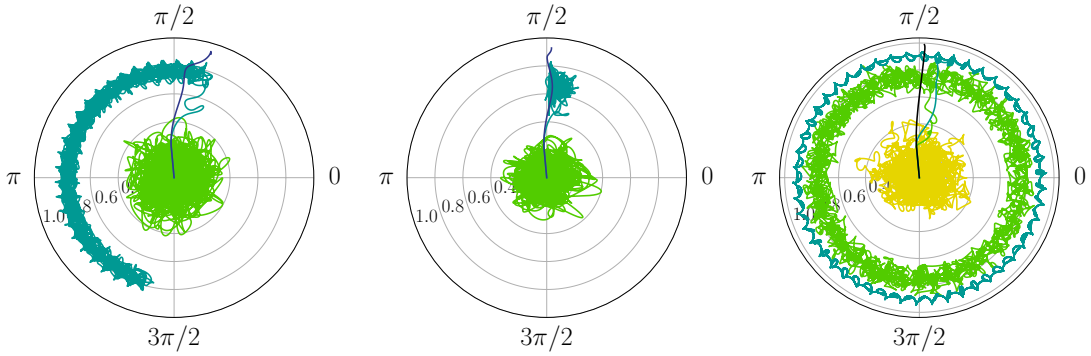

a) random Gaussian **b)** regular Gaussian **c)** random Lorentzian

coupling strengths

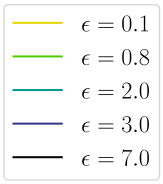

central moments

	μ	σ^2	γ_1	β_2
a)	0	1	0.07	3.8
b)	0	1	0.00	2.5
c)	0	1	1.80	16.1

FIG. 3.1: **Time evolution of the complex order parameter Z in polar representation** at different values of coupling strength ϵ for 50 oscillators with frequencies 3.1a) randomly sampled from the normal distribution, 3.1b) regularly sampled via quantiles from the normal distribution, and 3.1c) randomly sampled from the Lorentz distribution over $t = 10^5$ RK4 time steps of size 0.01. We will see that the decisive difference between random and regular Gaussian sample is the pairwise symmetry of the latter ($\forall i \, \exists$ exactly one $j : \omega_i = -\omega_j$). Note that in 3.1a), 3.1b) we display only $\epsilon = 0.8$, 2.0, and 3.0, while in 3.1c) we show $\epsilon = 0.1$, 0.8, 2.0, and 7.0 – because the Lorentzian distributed oscillators reach partial synchronization at much lower coupling strength compared to the two Gaussian samples but need much stronger coupling to achieve complete frequency locking. The table contains the first central moments of the three natural frequency samples: mean μ, variance σ^2, skewness γ_1, and kurtosis β_2 (see (3.34) and (3.22) for definitions of the latter two). All trajectories start from the same 50 initial phases, randomly picked from a uniform distribution in $[0, 2\pi)$, therefore $R(t_0) \approx 0$.

In this section, we first discuss the typical time evolution of the complex order parameter Z in different setups and compare it to the infinite model. What we observe will then motivate the definition of an alternative order parameter R_{min} which is necessary for a meaningful definition of the global phase. The second part of the section is then devoted to the discussion of this new quantity.

General time evolution of the complex mean field in finite ensembles

This chapter takes a different, less thermodynamic, view on the Kuramoto model-specific finite-size effects. We aim to grasp the different outcomes of the quenched noise stemming from the sample-to-sample variability of the frequency distribution that imprints different features to each realization of the model. In order to gain some intuition about the different parameters in the finite model, we first discuss time series of the order parameter for different coupling strengths, natural frequency distributions and ensemble sizes. We will state three main observations, one of which will motivate the definition of an alternative order parameter for the detection of a collective dynamics.

In Fig. 3.1, we compare the time evolution of the order parameter for three typical natural frequency distributions. The random Lorentzian sample in panel 3.1c) traditionally

appears in connection with the infinite Kuramoto model due to the above-mentioned analytical tractability. The random Gaussian distribution in panel 3.1a) dominates the set of all examples of distributions in nature due to the classical central limit theorem. The regular Gaussian in panel 3.1b) might serve as representative for the set of Gaussian samples in certain aspects and potentially eases comparisons between different sample sizes.

In all three cases, the order parameter strays around zero for small coupling strengths. For stronger coupling, apparently an inner disc is avoided after a transient period, i.e. the order parameter arrives at a certain degree of order that it seemingly never undercuts again. Like in the infinite case, where the synchronized state is stable and attractive, the partially synchronous state might correspond to a stable and attractive region in phase space to which the dynamics migrates within the transient time, further corroborated by results in Sect. 3.6. Already at this point, we note the transition with increasing coupling strength from an incoherent regime with arbitrarily small order parameter to a partially ordered regime, where the order parameter complies with a lower bound. We soon discuss $R_{\min}$ as an indicator of this transition that serves as an alternative order parameter in Sect. 3.1.

The critical coupling corresponding to this transition point varies considerably between different natural frequency distributions, as the comparison between random Gaussian and random Lorentzian sample indicates: At coupling strength $\epsilon = 0.8$, while the Gaussian ensemble still fluctuates close to zero, the Lorentzian ensemble already clearly forms a ring with considerable minimum, $R(t) > 0.6$. At stronger coupling, on the contrary, the Gaussian population reaches complete frequency locking, indicated by constant mean field after a transient, with constant order parameter already at $\epsilon = 2$, while it requires a coupling strength of $\epsilon = 7$ to synchronize the Lorentzian ensemble completely. This effect is quite plausible considering the peakedness and comparably fat tails of the Lorentz distribution which typically produces samples with many close frequencies densely packed around the mean and a few extreme outliers. While weak coupling suffices to synchronize the central cluster of almost equal frequencies, the few outliers deviate strongly from the majority and necessitate significantly stronger forcing by the mean field to join the central cluster. The dependence of the typical behavior of order parameter $R(t)$ on the natural frequency distribution in the infinite case and on finite frequency samples merits discussion in Sect. 3.3.

The third important observation concerns the rotation and fluctuation of the global phase. We discuss in Sect. 3.1 that the global phase deserves its name only when a finite minimum of the order parameter can be assured. Then, the complex order parameter typically forms a characteristic ring structure (see Fig. 3.1) that reflects a finite drift and small fluctuations of the global phase. Perfectly symmetric samples (in which for each oscillator there is exactly one oscillator that rotates with the same frequency but in the opposite direction) are a notable exception from this typical behavior. Here, the global phase converges to a constant, while the order parameter fluctuates persistently. Fig. 3.2 shows typical trajectories of the global phase and the dependence on initial conditions[3]. We discuss the relation between the symmetry of the natural frequency distribution (or sample) and the drift of the global mean field in Sect. 3.4.

[3]Note that for large coupling strengths, the motion appears more regular – the only respective publication known to the author indicates weak chaoticity, see [Bar13].

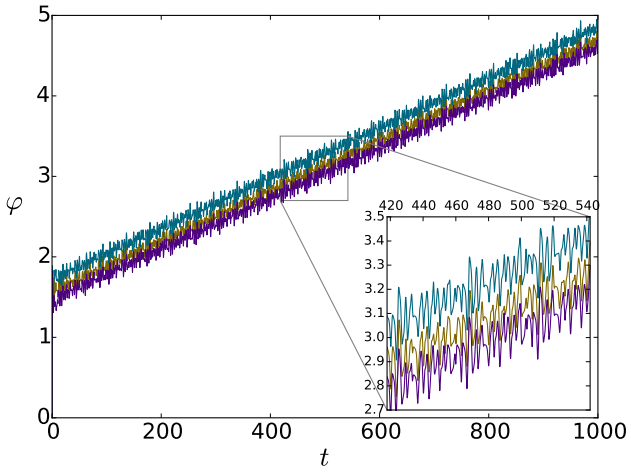

a) random Gaussian

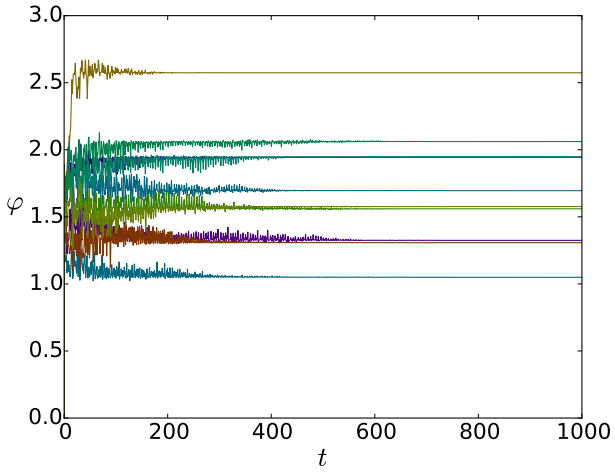

b) regular Gaussian

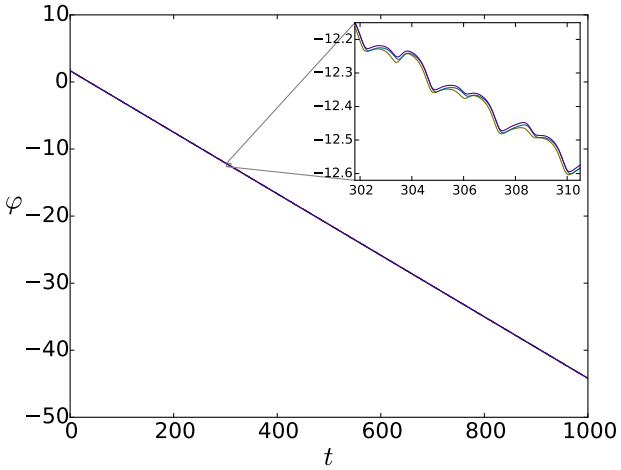

c) random Lorentzian

FIG. 3.2: **Time evolution of the global phase for different natural frequency samples** comparing different initial conditions for the same three natural frequency samples as in 3.1, at coupling strength 2. Different colors indicate different initial conditions (three, ten, and three initial conditions in 3.2a), 3.2b), 3.2c), respectively). They differ from each other only by a small phase vector of length 0.05 that points into a random direction. For (pairwise) symmetric samples, see 3.2b), the global phase converges to a constant that depends on the initial condition. Ensembles with asymmetric frequency sample adopt a finite drift with persistent fluctuations on top, see 3.2a) and 3.2c).

Three observations constitute the main body of this chapter:

- 1st, the transition to a finite minimum order parameter,
- 2nd, the relation between the shape of $g(\omega)$ and the critical coupling strength for the transition, and
- 3rd, the relation between the asymmetry of $g(\omega)$ and the global phase drift.

Aspects concerning fluctuations and chaoticity are discussed in Chapter 3.6.

Transition to a meaningful global phase definition

As discussed above, Fig. 3.1 suggests that sub-critical and super-critical regime can be distinguished via the existence of a minimal value of the order parameter. In the two random cases of this figure, Fig. 3.1a) and Fig. 3.1c), this corresponds to a ring shape of the complex order parameter's time evolution. We therefore define an indicator $R_{\min}$ as the minimum of a sufficiently long time evolution after a transient.

The idea already proved useful in [TZT$^+$12]. There, 20 coupled Wien-bridge oscillators exhibited partial synchrony[4] with a mean field frequency different from the frequency of the single units. The minimum value of the mean-field amplitude indicated the transition from a fluctuating incoherent to an oscillatory coherent regime. The motivation becomes apparent when plotting the recorded outputs of the mean-field voltage against its Hilbert transform: In the oscillating regime, the resulting phase portrait avoids an inner circular disk giving meaning to a phase definition, while in the fluctuating regime the whole disk is covered and thus any interpretation as periodic behavior must fail.

Likewise in the finite-size Kuramoto model (see Fig. 3.1) a global phase describes a collective oscillation only above the transition to a finite value of $R_{\min}$. This is due to two main reasons: First, when $R = 0$ in $Z = Re^{\imath\varphi}$ then φ can take arbitrary values, i.e. the phase is mathematically not well defined; second, for a physical meaning of a collective phase the system must, at least partially, exhibit collective phase evolution. The term global phase is conceptually justified only when a sufficient amount of coherence indicates collective oscillations. We quantify this amount by a non-vanishing $R_{\min}$.

In Fig. 3.3 (the top panel), we juxtapose the minimum and mean of the order parameter, and the individual observed frequencies of an ensemble of 50 Kuramoto oscillators – dependent on the coupling strength. The mean is finite at zero coupling strength and hardly informs about the dynamical state. The minimum, in contrast, clearly identifies the transition. The observed frequencies in the background show which oscillators' frequencies lock at which coupling strength.

The minimum of the order parameter is determined recording all updates of the minimum of $R(t)$ after cutting a transient. In the bottom panel, we color-code $R_{\min}(t)$ according to whether its final value after 10^5 time units exceeds 0.01 or not. Sub-critical $R_{\min}(t)$ approach zero with $\approx t^{-1/2}$, while super-critical saturate quicker. A clearer distinction around the critical value can be achieved by extending the time evolution.

Whenever we speak of sub- or super-critical regimes or coupling strengths (and do not say otherwise), we refer to the critical coupling strength with respect to $R_{\min}$.

By means of this new indicator, we can now compare the collective dynamics of different natural frequency samples. We first present a method for finding a parametric solution for the dependence of the order parameter on coupling strength for general natural frequency distributions in the thermodynamic limit. This later helps us to explain observations in the finite case by comparison to the infinite case.

[4] This is a different notion of partial synchrony than we use in this thesis, see footnote 6.

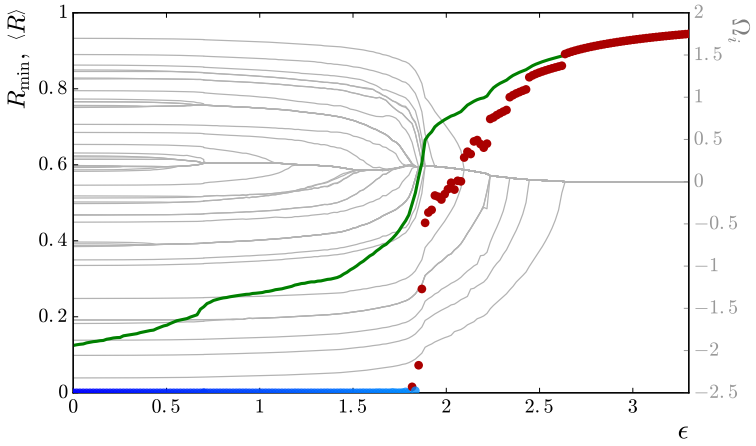

a) Red and blue dots: $R_{\min}(t = 10^5)$ lesser or greater than 10^{-2}, respectively. Green line: mean of $R(t)$. Gray lines and right ordinate axis: individual observed frequencies $\Omega_i = \langle \dot{\varphi}_i \rangle_t$.

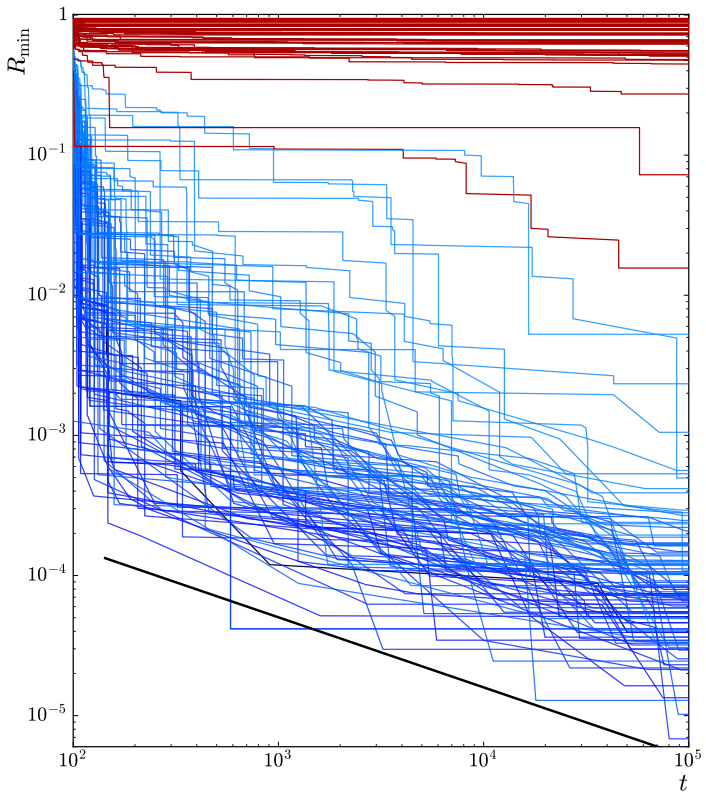

b) Time dependence of the minimum of the order parameter. The black line $\sim t^{-1/2}$ approximates the scaling of $R_{\min}(t)$ at subcritical coupling strengths.

FIG. 3.3: Statistical characterization of the minimum of $R(t)$, for $N = 50$ oscillators and a fixed random sample of a Gaussian frequency distribution with sample moments $\mu = 0$, $\sigma^2 = 1$, skewness $\gamma_1 = -0.45$ (see Eq. (3.34)), excess kurtosis $\gamma_2 = -0.55$ (see Eq. (3.23)). Time evolution starts from uniformly distributed phases in $[0, 2\pi)$. (a) $R_{\min}$, $\langle R \rangle$, and Ω_i vs. coupling strength ϵ. Here $R_{\min}$ is shown vs. ϵ at $t = 10^5$ (after transients of length 10^2) for an ϵ-grid with $\Delta\epsilon \approx 0.02$. The green solid line shows the mean value $\langle R \rangle_T$ averaged over a time interval of $T = 10^4$. The observed individual frequencies Ω_i shown in gray (right hand scale) reveal which oscillators synchronize already at small frequencies, and which join the synchronous cluster only at stronger coupling. The sampled natural frequencies ω_i equal the observed frequencies Ω_i at zero coupling. Note that several gray lines join far below critical coupling, indicating early synchronization of small clusters due to time-scale separation. (b) Dependence of $R_{\min}$ on the observation time. The bold black line gives an estimate $t^{-1/2}$ for the scaling behavior. In both panels, red indicates $R_{\min} > 0.01$ at $t = 10^5$; blue marks $R_{\min} < 0.01$.

3.2 Solving the self-consistency equation (SCE) in the infinite case

The startling beauty of Kuramoto's theory lies in the concert of different approximations that allowed him to find an exact self-consistent solution[5]. After this groundbreaking derivation, for more than 40 years now, all sorts of different generalizations remain in vivid discussion. The model assumptions are partially disputed as unrealistic, especially the combination of all-to-all coupling in combination with the infinite limit in the number of oscillators, but also the assumption of a Lorentzian natural frequency distribution with its heavy tails. The efforts presented in this section aim at extending the applicability of the theory especially in the last aspect. The normal distribution covers a wide range of applications due to the central limit theorem. Furthermore, with its exponentially bounded tails, it better meets the stipulation of small frequency dispersion.

We now present a self-consistent equation for the Gaussian frequency distribution, linking order parameter and coupling strength. Although this dependence cannot be expressed by elementary functions, its expression via modified Bessel functions allows for approximation of the relation $R(\epsilon)$ to arbitrary precision. In preparation for the later discussion of the effect of shape and symmetry of the natural frequency distribution on the dynamics of the complex order parameter, we also present a scheme for solving the SCE in parametric form for general unimodal symmetric or asymmetric distributions.

3.2.1 Solving the SCE for Gaussian distribution of natural frequencies

To find the dependence of the order parameter on the coupling strength in the case of a Gaussian natural frequency distribution, we start from the self-consistency equation for symmetric unimodal distributions given in Eq. (5.4.27) in [Kur84], after changing to our notation ($K \to \epsilon$, $\Omega \to \bar{\omega}$, $\sigma \to R$), or likewise Eq. (2.8), where solution $R = 0$ is already excluded:

$$1 = \epsilon \int_{-\pi/2}^{\pi/2} \cos^2\theta \cdot g(\bar{\omega} + \epsilon R \sin\theta)\, \mathrm{d}\theta \tag{3.1}$$

with absolute value of the order parameter R, coupling strength ϵ and mean frequency $\bar{\omega}$. We insert a Gaussian with zero mean and unit standard deviation

$$1 = \frac{\epsilon}{\sqrt{2\pi}} \int_{-\pi/2}^{\pi/2} \cos^2\theta\, \mathrm{e}^{-\frac{1}{2}(\epsilon R)^2 \sin^2\theta}\, \mathrm{d}\theta =: \frac{\epsilon}{\sqrt{2\pi}}\, \mathcal{I}_{\epsilon,R} \tag{3.2}$$

To make calculations easier, we define $A := \epsilon^2 R^2/2$ and just look at

$$\mathcal{I}_{\epsilon,R} = \int_{-\pi/2}^{\pi/2} \cos^2\theta\, \mathrm{e}^{-A\sin^2\theta}\, \mathrm{d}\theta. \tag{3.3}$$

Replacing the squared trigonometric functions by their double-angle expressions we write

$$\mathcal{I}_{\epsilon,R} = \frac{1}{2} \int_{-\pi/2}^{\pi/2} (1 + \cos 2\theta)\, \mathrm{e}^{-\frac{A}{2}(1-\cos 2\theta)}\, \mathrm{d}\theta. \tag{3.4}$$

[5]Take "It is difficult to explain how this emission of light is simultaneous for several thousands of individuals" as a quote that expresses the magic inherent in this phenomenon – quote from Bishop Pallegoix from 1854, an apostolic vicar in Eastern Siam at the impression of synchronous fireflies. Citation taken from John Bonner Buck, *Synchronous Rhythmic Flashing of Fireflies*, The Quarterly Review of Biology, Vol. 13, No. 3 (Sep., 1938), p. 302 – Kuramoto rather referred to chemical oscillators than to fireflies in his early publications, it is now considered a most illustrative example to which the theory applies.

Respecting that the function under the integral is symmetrical w.r.t. the y-axis and replacing $x = 2\theta$, we obtain

$$\mathcal{I}_{\epsilon,R} = \frac{\mathrm{e}^{-\frac{A}{2}}}{2} \int_0^\pi (1 + \cos x)\, \mathrm{e}^{-\frac{A}{2}\cos x}\, \mathrm{d}x \tag{3.5}$$

$$= \frac{\mathrm{e}^{-\frac{A}{2}}}{2} \left(\int_0^\pi \mathrm{e}^{-\frac{A}{2}\cos x}\, \mathrm{d}x + \frac{\mathrm{e}^{-\frac{A}{2}}}{2} \int_0^\pi \cos x\, \mathrm{e}^{-\frac{A}{2}\cos x}\, \mathrm{d}x \right), \tag{3.6}$$

which corresponds to the modified Bessel functions of first kind I_ν [AS65] p. 374 ff., especially Eq. 9.6.19 therein. Eq. (3.2) can thereby be expressed as

$$R = \sqrt{\frac{\pi}{2}}\, \sqrt{x}\, [I_0(x) + I_1(x)]\, \mathrm{e}^{-x} \quad \text{where} \quad x = \epsilon^2 R^2/4 \tag{3.7}$$

Note that $[I_0(x) + I_1(x)]\, \mathrm{e}^{-x} = 1$ at $x = 0$, such that we recover equation $\epsilon_c = 1/(2g(\bar{\omega})) = 2\sqrt{2}/\sqrt{\pi}$. For $x \to \infty$, $I_\nu(x) \approx \mathrm{e}^x/\sqrt{2\pi x}$ (compare [AS65] Eq. 9.7.1) such that $R \to 1$ as $\epsilon \to \infty$, reflecting that the width of the phase distribution of the synchronized oscillators decreases with increasing coupling strength. After treating this special case which is the central example in this thesis, we now develop a method for solving self-consistency equations for general, also asymmetric, distributions in parametric form.

3.2.2 Expressing the solution of the SCE in parametric form for a general natural frequency distribution

In order to find parametric solutions for more general (also asymmetric) frequency distributions, we adopt a technique developed in [OW12, OW13, ZPL17, KP14] and extend it to asymmetric natural frequency distributions. We start from Eqs. (2.5) and (2.6) and assume that the mean field $R\exp(\imath\varphi)$ rotates at constant frequency Ω and reaches a constant absolute value after some transient. We determine these two values self-consistently.

$$\dot{\theta} = \omega + \epsilon R \sin(\varphi - \theta) \quad \text{with} \quad R\mathrm{e}^{\imath\varphi} = \langle \mathrm{e}^{\imath\theta} \rangle \quad \text{and} \quad \dot{\varphi} = \Omega \tag{3.8}$$

Substituting $\psi = \theta - \varphi$ compensates for the uniform rotation of the mean field, which in this model is equal to the rotation of all locked individual oscillators[6]. Furthermore, we define a parameter $a := \epsilon R$, which together results in an Adler-equation

$$\dot{\psi} = \omega - \Omega - a \sin\psi. \tag{3.9}$$

This equation has only one relevant parameter, so for the discussion of its solutions we can rescale to $\dot{\psi} = \Delta - \sin\psi$ (where the dot now refers to a different time scale) and consider $\psi \in (-\pi, \pi]$. This first order nonlinear differential equation undergoes a saddle-node bifurcation at both, $\Delta = 1$ and $\Delta = -1$. For $\Delta \in (-1, 1)$, a pair of stable and unstable fixed points exists with ψ in $(-\pi/2, \pi/2)$ and with $|\psi|$ in $(\pi/2, \pi)$, respectively. We recall that ψ is the difference between an oscillators' individual phase and the phase of the global mean field. The stable fixed point, with constant frequency difference, thus corresponds to frequency locking between the two. For $|\Delta| > 1$, there is only the free-running periodic solution, which corresponds to asynchrony between mean field and individual oscillator.

[6] Recently, systems exhibiting partial synchrony (ps) raised attention [MP06, RP15, CPR16]. Other than in this thesis, ps refers to a periodic collective dynamics when individual oscillators rotate at frequencies different to the mean field phase.

The integral form of the definition of the order parameter as in Eq. (3.8) can be interpreted as a self-consistent equation for the order parameter, as first presented by Kuramoto [Kur75].

$$R = \int_{-\pi}^{\pi} \mathrm{e}^{\imath\psi} \left(\int_{-\infty}^{\infty} g(\omega)\, w(\psi, \omega|\Omega, a) \mathrm{d}\omega \right) d\psi = F(\Omega, a)\, \mathrm{e}^{\imath Q(\Omega,a)} \tag{3.10}$$

$$=: \int_{-\pi}^{\pi} \mathrm{e}^{\imath\psi} \left(n_{\mathrm{s}}(\psi) + n_{\mathrm{as}}(\psi) \right) d\psi \tag{3.11}$$

where $n_{\mathrm{s}}(\psi)$ and $n_{\mathrm{as}}(\psi)$ are the distributions of the phase differences to the global mean field phase of the synchronous and asynchronous solution, respectively. The trick now is to interpret the right hand side of Eq. (3.10) as a function $F\,\mathrm{e}^{\imath Q}$ which depends on the frequency of the global mean field Ω and on parameter a. As $R = F(\Omega, a)\,\mathrm{e}^{\imath Q(\Omega,a)}$ but $R \in [0, 1]$ is real, the order parameter is given as a function of Ω and a and the imaginary part must vanish[7]. With $\epsilon = a/R$, the set of parametric equations is complete.

As derived in [Kur84] Chap. 5 or [PRK03] Chap. 12, the oscillators fall in either of the two groups corresponding to the two types of solutions of the Adler equation, according to their natural frequency. Oscillators with frequencies $|\Omega - \omega| < a$ lock to the mean frequency (the unstable fixed point is occupied by a set of oscillators of Lebesgue measure zero). Oscillators with frequencies $|\Omega - \omega| > a$ rotate according to Eq. (3.9). The respective densities n_{s} and n_{as} can thus be written as

$$n_{\mathrm{s}} = \int_{-\infty}^{\infty} g(\omega)\, \delta \left(\psi - \arcsin \left[\frac{\omega - \Omega}{a} \right] \right) \mathrm{d}\omega \tag{3.12}$$

$$= a g(\Omega + a \sin\psi) \cos\psi \quad \text{with} \quad -\frac{\pi}{2} \leq \psi \leq \frac{\pi}{2} \tag{3.13}$$

where we transformed the δ-distribution according to $\delta(f(x)) = \delta(x - x_0)/|f'(x_0)|$, which applies for sufficiently well-behaved functions f with only one root at x_0 and derivative f'. For the asynchronous part we have

$$n_{\mathrm{as}}(\psi) = \int_{|\omega - \Omega| > a} \mathrm{d}\omega\, g(\omega)\, P(\psi, \omega), \tag{3.14}$$

where $P(\psi, \omega)$ is the probability density of the individual phase differences which scales inversely to the velocity of the phase differences $P(\psi, \omega) \sim 1/|\dot{\psi}|$. By normalizing we obtain

$$P(\psi, \omega) = \frac{1}{\int_{-\pi}^{\pi} \mathrm{d}\psi/|\dot{\psi}|} \cdot \frac{1}{|\dot{\psi}|} \tag{3.15}$$

$$= \left(\int_{-\pi}^{\pi} \frac{1}{|\omega - \Omega - a \sin\psi|} \mathrm{d}\psi \cdot |\omega - \Omega - a \sin\psi| \right)^{-1} \tag{3.16}$$

$$= \frac{1}{2\pi} \cdot \frac{\sqrt{(\omega - \Omega)^2 - a^2}}{|\omega - \Omega - a \sin\psi|} \tag{3.17}$$

[7] ... in contrast to the Kuramoto-Sakaguchi model, where Q represents the phase delay β, see Sect. 2.1.3.

which yields[8]

$$F = a \int_{-\pi/2}^{\pi/2} \mathrm{e}^{\imath\psi} g(\Omega + a\sin\psi)\cos\psi \mathrm{d}\psi + \int_{-\pi}^{\pi} \mathrm{d}\psi \frac{\mathrm{e}^{\imath\psi}}{2\pi} \int_{|\omega-\Omega|>a} \mathrm{d}\omega\, g(\omega) \frac{\sqrt{(\omega-\Omega)^2 - a^2}}{|\omega - \Omega - a\sin\psi|}$$
$$= \text{synchronous} + \text{asynchronous oscillators} = I_\mathrm{s} + I_\mathrm{as} \tag{3.19}$$

Other than in the two cited derivations, we here assume unimodal but not necessarily symmetric natural frequency distributions, such that Ω in general is different from zero. Before solving the integral over frequencies in Eq. (3.14) for a special frequency distribution, the integral over phases can be solved for arbitrary $g(\omega)$, see Appendix A.1, where we calculate the ψ integrals in I_as. The imaginary part $\Im$ of the synchronous integral can be cast to an integral over ω by parameter transformation. The condition for Ω reads

$$\begin{aligned} 0 &\stackrel{!}{=} -\imath a I_\mathrm{as} + -\imath a \Im(I_\mathrm{s}) \\ &= \int_{a+\Omega}^{\infty} \mathrm{d}\omega\, g(\omega) \left((\omega - \Omega) - \sqrt{(\omega-\Omega)^2 - a^2} \right) \\ &\quad + \int_{-\infty}^{-a+\Omega} \mathrm{d}\omega\, g(\omega) \left((\omega - \Omega) + \sqrt{(\omega-\Omega)^2 - a^2} \right) + \int_{-a+\Omega}^{a+\Omega} (\omega - \Omega)\, g(\omega)\, \mathrm{d}\omega \end{aligned} \tag{3.20}$$

As $g(\omega)$ is positive definite and the weight, i.e. the integration kernel, grows monotonously, Ω is unique (compare Fig. 3.4). While the integrals are general and e.g. valid also for multimodal distributions, the uniqueness of Ω is only guaranteed for unimodal distributions.

Having found the Ω corresponding to a, we can solve the real part $\Re$ of the integral over synchronous oscillators for this pair

$$\Re\left(I_\mathrm{s}\right) = \int_{-a+\Omega}^{a+\Omega} g(\omega) \sqrt{1 - (\omega/a)^2}\, \mathrm{d}\omega = F(\Omega, a) = R \tag{3.21}$$

with $\Re\left(I_\mathrm{s}\right) = F(\Omega, a) = R$, and therefore by $a = \epsilon R$ we find $R(\epsilon)$. The presented scheme finds Ω and $R(\epsilon)$ for arbitrary distributions $g(\omega)$. For graphic representations of the integral kernels, see Fig. 3.4. When an analytical solution of the involved integration and root finding is either not necessary or intractable, this scheme allows for numerical integration as well (see Sections 3.3.2 and 3.4.2).

In the finite case, such a self-consistent approach does not apply. The order parameter varies in time – at a time scale comparable to individual oscillators. The effective decoupling found in the infinite case does therefore not apply in the finite case. However, the minimum of the order parameter R_min (introduced for the detection of a collective mode)

[8] The symbolic form of the asynchronous integral over frequencies means

$$\int_{|\omega-\Omega|>a} \frac{\cdots}{|\omega - \Omega - a\sin\theta|} = \int_{-\infty}^{\Omega-a} \frac{\cdots}{-\omega + \Omega - a\sin\theta} + \int_{\Omega+a}^{\infty} \frac{\cdots}{\omega - \Omega - a\sin\theta}. \tag{3.18}$$

Interestingly, as we will see in more detail in the following sections, the asynchronous integral balances the weighted tails (everything outside the integral $(-a, a)$) of the frequency distribution, while the synchronous integral quantifies the weighted probability mass contained in interval $(-a, a)$ around the mean – frequency Ω simply shifts these integrals left or right, see Fig. 3.4.

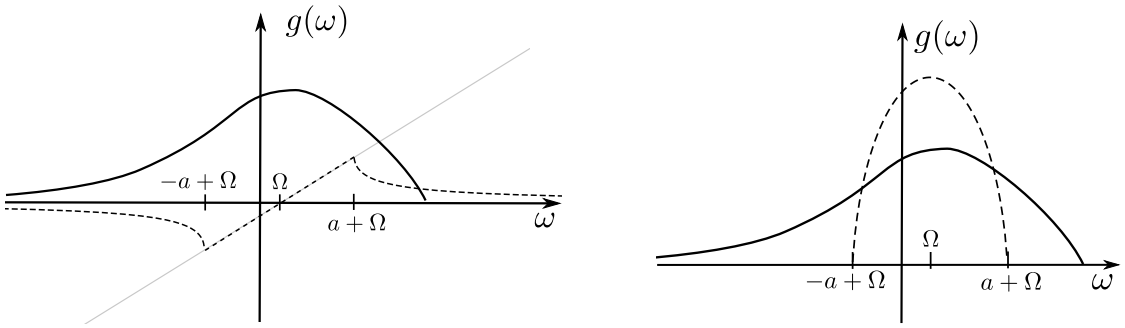

a) imaginary parts of $-aI_{\mathrm{as}}$ and $-aI_{\mathrm{s}}$ **b)** real part of I_{s}

FIG. 3.4: Graphical illustration Eq. (3.20) and of integral $\Re(I_{\mathrm{s}})$ as in (3.21). In both cases, the frequency distribution $g(\omega)$ (solid) is multiplied by a kernel (dashed) and then integrated over the support of the kernel. The thin gray line in 3.4a) marks $\omega - \Omega$. In 3.4a), with given a, Ω is defined as the (unique) frequency shift at which the three terms in Eq. (3.20) cancel each other. For given a and Ω, $R = \Re(I_{\mathrm{s}})$ corresponds to coupling strength $\epsilon = a/R$.

gives us an alternative for characterizing the mean field dynamics depending on the natural frequency distribution.

3.3 The shape of the distribution of natural frequencies determines the route to synchrony $R_{\min}(\epsilon)$

Synchronization is an emergent phenomenon. Macroscopic features result from individual characteristics of microscopic units. In this Section, we show how the transition point and the degree of synchronization at a certain coupling strength relate to the natural frequencies in a finite ensemble. In Fig. 3.1, we observed a strong difference between the two Gaussian samples and the Lorentzian case: the Lorentzian ensemble forms a collective mode, indicated by finite $R_{\min}$, at much smaller coupling than the Gaussian ensemble. On the other hand, much stronger coupling than in the Gaussian case is necessary to reach a constant order parameter, which (as can be concluded from the mean field phase, see Sect. 3.4) corresponds to complete frequency locking.

To understand this observation, let us characterize a typical Lorentzian sample in contrast to a typical Gaussian one: the central peak in the Lorentzian distribution most likely produces many small frequencies. Under the restriction of unit sample variance, this central pack needs to be compensated for by few comparably large outliers, compatible with the fat tails of the underlying distribution. The time scales of the central frequencies and the outliers are well separated. The outliers barely hinder the central oscillators to synchronize. The spread of the central oscillators is small, and weak coupling suffices to synchronize them. They are superior in number compared to the outliers. Their synchronization at weak coupling is directly reflected in a finite $R_{\min}$ at comparably weak coupling. On the other hand, when trying to synchronize all oscillators, much stronger coupling is necessary to include the outliers. As this example shows, the shape of the distribution plays an important role in the synchronization transition.

Former studies indicated a connection between the shape of the natural frequency distribution and the transition to synchrony. Kuramoto noted already in [Kur84] that

uni-modal frequency distributions with non-vanishing second-order derivative at the maximum have a second-order phase transition, i.e. the order parameter is a smooth function of coupling strength at the critical point. Diego Pazó was the first[9][10] to investigate the non-hysteretic first order phase transition in Kuramoto ensembles with uniform frequency distribution [Paz05]. [BU07] correctly linked this property to the vanishing derivative at the maximum over a sufficiently large interval and thereby extended the class of frequency distributions with first-order transition to all distributions with a sufficiently flat maximum, which they call plateau. In [BU08], the same authors investigate asymmetric triangular distributions with and without flat top and observe the same effect of flat tops. [Cra94, MBS+09b] studied bi-modal frequency distributions, constructed as two Lorentzian distributions with the same scale (half-width at half-maximum) but different center frequencies. They find a parameter region with standing waves that in small regions coexists with the partially synchronized state in the bifurcation diagram. This so called Crawford state corresponds to locking within the two groups at two different frequencies. [PM09] found hysteresis in such bi-modal distributions when the central dip between the two maxima becomes sufficiently small. [TIAY17] find an even richer bifurcation diagram, e.g. with traveling waves, for different heights of the two Lorentzians and therefore asymmetry of the distribution. More surprising scenarios can be found e.g. by including a Kuramoto-Sakaguchi phase [OW12], where the order parameter decreases with increasing coupling strength for a clever choice of frequency distribution and phase delay. We generalize in this section the shape dependence of the transition in unimodal distributions (without such phase delay).

Shape in the above discussed sense of either peakedness combined with heavy tails or uniformity is well captured by the fourth moment, called kurtosis β_2. [BM88] interpret kurtosis " vaguely [...] as the location- and scale-free movement of probability mass from the shoulders of a distribution into its center and tails." The term *vaguely* refers to the fact that distributions with the same kurtosis can still have tremendously different shape. The last part of their definition, "movement of probability mass from the shoulders of a distribution into its center and tails", dispels former misinterpretations as "the lack of shoulders" or multi-modality and ends up being exactly what we want to describe, compare above Lorentzian example compared to the Gaussian one. The measure is location- and scale-free in that it is centered around the mean and normalized by the variance of the distribution:

$$\text{kurtosis} \qquad \beta_2 = \langle \omega_i^4 \rangle \langle \omega_i^2 \rangle^{-2}. \tag{3.22}$$

Regarding kurtosis, the Gaussian distribution with $\beta_2 = 3$ serves as a reference, leading to the definition of excess kurtosis

$$\text{excess kurtosis} \qquad \gamma_2 = \beta_2 - 3. \tag{3.23}$$

Distributions or samples with positive excess kurtosis, called *leptokurtic* distributions, typically have fat tails and a central peak. *Platykurtic* distributions with negative excess kurtosis resemble more the uniform distribution. The Gaussian distribution, and others with $\gamma_2 \approx 0$, are called mesokurtic.[11]

[9] Note that Winfree observed "explosive" synchronization, i.e. a first-order transition, for flat frequency distributions in the already in [Win67], in the last lines of the Appendix. In [Win80] he already generalizes this statement to flat-topped distributions, see Box on p. 115 therein.

[10] The term "explosive" synchronization is used in both contexts: synchronization due to a certain relation between node degree and frequency in that node in networks of Kuramoto oscillators [GGnGAM11] or due to a plateau in the distribution of natural frequencies [Paz05].

[11] In [Stu27], the two extremes of platykurtic and leptokurtic are illustrated as a mnemonic aid. Platypues with their chubby physique and short tail resemble distributions whose main probability mass is concentrated around the mean, i.e. platykurtic distributions. Leptokurtic distributions in contrast, with

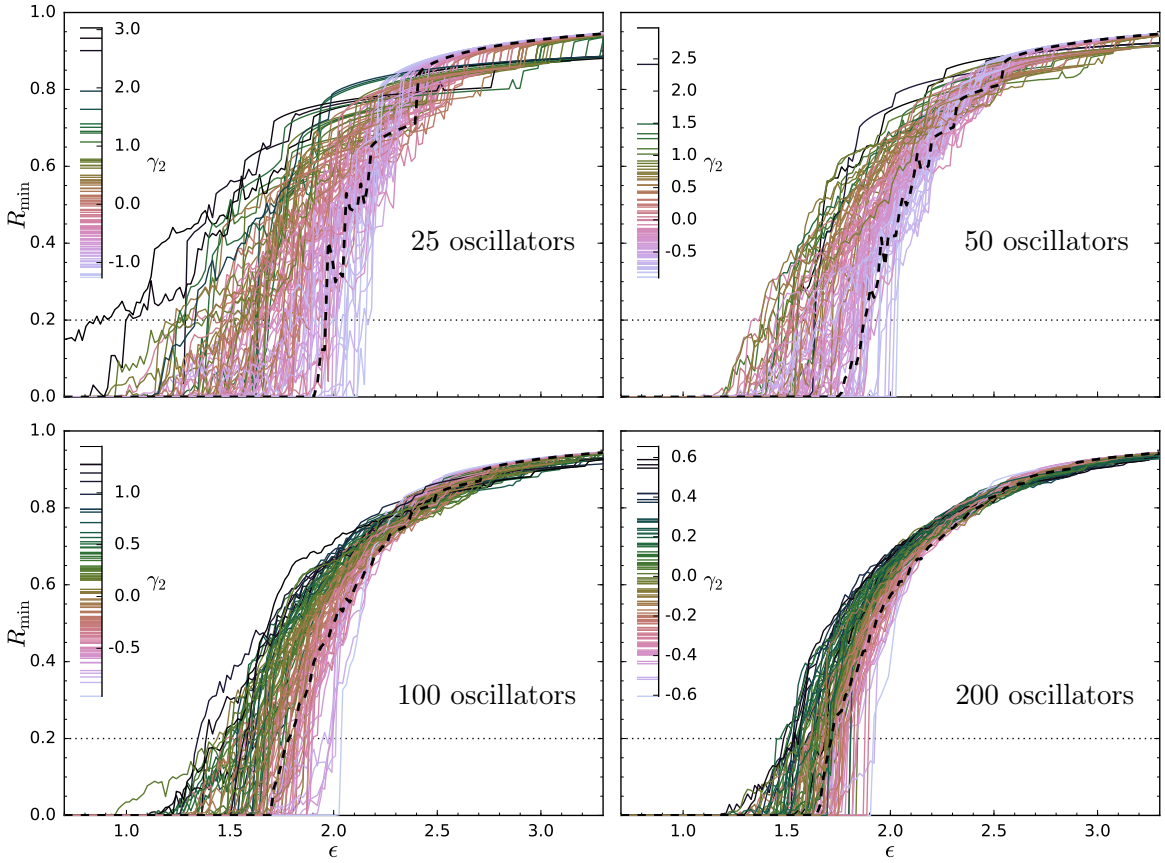

FIG. 3.5: Dependence of $R_{\min}$ on ϵ: Each panel shows results for 100 random samples of a Gaussian frequency distribution, for $N = 25, 50, 100, 200$. The curves are color-coded according to their respective excess kurtosis γ_2. Note that the range of γ_2 differs considerably between the panels. The black dashed line stems from regular sampling. The dotted black line marks the cut at $R_{\min} = 0.2$, at which the spread presented in Fig. 3.7 is measured.

With this knowledge, we now compare the transition to synchronization for different samples of the Gaussian. The sampling distribution of the kurtosis of the Gaussian has a wider spread for small sample sizes, so we naturally come across a considerable diversity of shapes for sample sizes of circa 50 oscillators, e.g. excess kurtosis γ_2 ranges from $\sim -1.$ to $\sim 3.$ in Fig. 3.5 top right panel.

3.3.1 Effect of kurtosis of natural frequency samples in finite ensembles

The introductory discussion and the observations made in Fig. 3.1 result in the hypothesis that the kurtosis of the natural frequency sample and the coupling strength dependence of the synchronization transition are correlated. We make use of the above discussed alternative order parameter $R_{\min}$ to track the emergence and coherence of the collective mode.

In the first experiment, we compare $R_{\min}(\epsilon)$ for 100 random samples and the regular sample (compare Sect. 3.0) of a Gaussian natural frequency distribution for each of four sample sizes $25, 50, 100, 200$. This means calculating time series of length $t = 10^5$ after a

their central peak but heavy tails, the author compares to two facing kangaroos with their heavy tails and upright posture. The author of this publication is "Student", also known as William Sealy Gosset was the inventor of the Student's t-test and a friend of Pearson and Fisher.

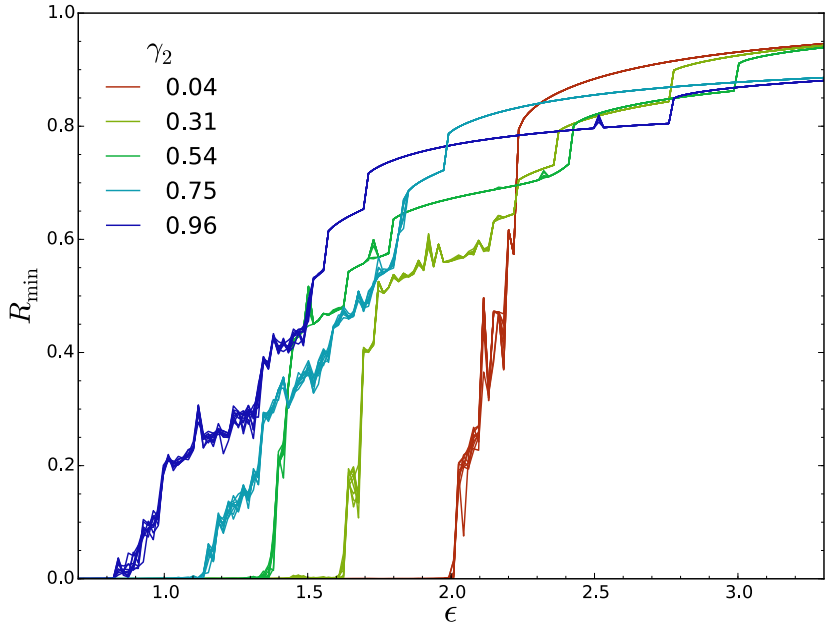

FIG. 3.6: $R_{\min}(\epsilon)$ for 10 different initial conditions but the same natural frequency sample. The non-monotonicity of $R_{\min}(\epsilon)$ could be linked to the effective multi-modality of finite ensembles and resulting multi-stability and hysteresis, compare [PM09]. Approximately starting at $R_{\min} \approx 0.6$, all curves from one frequency sample perform collective jumps to higher values of $R_{\min}$.

transient $t = 10^2$ for each frequency sample and coupling strength and evaluating $R_{\min}$ over time. The results are presented in Fig. 3.5.

The colors, going from bright for leptokurtic to dark for platykurtic, indicate a negative kurtosis-gradient in ϵ-direction for small $R_{\min}$. Leptokurtic samples who have typically many very small frequencies and few comparably large outlier frequencies form a collective mode at comparably weak coupling. Platykurtic samples that are rather flat but therefore confined to a smaller frequency interval achieve sufficient coherence to form a collective mode only at comparably strong coupling but then suddenly jump to high values of $R_{\min}$. For large $R_{\min}$, i.e. at strong coupling, the relation reverses: The strong outliers in the leptokurtic samples resist up to strong coupling against inclusion into the synchronized cluster, while platykurtic samples are completely locked at much lower coupling strength.

Let us shortly note some further observations from this figure. Non-monotonicities in individual curves partially stem from the finite measurement time of the minimum of the order parameter; as we saw, the waiting times between updates of the minimum become longer with time. An other reason might be the effective multi-modality of the finite frequency sample, with the above mentioned hysteresis. Additional tests show that the spread of $R_{\min}$ varies between different initial conditions, depending on the coupling strength (see Fig. 3.6). Further experiments are necessary to clarify this point.

Fig. 3.3 hinted to an effect that is now repeated for all frequency samples in Fig. 3.5. At stronger coupling strengths, the minimum of the order parameter jumps abruptly to a higher value (as we see in Fig. 3.6, these jumps are independent of the initial condition). The mean observed frequencies in Fig. 3.3a) show that these jumps stem from single or few oscillators that join the synchronized cluster. Still, the system of one large synchronized cluster and single asynchronous oscillators can be weakly chaotic, as the single oscillators perturb the collective mean field [Bar13]. A lower bound to the critical coupling strength

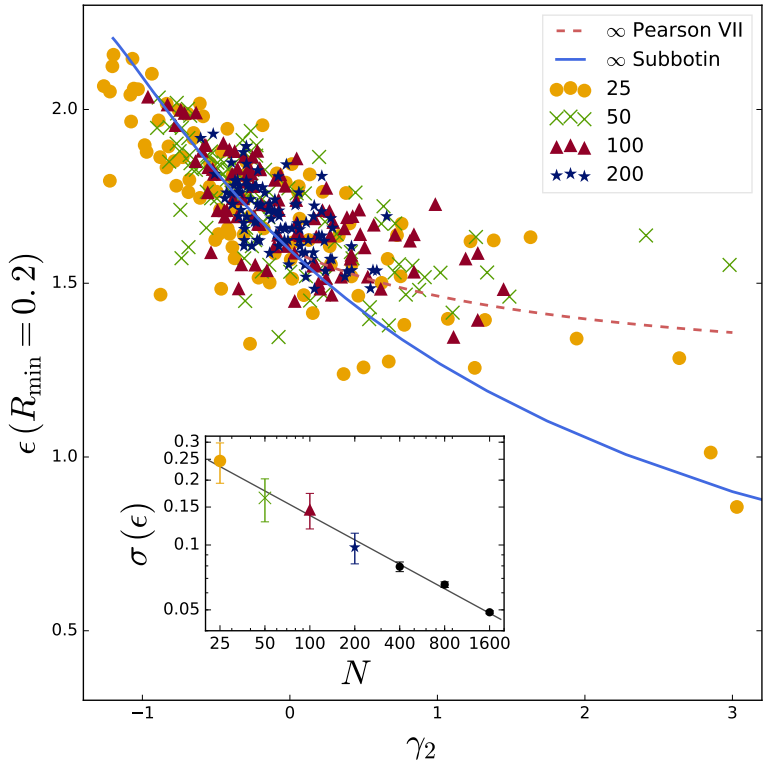

FIG. 3.7: Coupling strength at the level $R_{\min} = 0.2$ vs. sample kurtosis of the respective $g(\omega)$-sample; the same data as in Fig. 3.5. Solid (blue) and dashed (flamingo) lines give predictions from numerical integration of Eq. (3.21) for two families of distributions with kurtosis as a parameter, Subbotin and Pearson, respectively (see Sect. 3.3.2). Inset: Scaling of the standard deviation of ϵ corresponding to $R_{\min} = 0.2$ with the number of oscillators N; linearly fitted by power law $\sigma(\epsilon(R_{\min} = 0.2)) \approx N^{-0.38}$.

at which all oscillators lock (which always exists in finite samples, as their support is always bounded) was given in [VM07]. [Erm85] presented the critical width of different distributions in the infinite limit under which, assuming $\epsilon = 1$, the partial synchrony solution bifurcates from the incoherent branch. For the finite equidistant case [OLS16] derived the exact critical width, as well assuming $\epsilon = 1$.

To find the relation between the coupling strength for a certain $R_{\min}$ and the sample kurtosis of the respective natural frequency sample, we cut through all the curves at $R_{\min} = 0.2$ and plot the corresponding coupling strength (weighted between coupling strengths of the pair of closest $R_{\min} \lessgtr 0.2$) against excess kurtosis γ_2, see Fig. 3.7. The distribution of points in the figure shows a clear tendency: The smaller the kurtosis (i.e. the more comparable to a uniform distribution[12]), the larger the coupling strength necessary to form a collective mode. For $N = 25$, the spread of the cloud of points is large in both directions, because of the large spread also of higher moments (and therefore compatibility of the samples with a larger variety of underlying distributions). As sample size increases, the spread in kurtosis – and thereby the spread of coupling strengths at which $R_{\min} = 0.2$ – decreases (see inset of the figure). The cloud eventually collapses into a point, because in the infinite limit, $\gamma_2 = 0$ and $R(\epsilon = 0.2)$ is unique for the Gaussian distribution.

To check our hypothesis also in the infinite limit, we need a family of distributions, in which kurtosis is a parameter. We find two quite natural families and evaluate their

[12]We discuss the finite equidistant natural frequency sample in more detail in Chap. 4. The uniform distribution in the infinite case is analytically soluble in all details, see following Sect. 3.3.2.

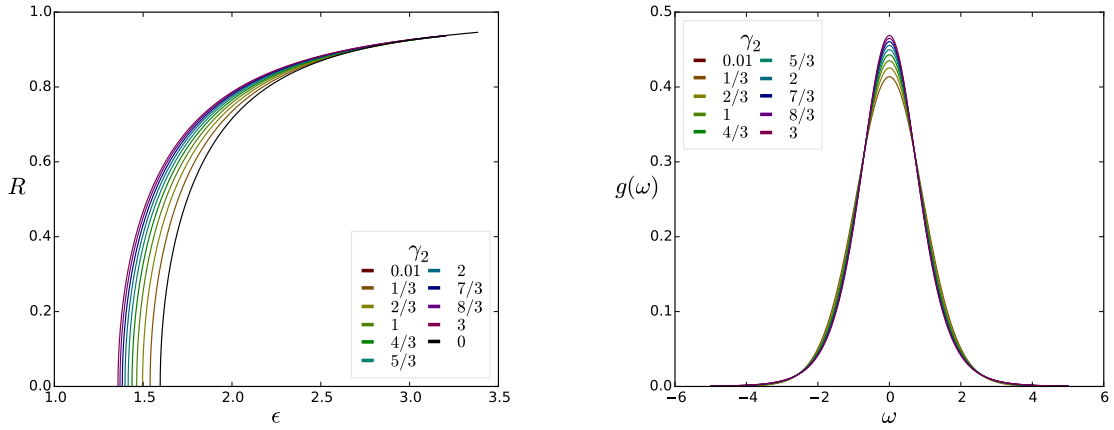

a) Self-consistent coherent solutions $R(\epsilon)$. **b)** Pearson VII frequency distributions.

FIG. 3.8: Numerical solution of the self-consistency integral for Pearson VII family members with different kurtosis. The kurtosis ranges from high, (violet; left in **a)**, top maximum in **b)**), to low kurtosis (red; right in **a)**, lowest maximum in **b)**). The analytical solution for $\gamma_2 = 0$ is given in black. Note that $\gamma \geq 0$ in this family.

$R(\epsilon)$ dependence in the next section. We juxtapose the results from finite samples and the infinite limit in Fig. 3.7. For larger numbers of oscillators N_{osc}, we use a computationally more efficient procedure, see App. B.1.

3.3.2 Effect of kurtosis of natural frequency distribution in the thermodynamic limit

We now show that the observed kurtosis dependence of the $R(\epsilon)$ relation is not a genuine finite-size effect. Above, we solved the self-consistency equation for a Gaussian distribution of natural frequencies, the result for a Lorentz distribution is known from the literature, see Sect. 2.1.3. Another frequency distribution that allows for in that case complete analytic solution is the uniform distribution that we treat as a special case of one two families of distributions, in which kurtosis is a parameter. For all these cases of symmetric distributions it suffices to integrate Eq. (3.21) with $\Omega = 0$.

We now dicuss two families of distributions with adjustable kurtosis. The Pearson family of distribution of type VII is part of Pearson's system of distributions that was constructed exactly for the purpose of having skewness and kurtosis as parameters. Members of the family VII are symmetric distributions with mean zero. For symmetric distributions, asymmetry integrals (Eq. (3.20)) cancel at $\Omega = 0$, which simplifies Eq. (3.21). Under two assumptions, the distributions possess the first four moments, allowing us to fix mean and variance and to vary kurtosis for their comparison. The probability densities

$$f(x; o, m) = \frac{\Gamma(m)}{o\sqrt{\pi}\Gamma(m - \frac{1}{2})}\left[1 + \left(\frac{x}{o}\right)^2\right]^{-m} \tag{3.24}$$

(with Gamma function $\Gamma(\cdot)$) have shape parameter m and scale o. For the kth moment to be defined, one needs $m > k + 1/2$, thus for kurtosis to be defined, we need $m > 5/2$. To obtain unit variance, we set $o^2 = 2m - 3$. m defines excess kurtosis γ_2 via $m = \frac{5}{2} + \frac{3}{\gamma_2}$. For $\gamma_2 \to 0$, the distribution converges to the standard normal distribution $\mathcal{N}(0, 1)$. For $\gamma_2 \to \infty$, the distribution converges to $g(x) = 3\,(2 + x^2)^{-\frac{5}{2}}$. The Pearson family VII,

symmetric around mean zero with unit variance and kurtosis $\gamma_2 = 3/(m - 5/2)$ reads

$$f(x;m) = \frac{\Gamma(m)}{\sqrt{2m-3}\sqrt{\pi}\Gamma(m-\frac{1}{2})}\left[1+\frac{x^2}{2m-3}\right]^{-m}. \tag{3.25}$$

Note that the family is purely leptokurtic, i.e. $\gamma_2 \geq 0$.

The self consistency equation as in Eq. (3.21) for this family of distributions and $a := \epsilon R$ reads

$$R = \frac{a\Gamma(m)}{\sqrt{2m-3}\sqrt{\pi}\Gamma\left(m-\frac{1}{2}\right)} \int_{-\frac{\pi}{2}}^{\frac{\pi}{2}} \left[1+\frac{a^2\,\sin^2\theta}{2m-3}\right]^{-m} \cos^2\theta\,\mathrm{d}\theta. \tag{3.26}$$

Apart from $\gamma_2 = 0$, we solve these integrals numerically for different m, see Fig. 3.8.

A much less known yet all the more natural family of distributions that ranges from platykurtic to leptokurtic members is the Subbotin distribution, also referred to as stretched exponential. It has three parameters μ, σ_p and p, with which mean, variance, and kurtosis can be set.

The general Subbotin distribution has the form [Chi00]

$$p(x) = \frac{1}{2\sigma_p p^{1/p}\Gamma(1+\frac{1}{p})}\exp\left[-\frac{|x-\mu|^p}{p\,\sigma_p^p}\right] \tag{3.27}$$

where μ is the mean value, and $\sigma_p > 0$ and $p > 0$ are shape parameters. The kurtosis is given by

$$\beta_2 = \frac{\mu_4}{\mu_2^2} = \Gamma\left(\frac{1}{p}\right)\,\Gamma\left(\frac{5}{p}\right)\Big/\left[\Gamma\left(\frac{3}{p}\right)\right]^2. \tag{3.28}$$

and excess kurtosis follows from $\gamma_2 = \beta_2 - 3$. Calculations are given in App. A.2. We leave mean at zero and scale variance to one and obtain the centered standardized Subbotin family suitable for our model

$$g(\omega;p) = \left[2\,\sigma_p\,p^{1/p}\,\Gamma(1+1/p)\right]^{-1}\cdot\exp\left(-\frac{|\omega|^p}{p\,\sigma_p^p}\right), \tag{3.29}$$

Leptokurtic members correspond to $0 < p < 2$, platykurtic are distributions with $p > 2$. $p = 1$ corresponds to the Laplace distribution, $p = 2$ to the Standard Normal distribution, for $p \to \infty$, $p(x)$ converges to the uniform distribution. For some of these special cases, the self-consistency approach gives analytical solutions for the order parameter, either explicitely or implicitely. We saw in the preceding section that for the Gaussian case with $p = 2$, the self-consistent solution is expressed via Bessel functions. For $p = 0$, $g(\omega;p)$ converges to the (normalized) δ-Distribution whereby the non-trivial self-consistent solution reads $R = 1$, i.e. unsurprisingly perfect phase locking or complete incoherence are the two only solutions for identical oscillators, independent of the coupling strength (which in that case merely scales the transient time before reaching full synchrony).

For $p \to \infty$, the Subbotin distribution converges to a uniform distribution, $g(\omega) = h$ for $|\omega| < \omega_{\max}$, $g(\omega) = 0$ else, with height $h = 1/(2\sqrt{3})$. Normalization sets $\omega_{\max} = \sqrt{3}$. The kurtosis converges to $\gamma_2 = -1.2$:

$$\lim_{p\to\infty}\beta_2 = \lim_{p\to\infty}\frac{\Gamma\left(\frac{1}{p}\right)\Gamma\left(\frac{5}{p}\right)}{\left(\Gamma\left(\frac{3}{p}\right)\right)^2} = \lim_{p\to\infty}\frac{\frac{p}{1}\Gamma\left(1+\frac{1}{p}\right)\frac{p}{5}\Gamma\left(1+\frac{5}{p}\right)}{\left(\frac{p}{3}\Gamma\left(1+\frac{3}{p}\right)\right)^2} = \frac{9}{5} \tag{3.30}$$

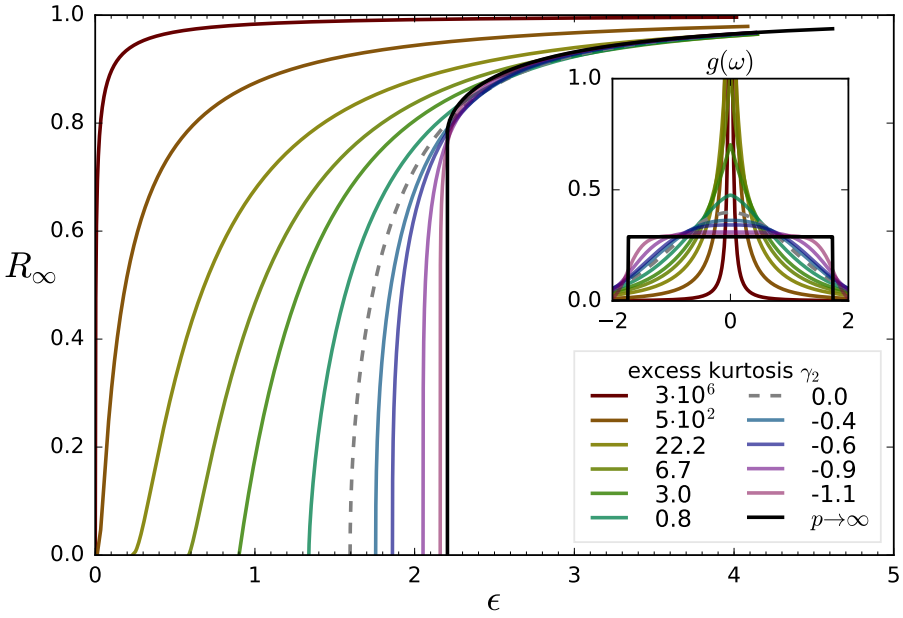

FIG. 3.9: Kurtosis-dependence of $R(\epsilon)$: We numerically integrate the self-consistent Eq. (3.21) with $\Omega = 0$ for the Subbotin family of frequency distributions, see Eq. (3.29). The integral for the uniform distribution stems from the analytical solution, see Eq. (3.33) with $\omega_{\max} = \sqrt{3}$. The curves (from left to right) correspond to values of the parameter $p = 0.1, 0.25, 0.5, 0.75, 1, 1.5, 2, 2.5, 3, 5, 10$ and to the uniform distribution with $p \to \infty$ (or likewise to the excess kurtosis values as given in the legend). The inset shows the respective probability densities.

and thus $\gamma_2 = \beta_2 - 3 = -1.2$, where we used that $\Gamma(1+z)$ converges to 1 for $z \to 0^+$.

In this limit case, we can find a parametric solution for $R(\epsilon)$ from the self-consistency equation. In the integral, we need $g(a \cdot \sin\theta)$ instead of $g(\omega)$, which is just $g(a \cdot \sin\theta) = \frac{1}{2\sqrt{3}}$ for $|\theta| \leq \arcsin\frac{\sqrt{3}}{a}$, zero else.

Then the self-consistency integral reads

$$R = \frac{a}{2\sqrt{3}} \cdot \frac{1}{2}\Big(x + \underbrace{\sin x \cos x}_{\frac{1}{2}\sin(2x)}\Big)\Big|_{x=-\min(\pi/2,\arcsin(\frac{\sqrt{3}}{a}))}^{x=\min(\pi/2,\arcsin(\frac{\sqrt{3}}{a}))} \tag{3.31}$$

If $\frac{\sqrt{3}}{a} \geq 1$, then

$$R = \frac{a}{2\sqrt{3}} \cdot \frac{1}{2}(\pi + 0) \Rightarrow \begin{cases} R = 0 \\ R \neq 0 \end{cases} \Rightarrow \epsilon = \frac{4\sqrt{3}}{\pi} \quad \Rightarrow \quad R = \frac{a}{\epsilon} \leq \frac{\pi}{4} \tag{3.32}$$

which means that at $\epsilon_c = \frac{4\sqrt{3}}{\pi}$, R can take all values between 0 and $\frac{\pi}{4}$. If on the other hand $\arcsin(\frac{\sqrt{3}}{a}) < \frac{\pi}{2}$, then

$$R = \frac{a}{2\sqrt{3}} \arcsin(\frac{\sqrt{3}}{a}) + \frac{1}{2}\sqrt{1 - \frac{3}{a^2}}, \tag{3.33}$$

that means $R < 1$ at any finite coupling strength. At ϵ_c, where R reaches $\pi/4$ we have that $\pi\epsilon_c/4 = \omega_{\max} = -\omega_{\min}$. This means that at the critical coupling strength, the ensemble already completely locks their frequencies.

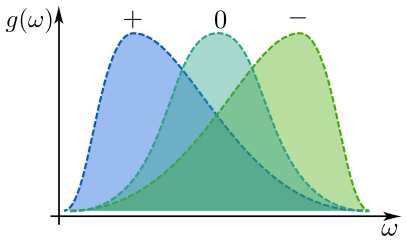

FIG. 3.10: Typical examples of frequency distributions with positive (heavier tail to the right), zero (symmetrical), and negative (heavier tail to the left) skewness.

For all other values of p, we solve Eq. (3.21) numerically for $\Omega = 0$. We solve the integral for different a and then plot $F(0, a)$ against $a/F(0, a)$, i.e. R against ϵ. The results are presented in Fig. 3.9. In the range of kurtosis of Fig. 3.5, results from finite ensembles and thermodynamic limit roughly coincide.

To conclude, the dependence of the order parameter on the coupling strength is mainly determined by the shape of the natural frequency distribution, both in finite and infinite ensembles.

3.4 The asymmetry of the natural frequency distribution drives the global phase

In Fig. 3.1, we observed a crucial difference in the super-critical (w.r.t. $R_{\min}$) time evolution of the complex order parameter between ensembles with random or regular natural frequency samples, respectively. The numerical experiments on the finite system in this and the analytical derivations in the next section show that the reason lies in the symmetry of the frequency sample (or distribution). As the mean of the samples is rotated to zero, one might, at first glance, expect that the mean field could fluctuate but that the mean field phase should have no drift.

The following calculations and numerical experiments in contrast show that the symmetry of the natural frequency distribution is of fundamental importance for the dynamics of the global phase in the regime of partial synchrony.

Asymmetry of probability distributions is reflected in all odd higher moments, starting with the third. As the higher moments are harder to estimate for small samples, we restrict our studies to this lowest moment[13] reflecting symmetry, called skewness.

$$\text{skewness} \qquad \gamma_1 = \langle \omega_i^3 \rangle \langle \omega_i^2 \rangle^{-3/2} \tag{3.34}$$

The above Fig. 3.10 is a quick reminder of what positive and negative skewness typically mean. Like all higher moments, the interpretation of skewness requires caution. The matter is simplified notably here, as we restrict our considerations to distributions and samples similar to the Gaussian distribution, i.e., approximately unimodal distributions[14] with exponentially decaying tails. With these two simplifications, a distribution or sample is positively (negatively) skewed, if the tail to right (left) is longer and heavier than that to the left (right) and, in most cases, the distribution seems to lean to the left (right).

[13] Shifting the mean to zero in all finite or infinite experiments and calculations in this chapter, there is no need to distinguish between central moments and moments about zero. Likewise, as the standard deviation is set to one, the moments we calculate are by construction normalized moments.

[14] Finite samples of unimodal distributions might be compatible with an interpretation as mixtures of two (or more) unimodal samples with different mean, i.e., be bi- (or multi-) modal. This effect is more likely for small samples.

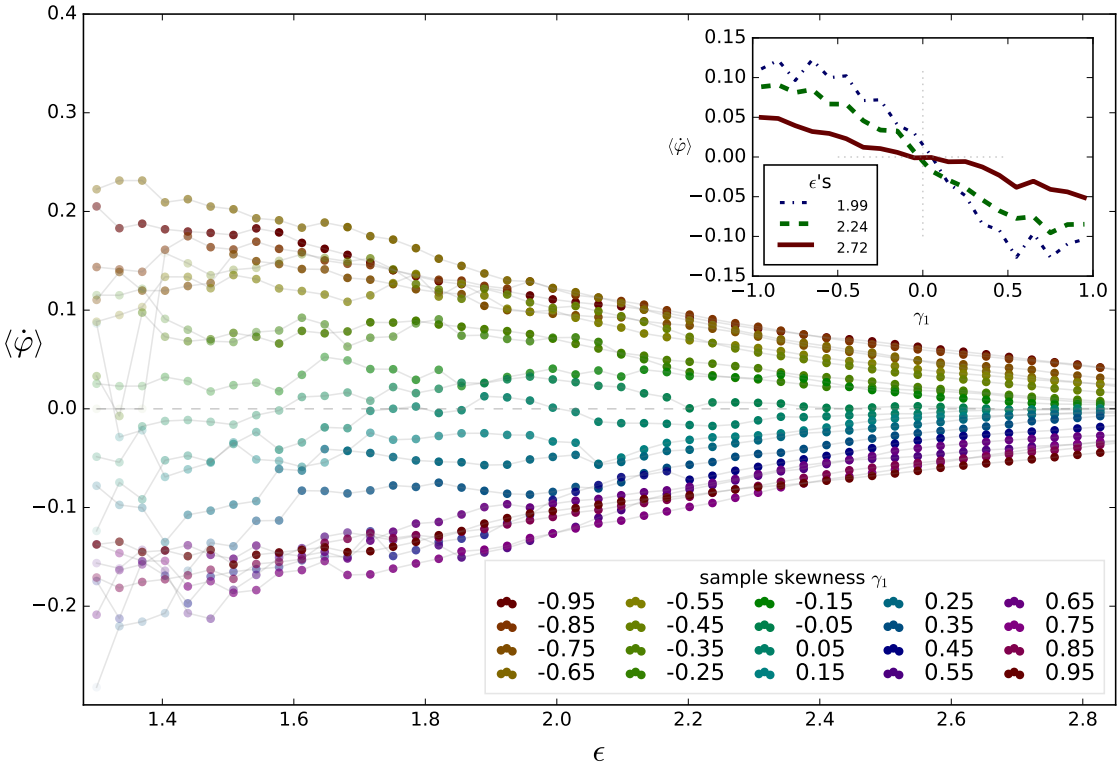

FIG. 3.11: Macroscopic phase $\Omega = \langle\dot{\varphi}\rangle$ for $N = 50$ oscillators versus coupling strength ϵ. Different colors indicate different sample skewnesses: from top $\gamma_1 = -0.95$, to bottom $\gamma_1 = 0.95$. Each chain of dots represents the mean over up to 20 phase velocities of distribution samples with the same ($\pm 10^{-5}$) skewness. The relative number of samples with $R_{\min} > 0.1$, i.e., for which a collective mode is actually defined at a given ϵ, increases with coupling strength, which we reflect in decreasing transparency. The frequencies are calculated by averaging over the time interval 10^3. The inset shows cuts through the main picture at three different values of ϵ: phase velocity vs. skewness.

Following the same order as in the former section that linked the shape of the natural frequency distribution to the curve of $R(\epsilon)$, we start with numerical findings in finite ensembles. Then we compare the findings with a family of distributions with tuneable asymmetry in the thermodynamic limit.

3.4.1 Effect of skewness of natural frequency distribution in finite ensembles

Regular samples, such as the one defined in Sect. 3.0, can be useful, e.g. for the comparison of different sample sizes. Chosen cleverly, such regular samples can circumvent the necessity of large statistics by generating an in the best case typical sample that captures most of the effects of interest in a representative way. The regular sample we described in Sect. 3.0 produces the first four moments fairly well, see table below Fig. 3.1, but panels a) and b) of the same figure show that the resulting dynamics crucially differs from the dynamics emerging in random samples. Above critical coupling w.r.t. $R_{\min}$, the global phase in a regular ensemble converges to a constant, in contrast to typical random samples for which we see a rotation of the mean field and persistent fluctuations of the global phase. The asynchronous self-consistent integrals Eq. (3.20) vanish for symmetric $g(\omega)$, i.e. the global phase assumes a constant value as well.

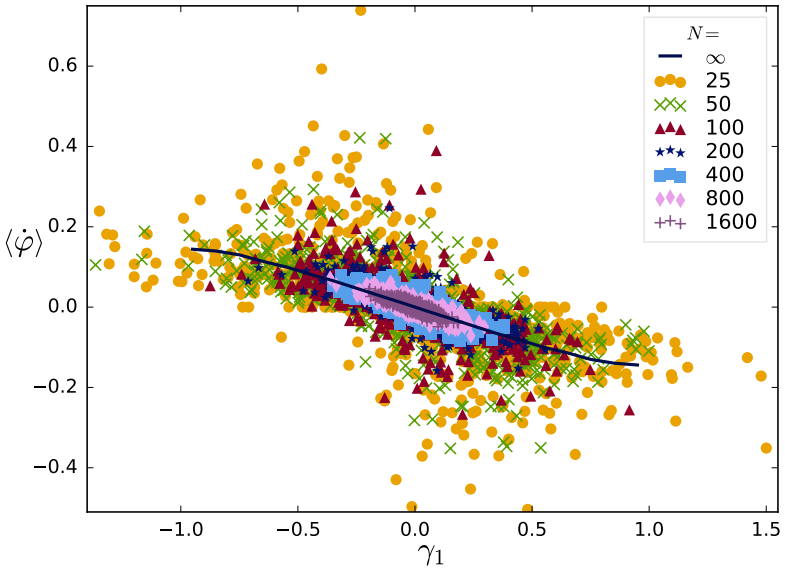

FIG. 3.12: Average frequencies of the mean field vs. skewness of the frequency sample for different ensemble sizes. The continuous curve stems from the numerical integration and root-finding in self-consistency Eq. (3.20) for skew-normal distributions with different skewness parameters α. Each marker shape corresponds to one ensemble size, for each of which 1000 samples of a Gaussian with mean zero and variance one are generated randomly. For each sample, the time evolution of φ at $\epsilon = 2$, performed over $t = 10^3$ plus 10^3 transient, gives $\langle\dot{\varphi}\rangle$ represented by one point in the plot.

To investigate the relation between asymmetry of the frequency sample and the resulting global phase dynamics further, we create skewed natural frequency samples and record their average observed mean field frequency. Therefore, we generate millions of Gaussian random samples of sample size 50 until we have 20 samples for each of 20 target sample skewnesses. That means, we find for each target skewness 20 samples close ($\pm 10^{-5}$) to this target skewness. For each of the 400 samples and for each of 50 super-critical coupling strengths, the time evolution is recorded after a transient of 10^2 time units. The observed frequencies are obtained from the unwrapped global phases' time evolution by linear regression. We then average over the 20 observed frequencies for each target skewness, thereby also averaging out other sampling effects such as varying kurtosis. The results are depicted in Fig. 3.11. The observed mean field frequencies have their largest value at small coupling strengths. An inset shows the profile of the observed mean field frequency over the skewness of the frequency sample at three different coupling strengths. The global frequency is roughly proportional to minus the sample skewness.

In a second experiment, we freely sample 1000 random Gaussian samples (without picking sample skewnesses and without averaging) for each of 7 ensemble sizes and plot the relation of observed mean field frequency in this sample against sample skewness. The coupling strength $\epsilon = 2$ is super-critical for all samples. Unsurprisingly, the spread of the cloud of points decreases with ensemble size, and would shrink to a point at $(0, 0)$ in the infinite limit. We also compare the results with solutions of the self-consistency equation in the thermodynamic limit for a family of distributions in which skewness is a parameter, where we observe a similar tendency.

To conclude, we observe that the global phase dynamics depends strongly on the symmetry of the natural frequency sample. Negatively skewed samples rotate in mathematically positive sense and vice versa. We now check this relation for the infinite case.

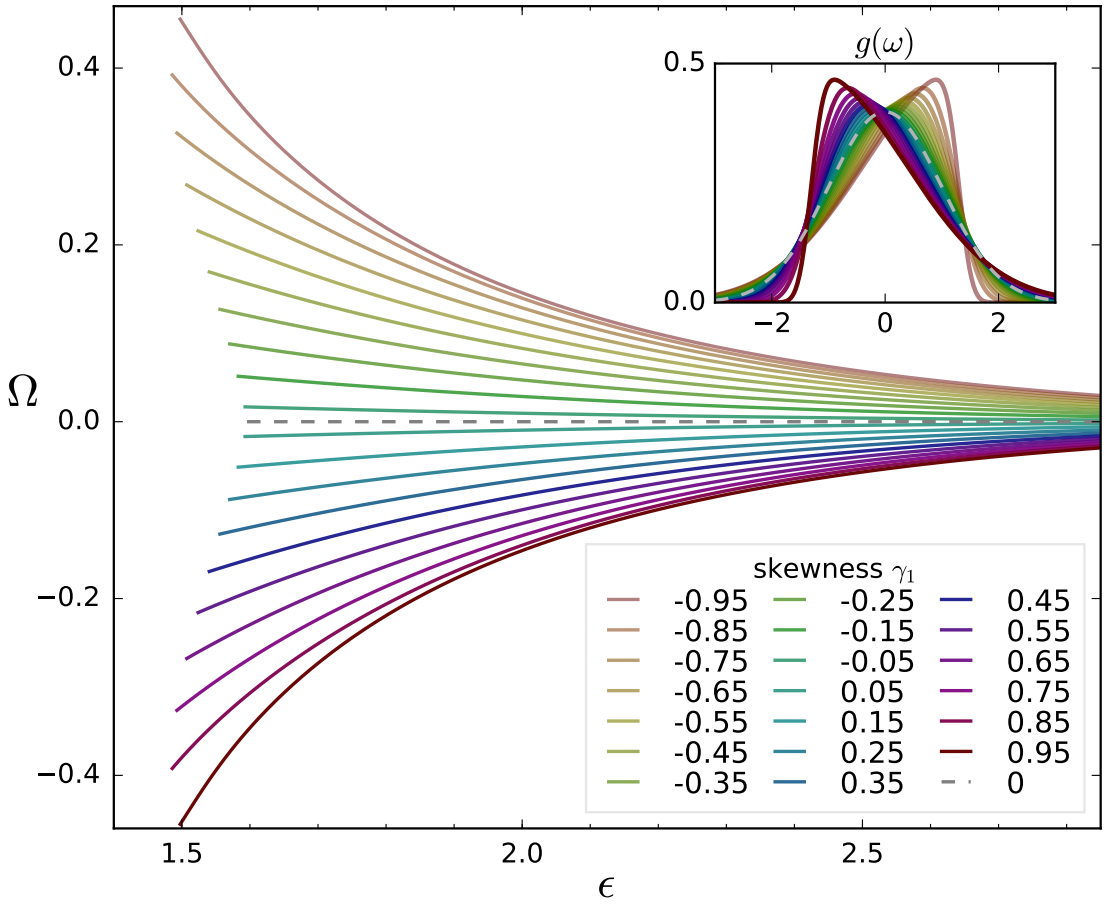

FIG. 3.13: Frequency of the macroscopic oscillations Ω for skew normal distributions as in Eq. (3.35), obtained by solving the self-consistency relation Eq. (3.20) for skewness from top $\gamma_1 = -0.95$ to bottom $\gamma_1 = 0.95$ against coupling strength $\epsilon \geq \epsilon_c$. The distributions are depicted in the inset.

3.4.2 Effect of skewness of $g(\omega)$ in the thermodynamic limit

With the framework we developed in Sec. 3.2.2, a family of distributions with asymmetry as parameter extends our findings from finite samples to infinite ensembles – similar to how we proceeded in Sec. 3.3.2 for the kurtosis. A natural choice is the family of skew normal distributions, [Azz13][15],

$$g(\omega) = \frac{1}{\sqrt{2\pi}\sigma} \mathrm{e}^{-\frac{(\omega-\mu)^2}{2\sigma^2}} \left[1 + \mathrm{erf}\left(\frac{\alpha(\omega-\mu)}{\sqrt{2}\sigma}\right)\right] \tag{3.35}$$

where erf is the error function[16] and α quantifies asymmetry. The Gaussian distribution corresponds to $\alpha = 0$ and positive (negative) α corresponds to positive (negative) skewness. The inset of Fig. 3.13 depicts members of this families with different α's and therefore different skewnesses γ_1. Mean and variance are additional parameters which we choose to

[15] Not the original but without doubt the most extensive publication on skew normal distributions.

[16] For numerical purposes or even for some analytical tricks, it might be useful to replace the error function (erf) by the tangens hyperbolicus (tanh).

be zero and one, respectively:

$$\mu + \sigma\delta\sqrt{\frac{2}{\pi}} \stackrel{!}{=} 0 \quad \text{and} \quad \sigma^2\left(1 + \frac{2\delta^2}{\pi}\right) \stackrel{!}{=} 1 \quad \text{where} \quad \delta := \frac{\alpha}{\sqrt{1+\alpha^2}}. \tag{3.36}$$

Therefore, with $\tilde{\delta} := 2\delta^2/\pi$,

$$\mu \stackrel{!}{=} -\mathrm{sgn}(\alpha)\sqrt{\tilde{\delta}/(1+\tilde{\delta})} \quad \text{and} \quad \sigma \stackrel{!}{=} 1/\sqrt{1+\tilde{\delta}}. \tag{3.37}$$

Skewness γ_1 already depends merely on α:

$$\gamma_1 = \mathrm{sgn}(\alpha)\frac{4-\pi}{2}\left(\frac{\tilde{\delta}}{1-\tilde{\delta}}\right)^{3/2}. \tag{3.38}$$

By inverting this formula, we generate the same target skewnesses as in the finite-size numerical experiment, see preceding Sect. 3.4.1. Kurtosis differs only slightly for different α.

In comparison to the self-consistent solution for the Subbotin family of distributions in Sec. 3.3.2, any family of skew distributions requires one additional calculation step. First, we need to find Ω such that the imaginary part of the self-consistency equation vanishes, see Eq. (3.20). (The corresponding integrals are hard to solve, and we turn to numerical integration.) We apply the Newton bisection method for the root finding, using the derivative of Eq. (3.35):

$$g'(\omega) = -\frac{\omega-\mu}{\sigma^2}\,g(\omega) + \frac{1}{\pi\sigma}\mathrm{e}^{-\frac{1+\alpha^2}{2}\left(\frac{\omega-\mu}{\sigma}\right)^2}. \tag{3.39}$$

With these preparations, we first find Ω for different $a = \epsilon R$ such that Eq. (3.20) is fulfilled. With the resulting pair (a, Ω), we integrate Eq. (3.21) to obtain $R(a, \Omega)$ and thereby $\Omega(\epsilon)$.

Fig. 3.13 displays the same tendency as Fig. 3.11. The curves for each target skewness start at the respective critical coupling strength; the difference in these critical couplings reflects on the variation in kurtosis among the distributions. Negatively skew ensembles rotate in mathematically positive direction and vice versa. The absolute global frequency increases with increasing absolute skewness and decreases with increasing coupling strength. Note that Ω at ϵ_c is not necessarily the frequency at the maximum of the distribution.

In conclusion, we find a relation between asymmetry of the natural frequency sample and the rotation frequency of the global phase. Remembering from [Kur84] that frequencies around the maximum of a unimodal frequency distribution synchronize first, and taking a look at Fig. 3.10, with the benefit of hindsight these results become plausible. The analytical results from the thermodynamic limit explain why in the finite case the global phase typically rotates with a constant drift.

3.5 Remark on the Lorentzian case

The Lorentz distribution arises in most of the literature on Kuramoto- and similar models, because it cracks the hard integrals in the self-consistency equation Eq. (3.21) for the mean field, see e.g. [Kur84, OA08]. In this section, we discuss, why the preceding discussion of Gaussian-like distributions[17] does not extend straightforwardly to the Lorentz distribution, especially the comparison between finite and infinite samples.

[17] Gaussian-like in the sense of (approximately) unimodal distributions that possess the higher moments that we need for our comparison.

Both the Lorentz and the Gaussian distribution belong to the family of (Lévy) alpha-stable distributions. Members of this family fulfill a generalized central limit theorem and are in this sense natural[18] distributions. They are leptokurtic, heavy-tailed and do not possess moments higher than the first – with the Gaussian distribution being the only exception in all three of these characteristics. The probability density function in most cases has no analytic expression, only the characteristic function does. It is therefore difficult to treat alpha-stable distributions in general. We restrict the discussion to the Lorentz distribution $g(\omega) = \gamma/[\pi(\omega^2+\gamma^2)]$ as a representative for the problematic features in this family.

There are three main problems: First, as stated above, the Lorentz distribution contradicts the model assumption of almost identical natural frequencies, as it possesses heavy tails. Second, finite Lorentzian samples are – due to the fat tails of the distribution – characterized by few strong outliers. Outliers with large positive or negative frequencies perform fast rotations. Their time scales separates from the time scale of the mean field. Third, the (infinite) distribution has no moments.

At least for the third problem, there are possible alternatives. Other than the moments, the quantiles of a probability distribution are always defined – by any of the abundant definitions, see e.g. [HF96]. Generally, the mth n-tile is obtained by dividing the support of a probability distribution into n pairwise disjoint intervals such that the probability distribution has an nth part of the probability mass in each of the intervals – then the mth n-tile is the lower boundary of the mth interval, counting from $-\infty$ to ∞.

We now describe combinations of quantile measures that should ideally resemble the sample moments: [Moo88][19] proposes a quantile-based measure for kurtosis, which applies to heavy-tailed distributions in the infinite case – where γ_2 diverges – and to finite samples. It combines the properties that we discussed as the crucial features for kurtosis, namely "(i) concentration of probability mass near [the mean]" and "(ii) concentration of probability mass in the tails of the distribution". The octiles E_m of a probability distribution symmetric around zero, i.e. distributions with $E_4 = 0$, derive for $m > 4$ from the integral

$$\int_0^{E_m} g(\omega)\,\mathrm{d}\omega = \frac{m-4}{8} \tag{3.40}$$

and for $m < 4$ it holds that $E_2 = -E_6$, $E_1 = -E_7$, and $E_3 = -E_5$. [Moo88] defines quantile kurtosis as

$$T := \frac{(E_7 - E_5) + (E_3 - E_1)}{E_6 - E_2} \quad \Rightarrow \text{ for symm. distribution: } \quad T = \frac{E_7 - E_5}{E_6} \tag{3.41}$$

A Gaussian distribution with standard deviation σ and mean 0 has octiles

$$\begin{aligned} E_{m>4} &= \sqrt{2}\sigma\,\mathrm{erf}^{-1}\left[(m-4)/4\right] \\ \text{and thus} \quad T &= \left[\mathrm{erf}^{-1}\left(\frac{3}{4}\right) - \mathrm{erf}^{-1}\left(\frac{1}{4}\right)\right] / \mathrm{erf}^{-1}\left(\frac{1}{2}\right) \sim 1.233, \end{aligned} \tag{3.42}$$

where erf^{-1} is the inverse error function.

[18] Natural frequency distributions are difficult to access experimentally in the many applications of the model – especially in biological systems where an in-vivo time-resolved observation of uncoupled individuals is necessary. The few publications on this topic we know of are an elaborate experiment recording the inter-flash intervals of at least 4 individuals [BBH+81] and the time-resolved recording of glycolytic cycles in starved yeast cells as observed in [WPZH12].

[19] Interestingly, the article uses the stretched exponential, i.e. the Subbotin family of distributions as an example. The α in their Eq. (3.6) corresponds to $1/p$ in our Eq. (3.27). Their kurtosis k minus 3 is our excess kurtosis γ_2.

For the Lorentzian distribution with scale γ integral (3.40) gives

$$E_5 = \gamma(\sqrt{2}-1) = -E_3, \quad E_6 = \gamma = -E_2, \quad E_7 = \gamma(\sqrt{2}+1) = -E_1 \tag{3.43}$$

and thereby $T = 2$.

When we plot $R_{\min}(\epsilon)$ with data from Fig. 3.5 (i.e. for Gaussian distributed frequencies) with colour scale proportional to this quantile based kurtosis, though, the correlation is not as clear as in Fig. 3.5. We conclude that the finite Lorentzian samples are a difficult matter to treat and that methods of separation of time scales can be used to discuss them fairly well.

3.6 The total volume contraction in the finite Kuramoto model phase space

The research on chaoticity in the finite Kuramoto model is limited to a handful of publications, see Sect. 2.2.2. The finite-size model is in most aspects elusive to analytical treatment and all previous publications estimate the Lyapunov exponents numerically. Here we derive the sum of all Lyapunov exponents that represents the average total volume contraction in the phase space. We use the same terminology as [PP16].

Starting from the Kuramoto model with finite ensemble size N

$$\dot{\theta}_i = \omega_i + \frac{\epsilon}{N}\sum_{j=1}^{N}\sin\left(\theta_j - \theta_i\right) =: f_i, \tag{3.44}$$

the time evolution of an infinitesimal perturbation $\vec{u}$ is given by

$$\dot{\vec{u}} = K(\vec{\theta})\vec{u}, \tag{3.45}$$

where the entries of matrix K read

$$K_{ik} := \frac{\partial f_i}{\partial \theta_k} = \begin{cases} -\frac{\epsilon}{N}\left(\sum_{j=1}^{N}\cos\left(\theta_j - \theta_i\right) - 1\right) & i = k \\ \frac{\epsilon}{N}\cos\left(\theta_k - \theta_i\right) & i \neq k. \end{cases} \tag{3.46}$$

The total volume contraction S_N is given as the sum of the Lyapunov exponents which is the trace of matrix K:

$$\mathcal{S}_N = \langle \operatorname{tr} K(t)\rangle = \lim_{t\to\infty}\frac{1}{t}\int_0^t \mathrm{d}t' \operatorname{tr}\left[K(\vec{\theta}(t'), t')\right] \tag{3.47}$$

$$= \lim_{t\to\infty}\frac{1}{t}\int_0^t \mathrm{d}t' \underbrace{-\frac{\epsilon}{N}\sum_{i=1}^{N}\left[\sum_{j=1}^{N}\underbrace{\cos(\theta_j - \theta_i)}_{\cos\theta_j\,\cos\theta_i + \sin\theta_j\,\sin\theta_i} - 1\right]}_{\frac{\epsilon}{N}\left(-N^2\,R(t')^2 + N\right)} \tag{3.48}$$

$$= -\epsilon N\langle R(t)^2\rangle + \epsilon. \tag{3.49}$$

Eq. (3.49) shows that the sign of the volume contraction depends only on the product $N\langle R^2(t)\rangle$. The time average $\langle R^2(t)\rangle$ is the sum of variance and squared mean of $R(t)$ and depends on ϵ and the natural frequency sample.

Unfortunately, we did not follow this direction of research any further, and the interpretation of this equation is still open. The obvious next step would be to either show that

the finite Kuramoto model is contracting for any positive ϵ or, if this is not the case, to find the minimal value $N\langle R(t)^2\rangle$ that undercuts 1.

The equation could potentially help to prove the existence of a finite minimum order parameter (compare Sect. 3.1) also below the thresholds given by [VM07]: we expect that the dynamics is contracted to a lower dimensional subspace, as known from the infinite case [OA08] and that configurations with vanishing order parameter cannot be visited already shortly above the critical ϵ corresponding to $R_{\min}$.

3.7 Conclusion

In this chapter we took an alternative viewpoint on the finite Kuramoto model – alternative to the otherwise usual thermodynamic framework of scaling of fluctuations. Instead we investigated how the collective dynamics depends on system parameters in finite ensembles. Therefore, it was necessary to first define an indicator for the emergence of a collective mode and thereby for a meaningful definition of a global phase. Inspired by [TZT$^+$12], we chose the minimum of the Kuramoto order parameter which allows for a numerical estimation of the corresponding critical coupling with arbitrary precision.

The dependence of this new indicator on the coupling strength varies strongly among different intermediate-size natural frequency samples. We find that most of this variability can be traced back to the sampling distribution of the fourth moment – kurtosis – of the distribution. In finite ensembles, we find a strong correlation between the coupling strength, at which a certain degree of synchronization is reached, and the sample kurtosis of the natural frequencies. In the infinite limit, solving the self-consistency equation of the order parameter for a family of distributions, in which kurtosis is a parameter, allows us to confirm this relationship. The results reconcile former results and draw a more complete picture.

The same approach helps to uncover the link between asymmetry of the natural frequency sample and resulting mean frequency of the global phase. We observe in both finite and infinite ensembles that negatively skewed natural frequency samples generate a global phase on average rotating in mathematically positive sense and vice versa. In skew finite ensembles, the phase drifts at constant frequency with fluctuations on top; in perfectly symmetric finite ensembles, the global phase converges to a constant.

We then remark that an analysis of finite samples of the Lorentz distribution requires a prudent approach. In particular, the moments we used above for the characterization of shape and asymmetry cannot be applied for the comparison of finite and infinite ensembles with Lorentz natural frequency distributions. Trying to circumvent this problems by combining quantile measures, we can not reproduce the kurtosis-dependence of the minimum order parameter curve for a quantile based kurtosis measure. For small sample sizes, extreme outliers as they are common in heavy-tailed distributions could be treated by time-scale separation.

We close the chapter by giving an analytical expression for the total volume contraction in the phase space of the finite-size Kuramoto model, a result that opens room for future research.

Chapter 4

Mean field fluctuations induce micro- and macroscopic correlations

Since Kuramoto presented the self-consistent mean field theory of sine coupled phase oscillators with distributed natural frequencies, countless publications refer to his picture of synchronizing ensembles consisting of synchronous and asynchronous oscillators. In the infinite limit, amplitude and angular velocity of the mean field assume constant values, whereby the oscillators effectively decouple. Then, each oscillator follows an Adler equation with slightly different parameters. The ratio of frequency detuning between oscillator and mean field on the one hand and coupling strength on the other decides over the oscillator either locking to the global mean field or rotating freely. The results from the thermodynamic limit associate synchronous oscillators with order and asynchronous with disorder: Synchronized oscillators rotate at a constant phase difference to the mean field and pairwise correlation among them is perfect. In contrast, asynchronous oscillators each rotate at a unique observed frequency, corresponding to disorder. The main question in this chapter is how radically this picture changes in the finite case.

We saw in Chap. 3 that the order parameter fluctuates persistently. In Chap. 2, we reviewed publications that report on a positive largest Lyapunov exponent in a large range of coupling strengths. We here investigate the action of this deterministic chaos in comparison to a random process.

A whole series of papers revealed the synchronizing effect of noise in a diverse range of theoretical models. Starting from [Pik84], many authors describe synchronization among uncoupled identical [GP04, TT04, GP05b], and non-identical oscillators [GP05a] forced by common noise, but also in coupled systems of identical [PGRP16] and non-identical [PGRP16, NK10] oscillators. All these publications assume Gaussian white noise as part of the driving force – employing the powerful corresponding apparatus of stochastic differential equations. We show in the following that more general fluctuating driving forces produce similar effects. The mean field fluctuations can thereby increase order in the disordered natural frequency interval of asynchronous oscillators.

Some experiments indicate positive effects of synchronization by external noise, such as increased spike timing reliability [MS95]. The most famous paper is maybe [GWF+98], where the population sizes of the sheep populations of two close – but with respect to sheep migration separated – isles were synchronized by the common weather impact. On the other hand, experiments also show how a complex system itself produces fluctuations due to finite-size effects, e.g. channel noise in neurons [FSL+12].

Combining these two facts, noise-induced synchronization and inherent fluctuations in finite ensembles, the following question arises: Can the weakly chaotic fluctuations from a

finite Kuramoto ensemble create order among disordered, incoherent oscillators?

We consider the effect of mean field fluctuations in finite ensembles with 1) Gaussian distributed natural frequencies (random or symmetric, see Sect. 3.0) at super-critical coupling and 2) equidistant natural frequencies at sub-critical coupling (super- and sub-critical in the $R_{\min}$-sense). In the latter case, fluctuations are much stronger than in the former, so in the Gaussian super-critical case we need a trick to make the effect of these weak fluctuations visible.

In both setups, we find a competition between the synchronizing effect of the noisy mean field fluctuations and the differences in the natural frequencies of the individual oscillators. In the Gaussian case, fluctuations are weaker and pairwise natural frequency differences among asynchronous oscillators are larger than in the equidistant case. The typical frequency difference could be decreased by increasing the number of oscillators, but with increasing ensemble size also fluctuations get weaker. We find a work-around for this (for our purposes unfortunate) relation between frequency difference and noise intensity. We decouple noise intensity from natural frequency difference by letting the mean field of few *active* Kuramoto oscillators act on uncoupled *passive* Kuramoto oscillators with arbitrarily small natural frequency differences[1].

In this chapter, we approach the topic of synchronization by Kuramoto finite-size fluctuations in three different ways:

First, in Sect. 4.1, we define a suitable model of active and passive oscillators for the detection of fluctuations.

In Sect. 4.2, we visualize the effect by taking snapshots of individual passive phases for different natural frequencies.

In Sect. 4.3, we quantify the pairwise correlation between the uncoupled oscillators with the same model. Locking to the observed frequencies of asynchronous active oscillators plays an important role.

Finally in Sect. 4.4, we model the effect on passive oscillators by uncoupled pairs of oscillators driven by common white Gaussian noise. In this analytical treatment, we derive an expression for the same pairwise correlation measure as in Sect. 4.3 and compare numerical experiment and analytical model.

A part of the research presented here is discussed in a publication we soon release, the other part gives research ground for a new project.

4.1 Active-passive Kuramoto model – Passive oscillators as tracers of the active field

In [PGRP16], an infinite ensemble of non-identical Kuramoto oscillators is subject to weak common Gaussian white noise. The authors prove analytically that the level of synchronization increases with noise intensity. For identical oscillators, they show that synchronization is associated with a negative Lyapunov exponent.

We instead want to measure to what extend phase differences between (coupled or uncoupled) oscillators are decreased under the action of noise (more precisely, of Kuramoto finite-size fluctuations) albeit their natural frequency difference. This effect will prove to depend on both natural frequency difference and strength of fluctuations. In finite Kuramoto ensembles, the two are strongly related: the larger the ensemble, the weaker the

[1] A similar system with passive (or testing) oscillators was discussed in [RPK+02].

fluctuations but also the smaller the natural frequency differences (under the premise of variance one of the frequency sample, w.l.o.g.). We therefore define an extended Kuramoto model, in which natural frequency difference and strength of finite-size fluctuations can be chosen independently.

Active-passive Kuramoto model
A small number $N_{\rm act} > 3$ of *active* phase oscillators ϕ_i generates a fluctuating Kuramoto mean field

$$Z_{\rm act} =: R_{\rm act}\, e^{i\phi_{\rm act}} =: \frac{1}{N}\sum_{i=1}^{N} e^{i\phi_i} \tag{4.1}$$

with order parameter $R_{\rm act}$ and global phase $\phi_{\rm act}$ by following the standard Kuramoto model

$$\dot{\phi}_i = \omega_i + \epsilon R_{\rm act}\, \sin(\phi_{\rm act} - \phi_i) \tag{4.2}$$

with global coupling strength ϵ and natural frequencies ω_i given as a sample of natural frequency distribution $g(\omega)$. Similar to sprinkling iron filings in a magnetic field, we now force *passive* oscillators with this active mean field at the same coupling strength.

$$\dot{\varphi}_i = \Omega_i + \epsilon R_{\rm act}\, \sin(\phi_{\rm act} - \varphi_i) \tag{4.3}$$

Passive natural frequencies Ω_i are comparable to natural frequencies of the active oscillators.

We want to discuss the synchronizing action of active ensembles with different natural frequency samples. First, we consider (random or symmetric[2]) Gaussian samples in the super-critical regime. As seen in Chap. 3, both cases display persistent fluctuations in the absolute value of the order parameter. Second, we investigate equidistant natural frequencies at sub-critical coupling. In the thermodynamic limit, the corresponding uniform distribution leads to a first order phase transition. As shown in [PMT05], the largest Lyapunov exponent is largest slightly below critical coupling, and fluctuations are much stronger than in the Gaussian super-critical case.

In the following section we visualize the action of a fluctuating active mean field on the phases of passive oscillators with distributed natural frequencies.

4.2 Cyclic alteration between formation and breakdown of phase synchronized bars

Passive oscillators φ_i in our model function as enhancers of the effect of increased correlation among asynchronous oscillators. We want to visualize these correlations by taking snapshots of the phases of these passive oscillators versus their natural frequencies, see e.g. Fig. 4.1. In a first experiment, we distribute these natural frequencies Ω_i equidistantly (with difference $\Delta\Omega$ between neighboring frequencies) into an interval outside the locking condition: $|\Omega_i| > \epsilon \min(R_{\rm act})$.

Let us shortly discuss the case of a static active mean field (from an infinite active ensemble or at complete synchrony). Then the passive oscillators follow Adler equations with different frequencies. The density of phases for a particular Ω_i converges to the invariant set of this Adler equation, which for $|\Omega_i| < \epsilon R_{\rm act}$ is a delta distribution and for $|\Omega_i| > \epsilon R_{\rm act}$, the passive oscillators rotate freely so their density is proportional to $1/|\dot{\varphi}_i| = |\Omega_i + \epsilon R_{\rm act}\, \sin(\phi_{\rm act} - \varphi_i)|^{-1}$ – a wrapped Cauchy distribution. The phases accumulate

[2]The regular sample defined in Sect. 3.0 is symmetric.

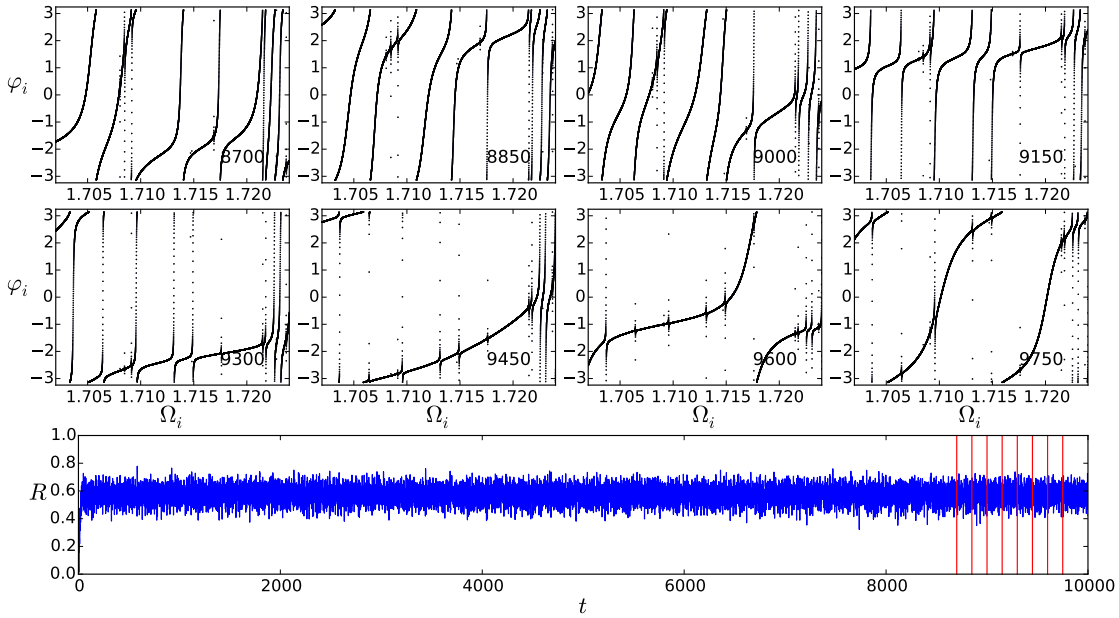

FIG. 4.1: Eight snap shots of passive phases against their natural frequencies in $[1.702, 1.724]$ (same magnification and frequency interval as in lowest panel of Fig. 3.1a) for a system of 50 active oscillators with random Gaussian natural frequency distribution shot at each 150 time units after 8700, indicated by vertical red lines in lower panel. Lower panel: time evolution of the absolute value $R = R_{\text{act}}$ of order parameter of active ensemble. Coupling strength $\epsilon = 1.85$. In comparison to the equidistant case, it takes more than ten times as long until phases concentrate on thin lines, compare also Fig. 4.2. Note that, e.g., the rupture at $\Omega_i = 1.716$ vanishes during the first four panels.

around the bottleneck of the Adler equation, $\phi_{\text{act}} \pm \pi/2$ for $\Omega_i \gtrless 0$. The spread of the phase distribution increases with increasing $|\Omega_i|$.

This picture changes considerably, when we now introduce finite-size fluctuations in $R_{\text{act}}(t)$, generated by 50 *coupled* oscillators.

The observations we describe in the following pages are of dynamical nature: Under the impact of finite-size mean field fluctuations, the phases of passive oscillators in small regions of natural frequencies achieve strong local coherence for a while but then get dragged apart by the difference in their natural frequencies, until fluctuations unify them again, see Fig. 4.1-4.3. This cyclic alteration between low and high coherence is harder to understand from static pictures and description, so we collect a series of videos [Pet18b, Pet18c, Pet18d] and others in a video playlist [Pet18a], see QR-code aside text or use `https://tinyurl.com/yawmkatw`. Descriptions of experiments below respective movies. This monograph, though, provides a comprehensive description of most aspects in these films.

Link to playlist.

In the two next sections we visualize and discuss correlations among passive oscillators in the Gaussian super-critical and the equidistant sub-critical case.

4.2.1 Weak fluctuations from a super-critical Gaussian ensemble

First, let us review the super-critical dynamics in the finite-size Kuramoto model with Gaussian natural frequency distribution (see Chap. 3). The Kuramoto transition to synchrony compares to a thermodynamic second-order phase transition. Above the critical

coupling (indicated by $R_{\min}$), a large synchronized cluster with a common observed frequency is formed by all oscillators with a natural frequency close to zero. The asynchronous oscillators in the wings of the natural frequency distribution already decrease their observed frequencies to join the central cluster at stronger coupling.

The exact critical coupling strength and its dependence on the particular frequency sample are extensively discussed in [PP18] and Sect. 3.

The pairwise phase differences within the central cluster fluctuate, due to the locking condition Eq. (2.7) being time-dependent. Oscillators with natural frequencies on the border of this central cluster are of particular importance for the phenomenon we aim to evince in this section, as they carry the strongest fluctuations.

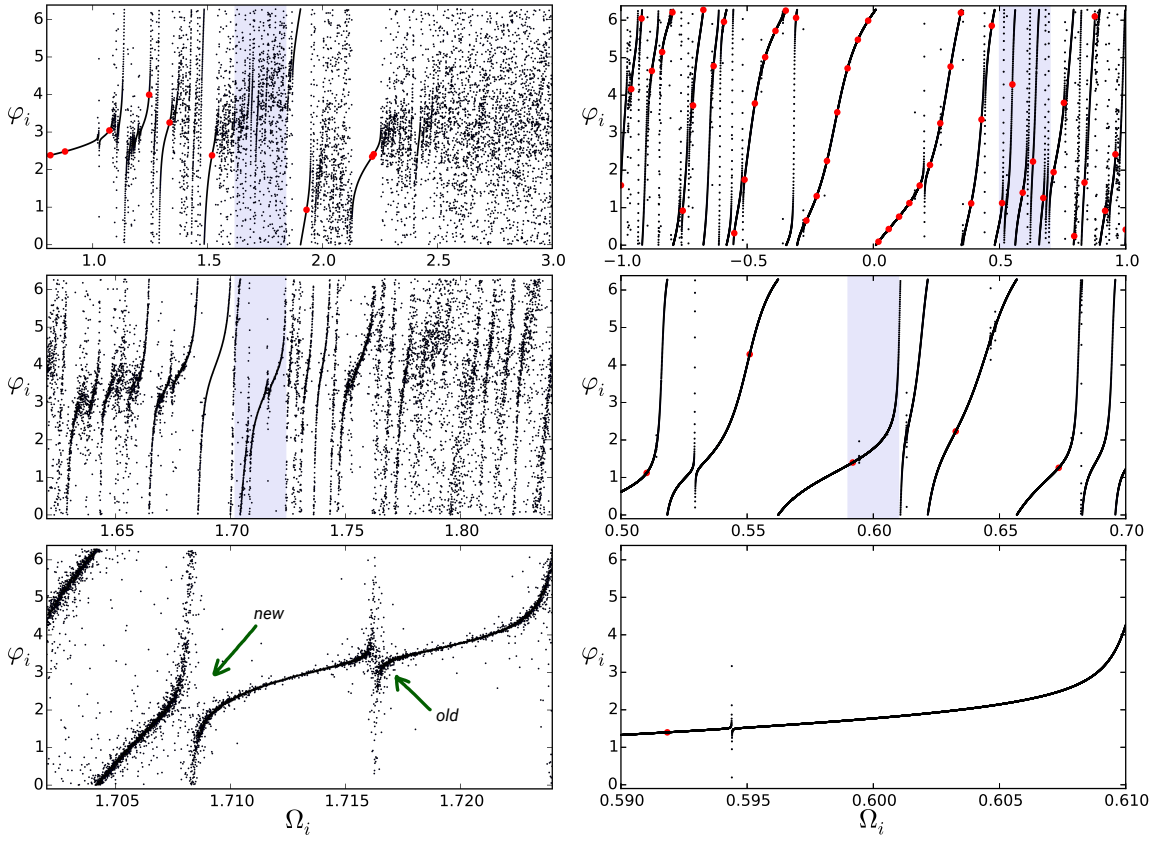

a) random Gaussian active ensemble **b)** equidistant active ensemble

FIG. 4.2: Snap shot at $t = 10^3$ of passive phases (small black dots) against their natural frequency for a system of 50 active oscillators (in red) with 4.2a) random Gaussian natural frequencies or 4.2b) equidistant natural frequencies and 10^4 passive oscillators with equidistant frequencies in three zoom levels with factor 10: Gaussian case $[0.8, 3.]$, $[1.6, 1.82]$, and $[1.72, 1.742]$ – equidistant case $[-1., 1.]$, $[0.5, 0.7]$, and $[0.59, 0.61]$. Coupling strengths $\epsilon = 1.85$ and $\epsilon = 1.25$, respectively. In the Gaussian case, the phases did not yet form a thin line as it occurs after $t \sim 5 \cdot 10^4$, compare Fig. 4.1. Both in the equidistant and in the Gaussian case, passive oscillators with natural frequencies close to an active oscillator lock to the latter (upmost panels). Correlation among neighboring passive oscillators decreases with difference to the central cluster, indicated by thinner and scarcer stripes. The green arrows in 4.2a) point to a rupture that is starting to close (old) and a recently born rupture (new). In 4.2b), there is only one rupture that is almost already closed.

The analogy of the synchronization transition to a thermodynamic phase transition suggests to investigate critical phenomena around the transition point. The vast majority of publications regarding the finite-size Kuramoto model therefore discusses the scaling of

fluctuations close to the criticality and concentrates on relatively large numbers of oscillators. Much less investigated is the chaoticity of the collective motion in the super-critical regime. The only reference known to the author is [Bar13]. In that work, small positive Lyapunov exponents in the direction of some of the oscillators' phases are found in a considerable range of super-critical coupling strengths – approximately between the critical coupling strength for a strictly positive order parameter after transient and the critical coupling strength for full synchrony. They produce noisy fluctuations in the Kuramoto order parameter – an important ingredient in the effect we show here.

We now observe the time-dependent phase profile (instantaneous individual phases vs. natural frequency) of passive oscillators forced by an active ensemble of 50 oscillators with Gaussian distributed frequencies at super-critical coupling $\epsilon = 1.85$, compare Figs. 4.1 and 4.2a)[3]. Initially the passive phases get attracted to the active global phase plus (minus) $\pi/2$ for passive oscillators faster (slower) than the active mean field – as in the case of periodic driving. The weak fluctuations of the driving active mean field then brings phases of passive oscillators closer together. After a long time of ~ 5000 time units, the passive phases align with other passive phases with similar natural frequency, forming a thin line. The natural frequency difference in contrast, drags phases apart, so that the thin line breaks and a "rupture" occurs (see e.g. bottom panels in Fig. 4.2). We call the approximately horizontal line between two such ruptures a bar. The fluctuating driving closes these ruptures in ~ 500 time units. The system seems to go into a dynamic equilibrium with certain density of ruptures, in which bars are constantly reformed and destructed. The typical bar width of ≈ 0.02 is indeed smaller than the typical natural frequency difference among asynchronous active oscillators ≈ 0.2; we therefore call these correlations microscopic. Note that passive oscillators with natural frequencies close to one of the active oscillators, frequency-lock to the latter.

4.2.2 Stronger fluctuations from a sub-critical equidistant ensemble

In the case of equidistant natural frequencies in the active ensemble and coupling strength $\epsilon = 1.25$ only slightly below the critical coupling $\epsilon \approx 1.275$, fluctuations are stronger than in the Gaussian super-critical case, assuming values between $R \approx 0$ and $R \approx 0.6$. Also the auto-correlation is larger than in the Gaussian case, as a comparison of the lower panels in Fig 4.1 and Fig 4.3 indicates. The effects are qualitatively equivalent to the above described Gaussian case, but occur on a shorter time-scale (approx. factor 10) and on larger passive-natural frequency intervals. Correlation 'lengths', i.e. typical interval lengths of passive frequencies in which bands are formed, become macroscopic, such that the concept of passive oscillators is not actually necessary in order to visualize (compare e.g. [Pet18c] for the case of 1000 active oscillators, although the effect is already visible for ~ 50 oscillators). The mean field fluctuations suffice to induce the bar-formation-and-destruction cycle among the central oscillators. The process happens cyclically but not periodically; after all the order parameter performs chaotic motion and the different cycle times reflect that.

As in the Gaussian case, we observe both, phase slips and closing of the ruptures they cause, *and* convergence of the phase distribution of individual passive oscillators to a narrow peak. As chaoticity is stronger than in the Gaussian case, both processes occur much quicker slightly below the critical coupling to complete synchrony, where both amplitude and Lyapunov exponents are significantly larger. Also, the correlation 'length',

[3]For comparability, the natural frequency sample, coupling strength, and initial condition are the same in Sect. 4.2 and 4.3.

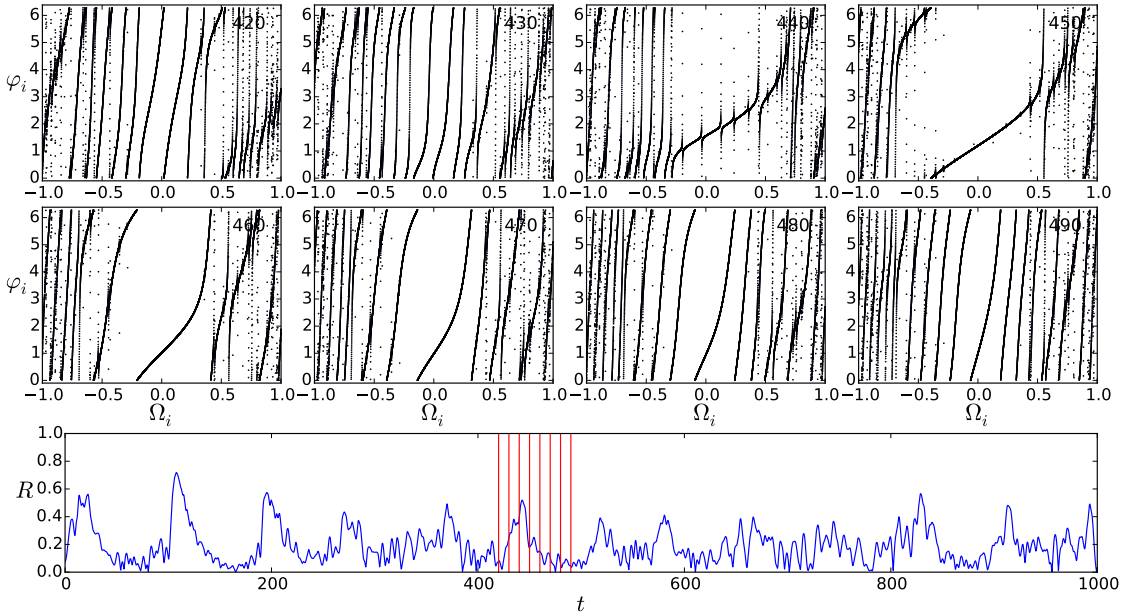

FIG. 4.3: Eight snap shots of passive phases against their natural frequencies in $[-1.01, 1.01]$ (same magnification as in upmost panel of Fig. 4.2b) for a system of 50 active oscillators with equidistant natural frequencies shot at each 10 time units after 420, indicated by vertical red lines in lower panel. Lower panel: time evolution of the absolute value $R = R_{\text{act}}$ of order parameter of active ensemble. Coupling strength 1.25. Note the closing of ruptures especially between 440 and 450 time units for the most central passive frequencies. First and eighth upper panel are similar, indicating beginning and end of a bar-formation-and-destruction cycle. Comparing to the lower panel, the cycle takes place between two local minima; the local maximum in the middle corresponds to the largest central 'bar'.

i.e. the typical interval length of passive natural frequencies in which the phases form such a band is considerably larger in the equidistant case. For a direct comparison of snapshots of the time evolution of passive phases in the Gaussian and equidistant case, respectively, see Fig. 4.2.

In the thermodynamic limit of infinitely many active oscillators, the uniform distribution is special in that, at the critical coupling, all oscillators at once lock to the mean frequency in a first order phase transition. Below critical coupling the order parameter vanishes, the oscillators decouple, and oscillators rotate at their natural frequencies. In the case of a finite ensemble, on the contrary, correlation among oscillators appear already at small coupling strength and increase when approaching critical coupling. With increasing coupling strength, the correlation length grows, and thereby the width of the central bar. The typical period of a cycle of formation and destruction of the central bar increases. As we discuss further in the next section, the transition to synchrony is quite elusive and deserves deeper discussion in a future project.

The above findings imply that finite-size fluctuations might play a crucial role in the stabilization of partial synchrony. Uncoupled equidistant oscillators driven by a constant mean field lock to the latter successively, as the coupling strength increases. In a coupled finite system of oscillators in contrast, fluctuations cause correlations almost across all natural frequencies that would in principle allow to lock all oscillators at once. This finding could be the path to a completely new understanding of the procedure of synchronization transitions in finite systems.

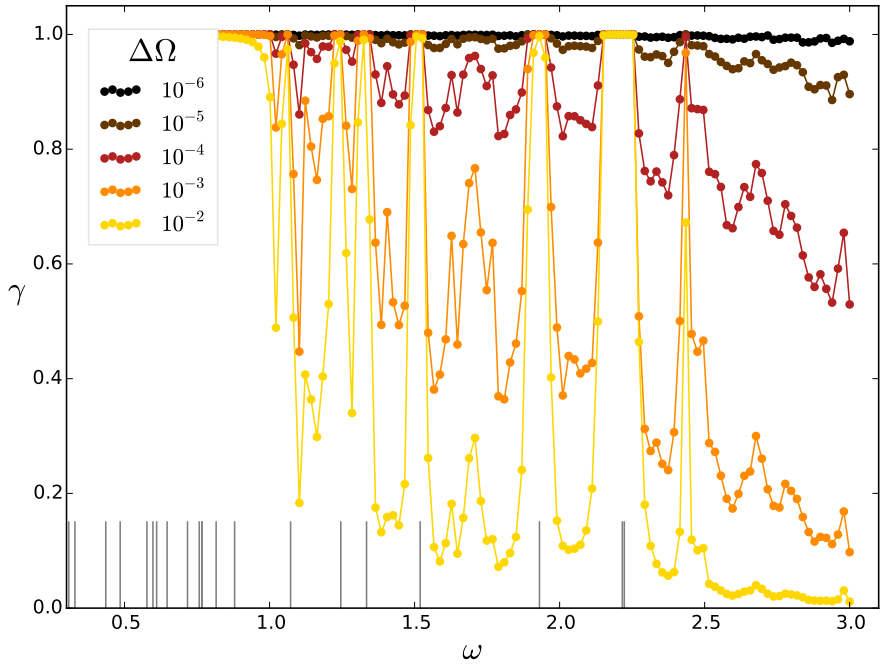

FIG. 4.4: Synchronization index γ of passive oscillators driven by the mean field of 50 active oscillators with Gaussian distributed natural frequencies against frequencies around which passive oscillator pairs are centered. (For numerical details see text.) γ decreases with passive natural frequency difference and with distance to the synchronized central cluster. Passive oscillators lock to active oscillators when natural frequencies of the former are similar to the natural frequency of the latter (indicated by gray vertical lines). Then, γ assumes values close or equal to one. The exceptional peak at natural frequency ~ 2.4 is discussed below Fig. 4.5.

4.3 Quantifying the correlations between neighboring passive frequencies via a synchronization index

The qualitative analysis in the former section should now be complemented with numbers that allow us to compare the result to the white-noise approximation. We observed that the typical width of the natural frequency interval in which phases stay close for some while ($\equiv$ correlation length) decreases with the natural frequency difference to the central synchronized cluster. We know that the variance of order parameter fluctuations decays with N^{-1}. And we are able to compare the impact on oscillators with different natural frequency difference by means of the method of passive oscillators.

Now we need a measure for correlation between pairs of passive oscillators. Before applying a correlation measure that is suitable for the circle topology, we need to compensate for a bias. Due to the movement of all oscillators in a common, nonlinear potential, spurious correlations occur, when the oscillators pass the same bottleneck. Speaking in the analogy of a particle sliding down a plane (as in [PRK03], Eq. (9.8)): all particles slide down the same tilted (time-dependent) potential, only that the tilt is a slightly different for each oscillator. We discussed that phases of oscillators with natural frequencies close to the synchronization transition have rather narrow phase distributions on the circle, due to their long stay close to the synchronized cluster interrupted only by short phase slips. Think of the temporal distribution of one passive oscillator on the circle as a snapshot of infinitely many identical oscillators at time t that started from uniformly distributed phases in $[0, 2\pi)$. Then, the attraction of these identical oscillators to a narrow distribution

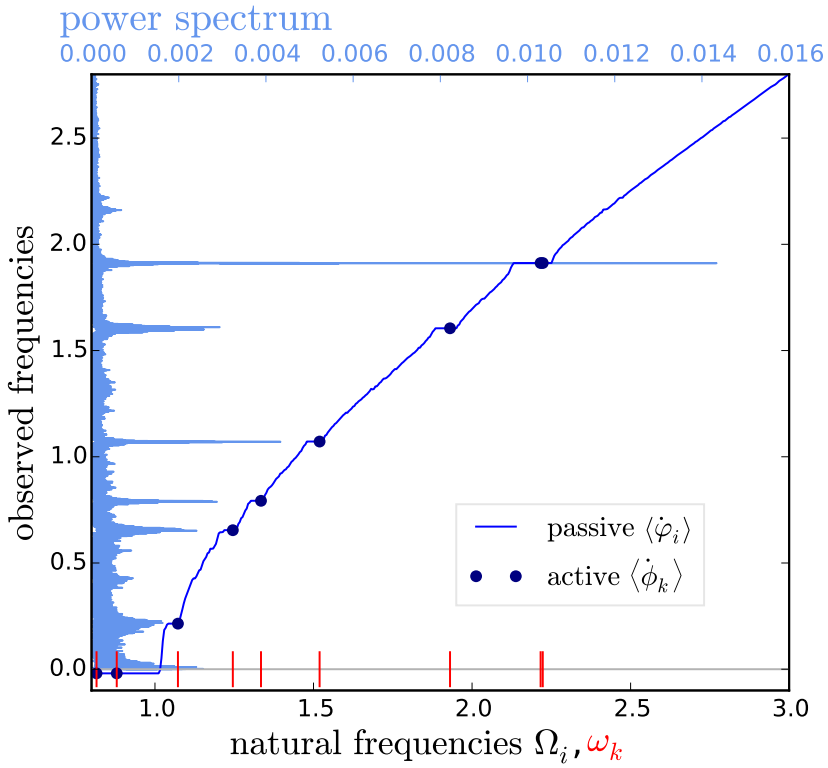

FIG. 4.5: Observed versus natural frequencies for active and passive oscillators. The natural frequencies of the seven asynchronous active oscillators are: $[1.0725, 1.2456, 1.3344, 1.5192, 1.9305, 2.2162, 2.2230]$, i.e. the two largest nat. frequencies are close in this random sample. Same active natural frequency sample as in Fig. 4.4. Averaging time $\sim 2 \cdot 10^9$ RK4 time steps of size 0.01. Unsurprisingly, the general shape compares to the observed frequency vs. frequency detuning graph of the Adler equation – as discussed in Chap. 2. Partially synchronized oscillators form a collective mode that in the infinite limit corresponds to a driving with the constant mean field frequency. The central oscillators on average rotate with the mean velocity of the order parameter phase $\langle \dot{\phi}_{\rm act} \rangle_t = -0.02$. Small steps beyond the central synchronized plateau stem from locking to asynchronous active oscillators. The power spectrum of $R_{\rm act} \exp(\phi_{\rm act})$ in light blue (from a time series of 10^5 units) consists of a noisy background and few pronounced peaks. The highest peak corresponds to two pairwise locked active oscillators with small natural frequency difference. Passive oscillators with similar natural frequencies lock $1:1$ to the two active oscillators. As the latter do not rotate at constant speed but rather linger around $\phi_{\rm act} + \pi/2$ between occasional phase slips, passive oscillators with smaller natural frequency are better synchronized, reflected in the slight asymmetry of the minor plateaus around active natural frequencies. What holds for the highest peak is also true for most of the minor peaks. Some though correspond to $2:1$ synchronization, e.g. the tiny step at natural frequency ~ 2.42 beyond the range of active natural frequencies. Comparison to multiples of the frequencies (measured from the observed frequency of the active mean field) at which the peaks appear reveals that this step corresponds to twice the peak at observed frequency ~ 1.07, i.e. the passive oscillators with natural frequency ~ 2.42 lock $2:1$ to the active oscillator with natural frequency ~ 1.52. The width of steps in general decreases with distance to the central synchronized cluster. Asymmetry of steps around active oscillators and width of these steps appear equivalently in a simplified model, where solutions of Adler equations with different ratios $|\Delta_i/a|$ drive passive Kuramoto oscillators. With the word "steps", we refer to the devils' staircase of a circle map, where – other than in the Adler equation – different winding numbers/ locking ratios occur.

around a certain phase θ_i is described by a Möbius transform, [WS94]. We therefore use

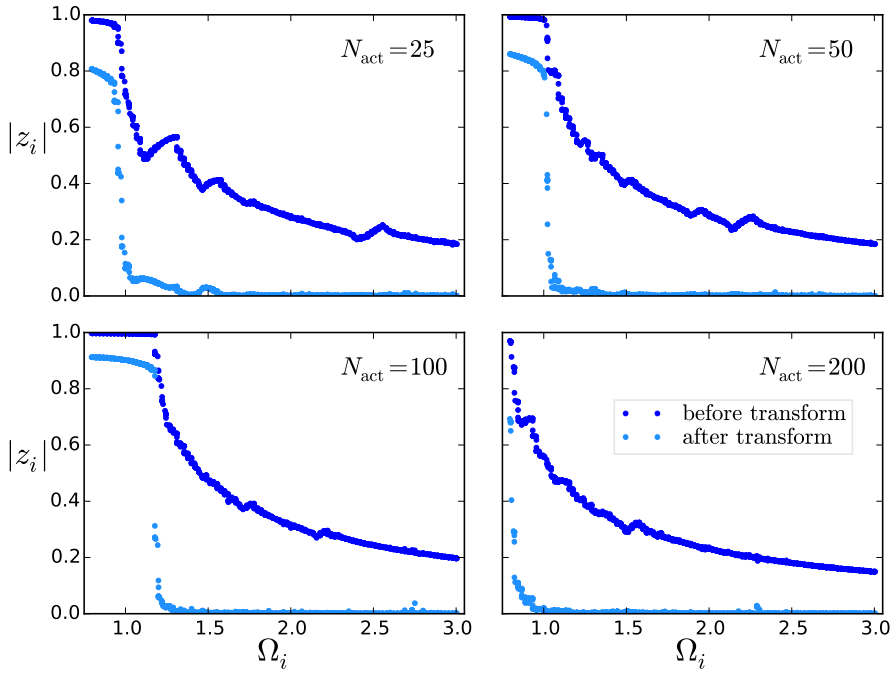

FIG. 4.6: Temporal order parameter $|z_i|$ for passive oscillators with natural frequency Ω_i for the four experiments in Fig. 4.7. The inverse Möbius transform as in Eq. (4.4) indeed leads to an approximately uniform rotation of individual passive phases, indicated by $|z_i|$ for all natural frequencies sufficiently far from the central synchronous cluster. The pairwise phase difference between oscillators in the synchronous cluster fluctuates. Therefore $|z_i| < 1$ before the transformation. Oscillators close to this cluster fluctuate strongest, entering and leaving the central cluster irregularly. They are thus not transformed to uniform distribution by the Möbius transform that can only smear out one global maximum of a phase distribution.

an inverse Möbius transform, with narrowness of the phase distribution and phase θ_i as parameters, to spread the narrow phase distribution to an approximately uniform one. We later check numerically, whether this trick indeed results in a flat distribution.

From a time series of individual passive oscillator i, we determine a temporal order parameter equivalent to the Kuramoto order parameter $z_i = |z_i| \exp[\imath\theta_i] = \langle \exp[\imath\varphi_i(t)] \rangle_t$. Absolute value $|z_i|$ lies between zero for uniform rotation and one for a constant phase. The following inverse Möbius transform stretches the time evolution of asynchronous oscillators which are constant interrupted by phase slips to approximately uniform rotation:

$$\mathrm{e}^{\imath\psi_i} = \frac{z_i - \mathrm{e}^{\imath(\varphi_i - \phi_{\mathrm{act}})}}{z_i^* \mathrm{e}^{\imath(\varphi_i - \phi_{\mathrm{act}})} - 1} \tag{4.4}$$

Measuring individual order parameter $|z_i|$ again after the Möbius transform quantifies the success of the transformation (see Fig. 4.6, where $|z_i|$ before and after transformation is plotted against passive natural frequencies for four different active ensemble sizes). As the active mean field typically rotates and fluctuates slowly due to asymmetries in the active natural frequency sample (compare Sect. 3.4), we apply the Möbius transform only after rotating into the reference frame of the active mean field $\varphi_i \mapsto \varphi_i - \phi_{\mathrm{act}}$.

An appropriate directional measure was suggested by [MJ00]. It measures "the mean phase coherence of an angular distribution". For transformed phases $\psi_{i,j}$, the pairwise synchronization index

$$\gamma = |\langle \exp[\imath(\psi_i - \psi_j)] \rangle_t|, \tag{4.5}$$

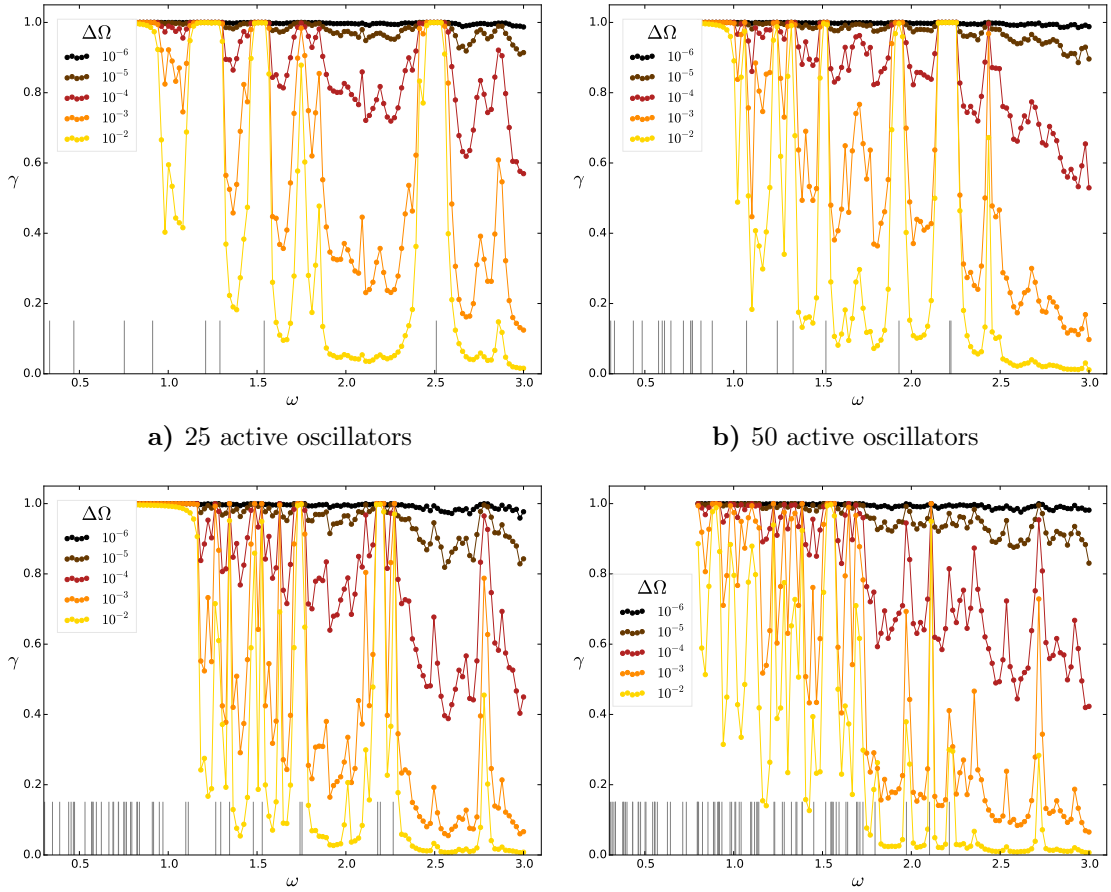

a) 25 active oscillators

b) 50 active oscillators

c) 100 active oscillators

d) 200 active oscillators

FIG. 4.7: Synchronization index γ as in Fig. 4.4, with same method, averaging time, and coupling strength as there, for active ensemble sizes 25, 50, 100, and 200. Natural frequencies of the active ensemble are drawn randomly from a Gaussian distribution; sample mean and standard deviation are unified to 0 and 1 after sampling.

is averaged over large times for pairs of passive oscillators with difference of natural frequencies $\Delta\Omega$.

In the following, we distinguish again between Gaussian and equidistant case. In the Gaussian case, we determine the index for one particular active natural frequency sample and discuss it thoroughly. Afterwards we shortly touch upon the scaling with active ensemble size, passive natural frequency difference, and intensity of active mean field fluctuations – to allow for a comparison to the analytical treatment in 4.4. In the equidistant case, we see in the same experiment as in the Gaussian case that the Möbius transform turns out less effective the closer the coupling approaches critical coupling.

4.3.1 Gaussian distribution

We focus at first on one particular Gaussian natural frequency sample for the active oscillators. We determine that the coupling strength 1.85 is super-critical for this sample. After a transient of 10^4 time units, the order parameter R_{act} fluctuates with variance ~ 0.0035 around mean ~ 0.575. Around each of 110 equidistant frequencies ω in $[0.8, 3.0]$, we center five pairs of passive oscillators with natural frequency differences $10^{-6}, 10^{-5}, 10^{-4}, 10^{-3}$, and 10^{-2}. Active and passive oscillators evolve jointly; the instantaneous order parameter

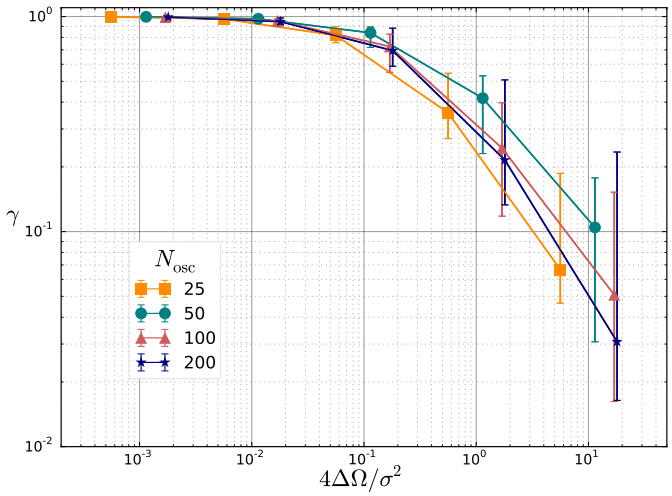

FIG. 4.8: Synchronization index versus ratio of pairwise natural frequency difference and variance of the active mean field. Data as in Fig. 4.7: In all four subplots, we average $\gamma(N_{\mathrm{active}})$ over all passive frequency indeces for which $\gamma(\Delta = 10^{-2})$ falls below an (arbitrary) threshold of $\gamma = 0.6$. Thereby, we mainly exclude the effect of locking to active asynchronous oscillators to focus on the effect of the noisy components of the driving. Compare to analytical white noise approximation, Fig. 4.13.

of the active mean field acts on the passive oscillators in each time step. After the transient, we use the average $z_i = \langle \exp[\imath(\varphi_i - \phi_{\mathrm{act}})] \rangle_t$ for each hundredth RK4 time step of size 0.01 over $t = 2.14 \cdot 10^7$ time units to inverse Möbius transform the trajectories of all 1100 passive phases. Only then, we measure the pairwise correlation of the transformed phases via γ as in Eq. (4.5), i.e. for each of the 110 frequencies we obtain five values. In the last 10^7 RK4 time steps, γ changed by less than 0.3%. The results are presented in Fig. 4.4.

As anticipated from the videos and snapshots from the former section, the results in Fig. 4.4 show a decreasing coherence with increasing distance to the central cluster. Comparing different $\Delta\Omega$, γ also quantifies what we formerly referred to as a correlation length: While the correlation of passive oscillators with natural frequency difference 10^{-6} almost equals one across all measured frequencies, the correlation between oscillators with a frequency difference of 10^{-2} amounts to less than 0.3 (excluding those oscillators for which γ is close to one) and for which $|z_i|$ is sufficiently small after transformation. The passive natural frequencies at which $\gamma \approx 1$ for all frequency differences are those close enough to one of the active oscillators to lock to them. We discuss this aspect in detail in Fig. 4.5. The upper right panel of Fig. 4.6 shows the success of the inverse Möbius transform in straightening the phase evolution of single passive oscillators. Passive oscillators with natural frequencies close to the synchronized cluster phase slip seldomly and irregularly; therefore the transformation is less successful and γ partly measures spurious correlations at these frequencies.

The intensity of fluctuations decreases with ensemble size. In Fig. 4.7-4.8, we evaluate the above experiment with parameters as above also for active ensembles with sizes 25, 100, and 200. As Fig. 4.7 shows, γ typically decreases with ensemble size for a specific passive natural frequency difference. To have a measure for this tendency, we pick all passive natural frequencies around which $\gamma(\Delta\Omega = 10^{-2})$ is smaller than a threshold 0.6, by which we aim to exclude both passive oscillators locked to an active one and passive oscillators close to the central synchronized cluster. Over these selected passive natural frequencies, we average γ to obtain one value for each of the five $\Delta\Omega$ and four active ensemble sizes. The error of γ is estimated as 25th and 75th percentile of γ of the respective selected

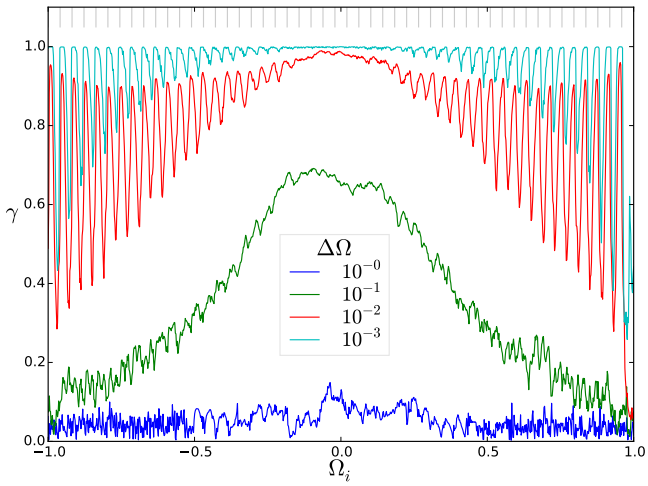

a) γ for equidistant active oscillators

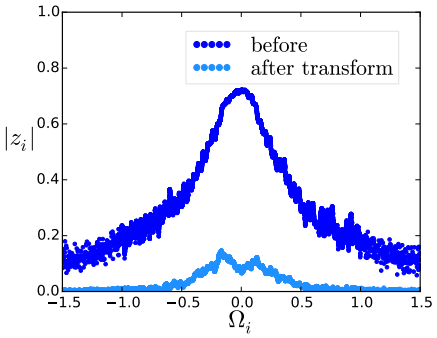

b) $|z_i|$ before and after inv. Mö transform

FIG. 4.9: Correlation for equidistant active ensemble. Panel 4.9a) γ of 1000×4 pairs of passive oscillators driven by mean field of 50 active oscillators with natural frequencies equidistant in $[-1, 1]$ (vertical gray lines above plot). Panel 4.9b) Temporal order parameter $|z_i|$ of passive oscillators, pairs of which are compared in panel 4.9a). (The small hump in $|z_i|$ after the transformation increases further when approaching the critical coupling – the applicability of the Möbius transform decreases.)

passive natural frequencies. Figs. 4.8 displays the results of this averaging against a ratio $4\Delta\Omega/\sigma^2$ that appears in the analytical derivation in Sect. 4.4. Noise intensity σ^2 is the variance of $R_{\text{act}}(t)$. The general curve compares very well to the analytical white noise result shown in Fig. 4.13.

4.3.2 Equidistant distribution

Correlations in slightly sub-critical equidistant active ensembles range over a passive natural frequency of the order of the active natural frequency range, as we saw in Fig. 4.3. Pairs with passive natural frequency differences $1, 0.1, 10^{-2}, 10^{-3}$ have sizable correlation. Moreover, fluctuations are stronger than in the Gaussian active ensemble. For both reasons, it suffices to average over 10^8 RK4 steps of size 0.01, after cutting a transient of 10^4 time units.

Fig. 4.9 shows synchronization index γ , similar to Fig. 4.8. Coupling strength $\epsilon = 1.25$ in this figure lies slightly below critical coupling $\epsilon \sim 1.275$. The strong macroscopic correlations observed in Fig. 4.3 are indeed reflected in large values of γ even for passive frequencies $\sim 10^{-2}$. As in the Gaussian case, we observe locking to active natural frequencies. With increasing $\Delta\Omega$ they smear out, as $\Delta\Omega$ exceeds the width of the locking interval of passive natural frequencies.

For a future project it would interesting to investigate changes of this picture when approaching the transition point. Temporal order parameter $|z_i|$ of the central passive oscillators before transformation increases until finally reaching 1. Our inverse Möbius transform becomes less efficient close to the transition. While in the thermodynamic limit the transition is clearly of first order, little is known about how the finite system undergoes the transition. For determining the exact transition point one might use [OLS16].

4.4 Approximation of chaotic mean field fluctuations as Gaussian white noise

The passive oscillators in Eq. (4.3) are mutually uncoupled and driven by a common chaotic forcing[4]. In the previous section, we measured a considerable pairwise correlation between these forced passive oscillators. Our observations from former Sects. 4.2 and 4.3 suggest that the chaotic driving acts similarly to a noisy forcing. Strong fluctuations close to criticalities are a universal phenomenon, described by scaling laws. Some authors also touched upon the corresponding increased Lyapunov exponents in systems similar to the here discussed finite-size model, see [Bar13, PMT05]. Synchronization by common noise appears in a variety of setups, as was mostly revealed by Goldobin et. al., e.g. [GPRP17] but also [TT04]. That motivates us to replace the chaotic mean field by Gaussian white noise as a first order approximation.

Clearly, the observed locking of passive oscillators to specific frequencies in the spectrum of the time-dependent mean field as observed in Sect. 4.3 are not captured by this approximation. The theories of Adler equation and circle map explain most aspects in this respect. We can therefore focus our attention on the effect of noise. This section is dedicated to the competition between noise and frequency difference in the passive-active system.

Therefore, we consider the synchronization index of a pair of two oscillators with natural frequency difference Δ and noisy forcing. We first bring the evolution equation of the passive oscillators in all three cases – equidistant sub-critical active forcing, random super-critical, and symmetric super-critical – into a common form. The Fokker-Planck equation of the phase differences' probability density then leads us to how the pairwise angular correlation depends on frequency difference and noise intensity.

4.4.1 Mean field driving of three active ensembles – approximation as stochastic differential equation

Three types of finite ensembles – one with equidistant natural frequencies at slightly sub-critical coupling, one with Gaussian randomly sampled natural frequencies and one Gaussian sample with symmetry $\forall i \exists! j : \omega_j = -\omega_i$, the latter two at slightly super-critical coupling – all exhibit the effect of bar formation that we discussed in Sect. 4.2. We thus expect the formalism of noise-induced synchronization to apply to all three systems. The dynamic equation for two passive oscillators φ_1, φ_2 is given by

$$\dot{\varphi_i} = \Omega_i + \epsilon R_{\mathrm{act}} \sin(\phi_{\mathrm{act}} - \varphi_i). \tag{4.6}$$

The time evolution of amplitude and phase of the active mean field, R_{act} and ϕ_{act}, differs considerably in the three cases. We will reduce this equation in the following to an equivalent form for all three cases:

$$\boxed{\dot{\psi_i} = \tilde{\Omega}_i + \chi(t) - h \sin\psi_i + \frac{a}{2}\sin(\psi_i)\xi_1(t) + \frac{b}{2}\cos(\psi_i)\xi_2(t)} \tag{4.7}$$

where ψ_i, $\tilde{\Omega}_i$, h, a, b, and white noise random processes $\xi_{1,2}(t)$ and $\chi(t)$ have different definitions, corresponding to the different ensembles. Random processes $\xi_{1,2}(t)$ represent two uncorrelated white noise processes $\langle \xi_{i,j}(t) \rangle = 0$ and $\langle \xi_i(t)\xi_j(t') \rangle = 2\delta_{ij}\delta(t-t')$.

[4]The setup should though not be confused with *generalized synchronization*, see [RSTA95], where a chaotic oscillator entrains an identical (chaotic) system.

4.4.1.1 Active mean field of equidistant ensemble at slightly sub-critical coupling

In Kuramoto ensembles at sub-critical coupling strength, both the phase and the absolute value of the Kuramoto order parameter fluctuate strongly. Roughly, the complex order parameter Z_{act} can be approximated to perform random white noise diffusion around zero: $Z_{\text{act}}(t) = \xi_X(t) + \imath\xi_Y(t)$ where $\xi_X(t)$ and $\xi_Y(t)$ are uncorrelated, real-valued Gaussian white noise processes with zero mean. The phase transition in the thermodynamic limit in case of a uniform distribution is of first order, compare Eq. (3.26). As order parameter fluctuations are stronger closer to the criticality, the standard deviation of the order parameter fluctuations should be estimated from numerical experiments at the corresponding coupling strength. We rewrite Eq. (4.6) accordingly[5]:

$$\begin{aligned}\dot{\varphi}_i &= \Omega_i + \epsilon R_{\text{act}} \sin(\phi_{\text{act}} - \varphi_i) \\ &= \Omega_i + \epsilon R_{\text{act}} \left[\sin\phi_{\text{act}} \cos\varphi_i - \cos\phi_{\text{act}} \sin\varphi_i\right] \\ &= \Omega_i + \epsilon \left[\xi_Y(t) \cos\varphi_i - \xi_X(t) \sin\varphi_i\right] \end{aligned} \tag{4.8}$$

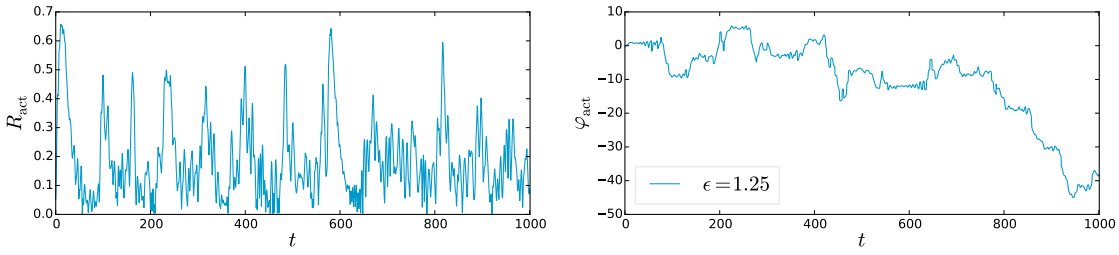

FIG. 4.10: Mean field absolute value $R_{\text{act}}(t)$ and phase $\varphi_{\text{act}}(t)$ of 50 Kuramoto oscillators with equidistant natural frequencies at coupling strength $\epsilon = 1.25$ slightly below critical coupling $\epsilon \sim 1.275$.

Eq. (4.8) already has the form of Eq. (4.7), with $\psi_i = \varphi_i$, $\tilde{\Omega}_i = \Omega_i$, $\chi(t) = 0$, $h = 0$, and $a\xi_1(t) = -2\epsilon\xi_X(t)$, $b\xi_2(t) = 2\epsilon\xi_Y(t)$.

Looking into details of our numerical findings, see also Fig 4.10 and [Pet18c], we observe recurring local plateaus which seem to be both the result of and the reason for bar formation – the white noise approximation might only capture part of the mechanisms involved.

4.4.1.2 Active mean field of Gaussian random ensemble at slightly super-critical coupling

As shown in [PP18], the super-critical order parameter $R_{\text{act}} =: R + \xi_R$ fluctuates around a finite constant value $R := \langle R(t)\rangle_t$, while the global phase ϕ_{act} on average rotates at constant frequency Ω, depending roughly linearly on the skewness of the natural frequency distribution (see Sect. 3.4), superimposed by small-amplitude fluctuations. We model the global frequency $\dot{\phi}_{\text{act}}$ as a constant plus white noise. With $\dot{\phi}_{\text{act}} \approx \Omega + \xi_\varphi$, we express the phases φ_i in the rotating reference frame of the global mean field $\tilde{\varphi}_i = \varphi_i - \phi_{\text{act}}$ and get

$$\dot{\tilde{\varphi}}_i = \Omega_i - \Omega - \xi_\varphi - \epsilon(R + \xi_R) \sin(\tilde{\varphi}_i). \tag{4.9}$$

This equation equals Eq. (4.7) by identifying $\psi_i = \tilde{\varphi}_i = \varphi_i - \phi_{\text{act}}$, $\tilde{\Omega}_i = \Omega_i - \Omega$, $\chi(t) = -\xi_\varphi$, $h = \epsilon R$, and $a\xi_1(t) = -2\epsilon\xi_R(t)$, $b = 0$.

[5] By $\dot{x}(t) = f(t) + g(t)\xi(t)$ we denote the stochastic differential equation (SDE) $\mathrm{d}X_t = f(t)\mathrm{d}t + g(t)\mathrm{d}W_t$ where X_t is a random process and W_t represents a Wiener process.

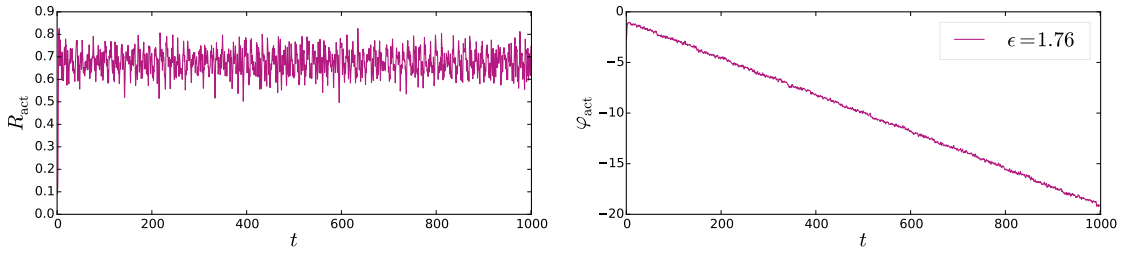

FIG. 4.11: Mean field absolute value and phase of 50 Kuramoto oscillators with Gaussian randomly sampled natural frequencies at coupling strength $\epsilon = 1.76$ slightly above critical coupling $\epsilon \sim 1.75$.

Fig. 4.11 shows a typical time evolution of absolute value and phase of the order parameter that motivates the approximation as white noise.

4.4.1.3 Active mean field of Gaussian symmetric ensemble at slightly super-critical coupling

One crucial observation in [PP18] was that the global phase ϕ_{act} converges to a constant Ω when the underlying natural frequency distribution is symmetric in the sense that $\forall i \exists! j : \omega_j = -\omega_i$. This facilitates calculations considerably, as we can set $\psi_i = \varphi_i - \phi_{\text{act}}$ (without generating an additional noise term). With $R := \langle R(t) \rangle_t$ and order parameter fluctuations ξ_R, Eq. (4.6) then becomes

$$\dot{\psi}_i = \Omega_i - \epsilon(R + \xi_R) \sin(\psi_i) \tag{4.10}$$

which is already of the form of Eq. (4.7) with $\psi_i = \varphi_i - \phi_{\text{act}}$, $\tilde{\Omega}_i = \Omega_i$, $\chi(t) = 0$, and $h = \epsilon R$, and $a\xi_1(t) = -2\epsilon\xi_R(t)$, $b = 0$.

Fig. 4.12 shows a typical time evolution of absolute value and phase of the order parameter that motivates the approximation as white noise and the convergence of the phase of the complex order parameter to a constant.

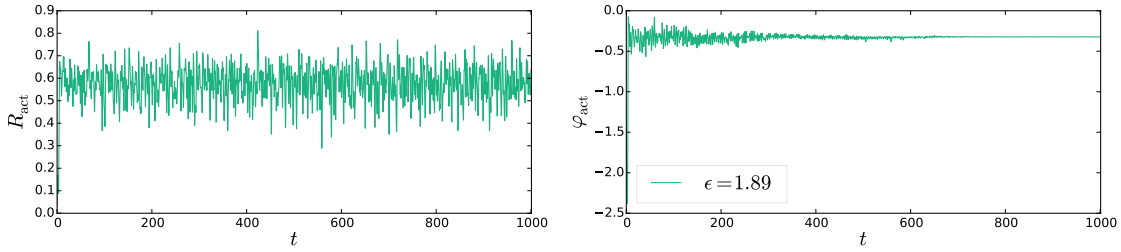

FIG. 4.12: Mean field absolute value and phase of 50 Kuramoto oscillators with *regular* Gaussian natural frequencies (see Sect. 3.0) at coupling strength $\epsilon = 1.89$ slightly above critical coupling $\epsilon \sim 1.87$. The global phase converges to a constant.

4.4.2 Removing bias in pairwise correlation via inverse Möbius transform

As in the numerical experiment, there is a bias in the pairwise correlation of passive oscillators, as they all move in a common nonlinear (time-dependent) potential. In the case of a unimodal natural frequency distribution and super-critical coupling strength, e.g., where the mean field is dominated by the approximately uniformly rotating central

synchronized cluster, both active and passive asynchronous oscillators sojourn longer time at a distance of $\pi/2$ to the mean field phase. By applying an inverse Möbius transform, we stretch the peaked distribution of instantaneous positions of individual phases in $[0, 2\pi)$ to an approximately uniform distribution.[6]

Starting from Eq. (4.7), we first shift phases ψ_i to $\tilde{\psi}_i = \psi_i - \pi/2$. Thereby, $\sin\psi = \cos\tilde{\psi}$ and $\cos\psi = -\sin\tilde{\psi}$, which proves practicable in the following calculation.

$$\dot{\tilde{\psi}}_i = \tilde{\Omega}_i + h\cos\tilde{\psi}_i + \frac{a}{2}\cos\tilde{\psi}_i\,\xi_1 - \frac{b}{2}\sin\tilde{\psi}_i\,\xi_2 + \chi(t). \tag{4.11}$$

We use the inverse Möbius transform in the form

$$\tan\frac{\phi_i}{2} = \sqrt{\frac{\tilde{\Omega}_i - h}{\tilde{\Omega}_i + h}}\tan\frac{\tilde{\psi}_i}{2}. \tag{4.12}$$

The time evolution of the transformed variables ϕ_i derives from these two equations and using derivative

$$\frac{\mathrm{d}}{\mathrm{d}x}(\tan x) = 1 + \tan^2 x \tag{4.13}$$

and half-tangent relations

$$t = \tan\frac{x}{2}, \quad \sin x = \frac{2t}{1+t^2}, \quad \text{and} \quad \cos x = \frac{1-t^2}{1+t^2}. \tag{4.14}$$

After a number of simple algebraic transformations, compare App. A.3, the dynamical equation for ϕ_i are of similar form as Eq. (4.7), namely

$$\dot{\phi}_i = \sqrt{\tilde{\Omega}_i^2 - h^2} + \frac{1}{\sqrt{\Omega_i^2 - h^2}}\left(\Omega_i\cos\phi_i + h\right)\cdot\left[\frac{a}{2}\xi_1 + \chi(t)\right] - \frac{b}{2}\sin\phi_i\,\xi_2. \tag{4.15}$$

As noises $\frac{a}{2}\xi_1$ and $\chi(t)$ are both Gaussian white noise processes centered around zero, their sum is a Gaussian process as well, with noise intensity being the sum of variances of both summands. Replacing the respective variables, Eq. (4.15) in the Möbius transformed variables ϕ_i takes the form

$$\boxed{\dot{\phi}_i = \sqrt{\Omega_i^2 - h^2} + \tilde{\chi}(t) + \frac{A}{2}\sin\phi_i\,\tilde{\xi}_1(t) + \frac{B}{2}\cos\phi_i\,\tilde{\xi}_2(t).} \tag{4.16}$$

New variables relate to the old as follows. $\tilde{\chi}(t)$ is a Gaussian white noise process with zero mean and intensity

$$\eta_i^2 = \frac{h^2}{\Omega_i^2 - h^2}[a^2/4 + \mathrm{Var}(\chi(t))]. \tag{4.17}$$

and $A = -b$ and

$$\frac{B_i^2}{4} = \frac{\Omega_i^2}{\Omega_i^2 - h^2}\left[a^2/4 + \mathrm{Var}(\chi(t))\right]. \tag{4.18}$$

Natural frequency differences $|\Omega_i - \Omega_j| \ll 1$, therefore we set $B = B_i = B_j$ and $\eta = \eta_i = \eta_j$. $\tilde{\xi}_{1,2}(t)$, $\tilde{\chi}(t)$ are Gaussian white noise processes with $\left\langle\tilde{\xi}_{i,j}(t)\right\rangle = \langle\tilde{\chi}(t)\rangle = 0$ and $\langle\xi_i(t)\xi_j(t')\rangle = 2\delta_{ij}\delta(t-t')$, $\langle\xi_i(t)\tilde{\chi}(t')\rangle = 0$, $\langle\tilde{\chi}(t)\tilde{\chi}(t')\rangle = 2\eta^2\delta(t-t')$. Note that, though

[6] This transformation was adapted from celestial mechanics to the synchronization of identical phase oscillators, see [SSW92]. There, the forward Möbius transform mediates the common rapprochement of phases in the synchronization process.

having the same statistics as former processes $\xi_{1,2}(t)$, $\chi(t)$, the transformed realizations generally differ. We drop the tilde in the following.

4.4.3 The synchronization index for a pair of noise driven oscillators

Only after that transformation, we can apply the correlation measure we formerly used in Sect. 4.3, namely

$$\gamma = \left| \langle \mathrm{e}^{\imath(\phi_1(t)-\phi_2(t))} \rangle_t \right| . \tag{4.19}$$

The comparison to the numerical estimation of the synchronization index under Kuramoto mean field driving is straightforward, as also there we compared pairs of oscillators.

In the following, approximating Eq. (4.6) as a stochastic differential equation, see Eq. (4.7), the probability density of the difference of two phases can be found by solving the corresponding Fokker-Planck equation.

4.4.3.1 Diffusion of the phase differences' probability density

The calculations in this subsection are partially adapted from [GPRP17]. We start from Eq. (4.7), where we introduce the mean of the natural frequencies of two oscillators as ω and their frequency difference as Δ:

$$\omega = (\sqrt{\Omega_1^2 - h^2} + \sqrt{\Omega_2^2 - h^2})/2 \quad \text{and} \quad \Delta = \sqrt{\Omega_1^2 - h^2} - \sqrt{\Omega_2^2 - h^2}. \tag{4.20}$$

Thereby, the equations for the two oscillators become

$$\begin{aligned} \dot{\phi}_1 &= \omega + \frac{1}{2}\Delta + \tilde{\chi}(t) + \frac{A}{2}\sin(\phi_1)\xi_1(t) + \frac{B}{2}\cos(\phi_1)\xi_2(t), \\ \dot{\phi}_2 &= \omega - \frac{1}{2}\Delta + \tilde{\chi}(t) + \frac{A}{2}\sin(\phi_2)\xi_1(t) + \frac{B}{2}\cos(\phi_2)\xi_2(t). \end{aligned}$$

It proves useful to reformulate to new variables: on the one hand the difference of phases $\theta = \phi_1(t) - \phi_2(t)$ that we need for the synchronization index, see Eq. (4.19), and on the other hand the sum of phases $\psi = \phi_1(t) + \phi_2(t)$ which we can later integrate over. These new variables relate to the former as follows:

$$\begin{aligned} \frac{1}{2}(\sin(\phi_1) - \sin(\phi_2)) &= \sin\frac{\theta}{2}\cos\frac{\psi}{2}, & \frac{1}{2}(\sin(\phi_1) + \sin(\phi_2)) &= \cos\frac{\theta}{2}\sin\frac{\psi}{2} \\ \frac{1}{2}(\cos(\phi_1) - \cos(\phi_2)) &= -\sin\frac{\theta}{2}\sin\frac{\psi}{2}, & \frac{1}{2}(\cos(\phi_1) + \cos(\phi_2)) &= \cos\frac{\theta}{2}\cos\frac{\psi}{2}. \end{aligned}$$

The evolution equations of θ and ψ are similar, only that the sum of phases rotates at faster speed.

$$\begin{aligned} \dot{\theta} &= \Delta + A\sin\frac{\theta}{2}\cos\frac{\psi}{2}\xi_1(t) - B\sin\frac{\theta}{2}\sin\frac{\psi}{2}\xi_2(t) \\ \dot{\psi} &= 2\omega + 2\tilde{\chi}(t) + A\cos\frac{\theta}{2}\sin\frac{\psi}{2}\xi_1(t) + B\cos\frac{\theta}{2}\cos\frac{\psi}{2}\xi_2(t) \end{aligned} \tag{4.21}$$

The above stochastic differential equation should be interpreted as of Stratonovich type, because the derivation of the Kuramoto model uses conventional differential calculus. In the Fokker-Planck equation for the probability density $W(\theta, \psi, t)$, the additive noise term $\tilde{\chi}(t)$ – which is independent of both θ and ψ – enters as a constant diffusion term with

differential operator D_ψ for the partial derivative w.r.t. θ, such that

$$\frac{\partial}{\partial t}W(\theta,\psi,t) + \frac{\partial}{\partial\theta}\left[\Delta W(\theta,\psi,t)\right] + \frac{\partial}{\partial\psi}\left[2\omega W(\theta,\psi,t)\right] = \left[\sigma^2(\hat{Q}_A^2+\hat{Q}_B^2) + 4\eta^2 D_\psi^2\right] W(\theta,\psi,t) \tag{4.22}$$

where $\hat{Q}_{A,B}$ are differential operators

$$\sigma\hat{Q}_A(\cdot) = \frac{A}{\sqrt{2}}\left[\frac{\partial}{\partial\theta}\left(\sin\frac{\theta}{2}\cos\frac{\psi}{2}(\cdot)\right) + \frac{\partial}{\partial\psi}\left(\cos\frac{\theta}{2}\sin\frac{\psi}{2}(\cdot)\right)\right] \tag{4.23}$$

$$\sigma\hat{Q}_B(\cdot) = \frac{B}{\sqrt{2}}\left[\frac{\partial}{\partial\theta}\left(-\sin\frac{\theta}{2}\sin\frac{\psi}{2}(\cdot)\right) + \frac{\partial}{\partial\psi}\left(\cos\frac{\theta}{2}\cos\frac{\psi}{2}(\cdot)\right)\right]. \tag{4.24}$$

For small Δ, A^2, B^2, σ^2, $\eta^2 \ll 2\omega$, Eq. (4.22) reduces to an easily solvable PDE:

$$\frac{\partial}{\partial t}W(\psi,t|\theta) + 2\omega\frac{\partial}{\partial\psi}W(\psi,t|\theta) = 0. \tag{4.25}$$

The equation carries θ as a mere parameter and can be solved, e.g. by the method of characteristics, to give $W(\psi,t|\theta) = f(\psi - 2\omega t|\theta)$, where the function f is determined by the initial condition. That means that in ψ-direction, assuming comparably large ω, the initial condition solely rotates at constant speed. We now average over these fast rotations by applying the method of multiple scales (compare [Nay81], e.g. Chap 4.5 therein). For Δ, A, B, σ, we define $\Delta = \sigma^2\Delta_1$, $A = \sigma^2 A_1$, $B = \sigma^2 B_1$, and $\eta^2 = \sigma^2\eta_1^2$. We express the time dependence of density $W(\theta,\psi,t)$ in different powers of the small parameter σ^2

$$W(\theta,\psi,t|\sigma^2) =: \hat{W}(\theta,\psi,t,\sigma^2 t,\sigma^4 t,\sigma^6 t...) =: \hat{W}(\theta,\psi,t_0,t_1,t_2,t_3...) \tag{4.26}$$

where we defined well-separated time scales $t_n = \sigma^{2n}t$. The differentiation with respect to time t becomes

$$\frac{\partial}{\partial t} = \frac{\partial}{\partial t_0} + \sigma^2\frac{\partial}{\partial t_1} + ... \tag{4.27}$$

We seek for a solution of the form

$$W = W^{(0)}(t_0,t_1,...) + \sigma^2 W^{(1)}(t_0,t_1,...) + ... \tag{4.28}$$

Inserting this into Eq. (4.22) gives in zeroth and first order

$$\begin{aligned}\left(\frac{\partial}{\partial t_0} + \sigma^2\frac{\partial}{\partial t_1}\right)&\left(W^{(0)} + \sigma^2 W^{(1)}\right) \\ &+ \frac{\partial}{\partial\theta}\left[\sigma^2\Delta_1\left(W^{(0)} + \sigma^2 W^{(1)}\right)\right] \\ &+ \frac{\partial}{\partial\psi}\left[2\sigma^2\omega\left(W^{(0)} + \sigma^2 W^{(1)}\right)\right] \\ &= \sigma^2\left[(\hat{Q}_A^2+\hat{Q}_B^2) + \eta_1^2\right]\left(W^{(0)} + \sigma^2 W^{(1)}\right).\end{aligned} \tag{4.29}$$

When we now sort the equations by time scales, we get in the zeroth order Eq. (4.25):

$$\frac{\partial}{\partial t}W^{(0)} + 2\omega\frac{\partial}{\partial\psi}W^{(0)} = 0 \tag{4.30}$$

Therefore, to the leading order, $W^{(0)}(\theta,\psi,t) = w(\theta,t)$. The first order in σ^2 gives

$$\frac{\partial}{\partial t_0}W^{(1)} + \frac{\partial}{\partial t_1}W^{(0)} + \frac{\partial}{\partial\theta}\left[\Delta_1 W^{(0)}\right] + 2\omega\frac{\partial}{\partial\psi}W^{(1)} = \left[(\hat{Q}_A^2 + \hat{Q}_B^2) + \eta_1^2\right]W^{(0)} \tag{4.31}$$

We now have to remove secular terms, i.e. spurious terms from the approximation that accumulate with integration time. Therefore, when we average Eq. (4.31) over ψ, we should set the monotonously growing term

$$\frac{\partial}{\partial t_0}\int_0^{2\pi} W^{(1)}\mathrm{d}\psi \stackrel{!}{=} 0 \tag{4.32}$$

to zero. Multiplying Eq. (4.31) with σ^2, we can omit subscripts $_1$ that formerly indicated the order in σ^2.

$$\frac{\partial}{\partial t}w(\theta,t) + \frac{\partial}{\partial\theta}\left[\Delta w(\theta,t)\right] + \omega\frac{\partial}{\partial\psi}(...) = \left[\sigma^2(\hat{Q}_A^2 + \hat{Q}_B^2) + 4\eta^2 D_\psi^2\right]w(\theta,t)$$

When now applying the operator $\frac{1}{2\pi}\int_0^{2\pi}\mathrm{d}\psi$, terms that have $\frac{\partial}{\partial\psi}$ as their outmost operation vanish, e.g. terms (4.31) and some terms in $\hat{Q}_A^2+\hat{Q}_B^2$ as well as the diffusion term stemming from additional noise $\tilde{\chi}(t)$.

$$\frac{\partial}{\partial t}w(\theta,t) = -\Delta\frac{\partial}{\partial\theta}w(\theta,t) + \left[\sigma^2(\hat{Q}_A^2 + \hat{Q}_B^2)\right]w(\theta,t) \tag{4.33}$$

We still need to solve integrals

$$\frac{\sigma^2}{2\pi}\int_0^{2\pi}\hat{Q}_A^2(\cdot)\mathrm{d}\psi \quad\text{and}\quad \frac{\sigma^2}{2\pi}\int_0^{2\pi}\hat{Q}_B^2(\cdot)\mathrm{d}\psi \tag{4.34}$$

where $(\cdot)$ does not depend on ψ. $\sigma\hat{Q}_{A,B}$ both have the form $\sigma\hat{Q}_{A,B} = \frac{\partial}{\partial\theta}[(...)(\cdot)] + \frac{\partial}{\partial\psi}[(...)(\cdot)]$, so when we square the operator we get

$$\sigma^2\hat{Q}_{A,B}^2 = \frac{\partial}{\partial\theta}\left\{(...)\frac{\partial}{\partial\theta}[...] + (...)\frac{\partial}{\partial\psi}[...]\right\} + \cancel{\frac{\partial}{\partial\psi}\left\{(...)\frac{\partial}{\partial\theta}[...] + (...)\frac{\partial}{\partial\psi}[...]\right\}} \tag{4.35}$$

where the second term vanishes when integrating over ψ. The equation now reads

$$\sigma^2\hat{Q}_A^2 = \frac{A^2}{2}\frac{\partial}{\partial\theta}\left\{\sin\frac{\theta}{2}\cos\frac{\psi}{2}\frac{\partial}{\partial\theta}\left[\sin\frac{\theta}{2}\cos\frac{\psi}{2}(\cdot)\right] + \sin\frac{\theta}{2}\cos\frac{\psi}{2}\frac{\partial}{\partial\psi}\left[\cos\frac{\theta}{2}\sin\frac{\psi}{2}(\cdot)\right]\right\}$$
$$\sigma^2\hat{Q}_B^2 = -\frac{B^2}{2}\frac{\partial}{\partial\theta}\left\{\sin\frac{\theta}{2}\sin\frac{\psi}{2}\frac{\partial}{\partial\theta}\left[-\sin\frac{\theta}{2}\sin\frac{\psi}{2}(\cdot)\right] + \sin\frac{\theta}{2}\sin\frac{\psi}{2}\frac{\partial}{\partial\psi}\left[\cos\frac{\theta}{2}\cos\frac{\psi}{2}(\cdot)\right]\right\}.$$

Both equations consist of two parts; the first can be integrated over all terms containing ψ right away, while in the second one first needs to perform the derivative. Summing both integrals yields

$$\begin{aligned}\frac{\sigma^2}{2\pi}\int_0^{2\pi}(\hat{Q}_A^2 + \hat{Q}_B^2)(\cdot)\mathrm{d}\psi &= \frac{A^2+B^2}{2}\left(\frac{\partial}{\partial\theta}\left[\sin\frac{\theta}{2}\frac{\partial}{\partial\theta}\left(\sin\frac{\theta}{2}(\cdot)\right)\right] + \frac{1}{2}\frac{\partial}{\partial\theta}\left[\sin\frac{\theta}{2}\cos\frac{\theta}{2}(\cdot)\right]\right)\\ &= \frac{A^2+B^2}{4}\frac{\partial^2}{\partial\theta^2}\left[(1-\cos\theta)(\cdot)\right].\end{aligned} \tag{4.36}$$

With that we now obtained the reduced Fokker-Planck equation for the phase difference of two oscillators obeying Eq. (4.33). The solutions with stationary flux $J = \Omega_{\mathrm{obs}}/2\pi$, where

Ω_{obs} is the difference between the observed frequencies obey

$$\boxed{\Delta w(\theta) - \frac{A^2+B^2}{4}\frac{\partial}{\partial\theta}\left[(1-\cos\theta)w(\theta)\right] = J} \tag{4.37}$$

This equation merely depends on $A^2 + B^2$, i.e. only the strength of the noisy forcing matters, not its direction. We therefore set $A^2 + B^2 = \sigma^2$ and quantify noise intensity by new variable σ. We define parameters

$$\frac{4\Delta}{\sigma^2} =: a \quad \text{and} \quad \frac{4J}{\sigma^2} =: j. \tag{4.38}$$

Integrating the resulting equation

$$aw - \frac{\partial}{\partial\theta}\left[(1-\cos\theta)w\right] = j \tag{4.39}$$

over θ in $[0, 2\pi)$ yields $2\pi j = a$.

Note that in Eq. (4.37), only the frequency difference between the two oscillators and the noise amplitude enter.

4.4.3.2 Numerical approximation of γ from static flux

In the former equation relating the static flux J to the probability density of the pairwise phase difference w

$$aw(\theta) - \frac{\partial}{\partial\theta}\left[(1-\cos\theta)w(\theta)\right] = \frac{a}{2\pi}, \tag{4.40}$$

we substitute w by a Fourier series with coefficients w_k

$$w(\theta) = \frac{1}{2\pi}\sum_{k=-\infty}^{\infty} w_k\, \mathrm{e}^{\imath k\theta}. \tag{4.41}$$

Inserting Eq. (4.41) into Eq. (4.40) gives

$$\sum_{k=-\infty}^{\infty} \mathrm{e}^{\imath k\theta}\left[a\, w_k - \imath k\, w_k + \imath k(w_{k-1} + w_{k+1})/2\right] = a. \tag{4.42}$$

For $k = 0$, the equation represents the normalization condition $w_0 = 1$. To be valid for all θ, terms with other k, i.e. $k \lesseqgtr 0$, should vanish independently. As $w_{-k} = w_k^*$, we restrict our attention to positive k.

$$\frac{\imath k}{2}\, w_{k-1} + (a - \imath k)\, w_k + \frac{\imath k}{2}\, w_{k+1} = 0 \tag{4.43}$$

which gives the following recursive definition for their ratios $r_k := w_{k-1}/w_k$:

$$\boxed{r_k = 2\frac{k+\imath a}{k} - \frac{1}{r_{k+1}}.} \tag{4.44}$$

Reinserting r_{k+1} successively, r_k represents an infinite (generalized) continued fraction. It facilitates further calculations considerably to transform the fraction slightly to a simpler

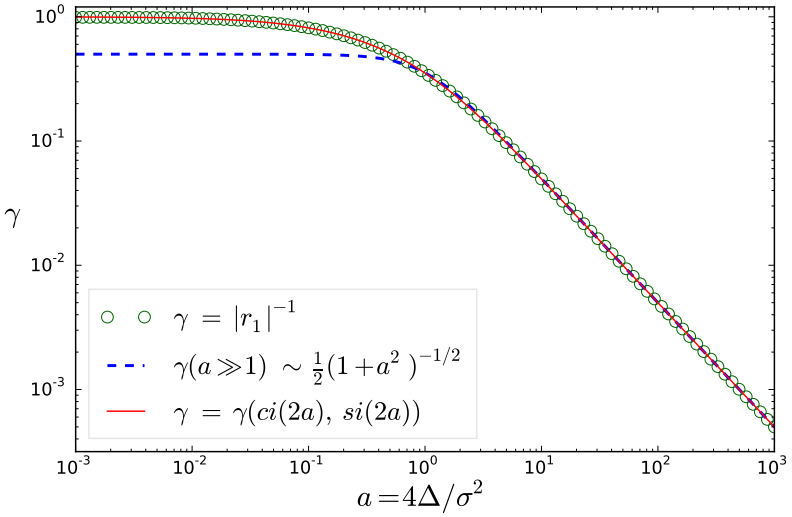

FIG. 4.13: Approximations of γ. Circles: representation of γ as the absolute value of the first Fourier mode, truncation of continued fraction r_k at $k = 100$. Dashed line: Truncation of continued fraction r_k at $k = 1$, i.e. $1/|r_2| \approx 0$. Solid line: representation of γ via trigonometric integrals, approximated via Taylor series up to 100th order for $a \leq 1$ and via the asymptotic expansion of the auxiliary functions f and g for $a > 1$. For detailed explanation of the first two see Sect. 4.4.3.2, the latter procedures are described in Sect. 4.4.3.3.

form and to represent it as a series:

$$a_0 - \cfrac{1}{a_1 - \cfrac{1}{a_2 - \cfrac{1}{a_3 - \cdots}}} = a_0 + \cfrac{1}{-a_1 + \cfrac{1}{a_2 + \cfrac{1}{-a_3 + \cdots}}} = [a_0, -a_1, a_2, -a_3, \cdots] \tag{4.45}$$

where for the ratios r_k:

$$a_{k-1} = 2(-1)^k \frac{k + \imath a}{k}, \quad k = 1, 2, 3, \cdots \tag{4.46}$$

For $a = 0$, the continued fraction can be denoted as $[2, -2, 2, -2, \dots]$ and the sequence of convergents reads

$$2, \frac{3}{2}, \frac{4}{3}, \frac{5}{4}, \cdots \tag{4.47}$$

such that the continued fraction converges to one. For large a, i.e. for large natural frequency difference Δ or small-amplitude noise, we observe that $1/|r_2|$ is of order $1/a^2$, so we approximate

$$r_1 = 2(1 + \imath a) \quad \text{and} \quad w_1 = w_0/r_1 = 0.5/(1 + \imath a). \tag{4.48}$$

For intermediate values of a, both convergence and limit of r_k are not so easily accessible, and we switch to numerical approximation. The value of the continued fraction is given as the limit of the sequence of convergents p_k/q_k, where

$$\begin{aligned} p_0 = a_0, \quad p_1 = a_0 a_1 + 1, \quad q_0 = 1, \quad q_1 = a_1 \\ \text{and} \quad p_k = a_k p_{k-1} + p_{k-2}, \quad q_k = a_k q_{k-1} + q_{k-2}. \end{aligned} \tag{4.49}$$

We iterate this scheme until $k = 100$ (in the last iteration step, γ changed less than

10^{-5} for $a = 10^{-3}$, and less than 10^{-15} for $a = 10^3$) and represent $1/|r_1|$ by green circles in Fig. 4.13 – namely because the synchronization index equals the absolute value of the first Fourier coefficient:

$$\gamma = \left|\langle \mathrm{e}^{\imath(\phi_1(t)-\phi_2(t))}\rangle_t\right| = \left|\langle \mathrm{e}^{\imath\theta(t)}\rangle_t\right| = |\int_{-\pi}^{\pi} w(\theta)\,\mathrm{e}^{\imath\theta}\,\mathrm{d}\theta| = |w_1| = \left|\frac{w_0}{r_1}\right| = \frac{1}{|r_1|} \tag{4.50}$$

By Eq. (4.48), synchronization index γ is approximated as $0.5/\sqrt{a^2+1}$ which we also depict in Fig. 4.13.

4.4.3.3 Expressing γ by trigonometric integrals

Alternatively, the synchronization index can be expressed as a function of sine and cosine integrals. Therefore, we transform the density w of phase difference θ to density p of the cotangent half-angle x of θ:

$$x = \cot\frac{\theta}{2} \quad \sin^2 t\frac{\theta}{2} = \frac{1}{1+x^2} \quad \cos\theta = \frac{x^2-1}{x^2+1} \quad \sin\theta = \frac{2x}{1+x^2} \quad \mathrm{d}x = -\frac{1+x^2}{2}\mathrm{d}\theta.$$

Thereby, with $p(x)\mathrm{d}x = w(\theta)\mathrm{d}\theta$, the transformed density reads

$$p(x) = w(\theta(x))\,\frac{2}{1+x^2}. \tag{4.51}$$

While $\theta \in [0, 2\pi)$, cotangent x extends over the whole real line. It is therefore necessary to check the proper decay of $p(x)$ for $|x| \to \infty$, especially for delta-distributed $w(\theta)$. Singularities around $\theta = \pi$, i.e. $x = 0$ are harmless. The problematic case is $\theta \to 0$, i.e. $x \to \pm\infty$. We represent the delta distribution in w as

$$w(\theta) = \lim_{\epsilon\to 0} \frac{1}{\sqrt{\pi}\epsilon}\,\exp(-\theta^2/\epsilon^2). \tag{4.52}$$

Around $\theta = 0$, we use the approximation $\sin\theta \sim \theta$ to simplify the transformation to $p(x)$ and obtain

$$p(x) = \lim_{\epsilon\to 0} \frac{1}{\sqrt{\pi}\epsilon}\frac{2}{1+x^2}\,\exp\left[-\frac{1}{\epsilon^2}\left(\frac{2}{1+x^2}\right)^2\right] \tag{4.53}$$

which decays as

$$\lim_{|x|\to\infty} p(x) \sim \lim_{\substack{|x|\to\infty\\ \epsilon\to 0}} \frac{1}{\sqrt{\pi}\epsilon}\frac{2}{x^2}\,\exp\left[-\frac{1}{\epsilon^2}\left(\frac{2}{x^2}\right)^2\right] \sim \begin{cases} 0 & \text{if } x < 1/\epsilon \\ \frac{1}{x^2\epsilon} & \text{if } x > 1/\epsilon \end{cases} \tag{4.54}$$

The normalization of $p(x)$ is also still fulfilled. Function $p(x)$ thereby is a probability density. Converting Eq. (4.40) gives

$$\frac{\mathrm{d}p(x)}{\mathrm{d}x} + a\,p(x) = \frac{a}{\pi(1+x^2)}. \tag{4.55}$$

We define a potential function $V(x) = ax$ and solve the differential equation formally by Variation of Parameters:

$$\frac{\mathrm{d}p(x)}{\mathrm{d}x} + V'(x)p(x) = \frac{a}{\pi(1+x^2)} \qquad p(x) = p_0(x)\mathrm{e}^{-ax} \tag{4.56}$$

$$p_0(x) = \int_{-\infty}^{x} \frac{a}{\pi(1+y^2)}\,\mathrm{e}^{ay}\,\mathrm{d}y \tag{4.57}$$

$$p(x) = \frac{a}{\pi}\int_{-\infty}^{x} \frac{a}{\pi(1+y^2)}\,\mathrm{e}^{a(y-x)}\,\mathrm{d}y. \tag{4.58}$$

For synchronization index γ we need

$$S = \langle \sin\theta \rangle = \int_{-\infty}^{\infty} \frac{2x}{1+x^2}\,p(x)\,\mathrm{d}x \quad \text{and} \quad C = \langle \cos\theta \rangle = \int_{-\infty}^{\infty} \frac{x^2-1}{1+x^2}\,p(x)\,\mathrm{d}x. \tag{4.59}$$

Inserting Eq. (4.58) into the integral for S and substituting $u = x - y$, $v = x$, where $0 < u < \infty$ and $-\infty < v < \infty$, we obtain

$$S = \frac{a}{\pi}\int_{-\infty}^{\infty} \mathrm{d}v \int_{0}^{\infty} \mathrm{d}u\,\frac{2v\mathrm{e}^{-au}}{(1+v^2)(1+(v-u)^2)}, \tag{4.60}$$

where the integral over v solves, e.g. by complex integration, to

$$\int_{-\infty}^{\infty} \mathrm{d}v\,\frac{2v}{(v^2+1)((v-u)^2+1)} = \frac{2\pi u}{u^2+4}. \tag{4.61}$$

As a is real and positive in our definition, we apply formula 3.354.2 in the integral tables of Gradsteyn & Ryzhik [GR80] and express S via sine and cosine integrals:

$$S = 2a\int_{0}^{\infty} \mathrm{d}u\frac{u\mathrm{e}^{-au}}{u^2+2^2} = 2a[-ci(2a)\cos(2a) - si(2a)\sin(2a)]. \tag{4.62}$$

where cosine and sine integrals are defined as

$$ci(x) = -\int_{x}^{\infty} \frac{\cos t}{t}\,\mathrm{d}t = Ci(x) \quad \text{and} \quad si(x) = -\int_{x}^{\infty} \frac{\sin t}{t}\,\mathrm{d}t = Si(x) - \pi/2. \tag{4.63}$$

For the cosine case C, we proceed equivalently. Substituting $p(x)$ from Eq. (4.58) in the equation for C in Eq. (4.59) and, as above, transforming to variables u, v with $u = x - y$, $v = x$, where $0 < u < \infty$ and $-\infty < v < \infty$ we get

$$C = \frac{a}{\pi}\int_{-\infty}^{\infty} \mathrm{d}v \int_{0}^{\infty} \mathrm{d}u\,\frac{(v^2-1)\mathrm{e}^{-au}}{(1+v^2)(1+(v-u)^2)}. \tag{4.64}$$

Again by complex integration, we solve the integral over v:

$$\int_{-\infty}^{\infty} \mathrm{d}v \, \frac{v^2-1}{(v^2+1)((v-u)^2+1)} = \frac{\pi u^2}{u^2+4}. \tag{4.65}$$

Gradsteyn & Ryzhik's equation 3.354.1 helps us to express C as

$$C = a\int_0^{\infty} \mathrm{d}u \frac{u^2 \mathrm{e}^{-au}}{u^2+2^2} = 1-4a\int_0^{\infty} \mathrm{d}u \frac{\mathrm{e}^{-au}}{u^2+2^2} = 1-2a[ci(2a)\sin(2a)-si(2a)\cos(2a)]. \tag{4.66}$$

Synchronization index γ is the square root of

$$\boxed{\gamma^2 = 1+4a^2(ci^2(2a)+si^2(2a))-4a[ci(2a)\sin(2a)-si(2a)\cos(2a)]} \tag{4.67}$$

where the expression in brackets equals auxiliary function f represented as an other integral, see [AS65] Chapter 5,

$$[\cdots] = \int_0^{\infty} \frac{\sin t}{t+2a}\,\mathrm{d}t = \int_0^{\infty} \frac{\mathrm{e}^{-2at}}{t^2+1}\,\mathrm{d}t. \tag{4.68}$$

For graphical representation, Ci and Si are well approximated by their respective Taylor expansions [AS65]:

$$Si(z) = \sum_{n=0}^{\infty} \frac{(-1)^n z^{2n+1}}{(2n+1)(2n+1)!} \quad \text{and} \quad Ci(z) = \gamma_{\mathrm{EM}} + \ln z + \sum_{n=1}^{\infty} \frac{(-1)^n z^{2n}}{(2n)(2n)!} \tag{4.69}$$

with Euler-Mascheroni constant γ_{EM}. As the Taylor expansion converges slowly for large arguments, it is beneficial to switch to a representation via auxiliary functions

$$f(z) = ci(z)\sin(z) - si(z)\cos(z) \quad \text{and} \quad g(z) = -ci(z)\cos(z) - si(z)\sin(z) \tag{4.70}$$

with (for $|\arg(z)| < \pi$)

$$f(z) \approx \frac{1}{z}\left(1 - \frac{2!}{z^2} + \frac{4!}{z^4} - \frac{6!}{z^6}\cdots\right), \quad g(z) \approx \frac{1}{z^2}\left(1 - \frac{3!}{z^3} + \frac{5!}{z^5} - \frac{7!}{z^7}\cdots\right). \tag{4.71}$$

Results from this and the previous section are compared in Fig. 4.13.

4.4.3.4 Comparison between numerical experiment and analytical model

Fig. 4.14 allows for a direct comparison of the results from Sect. 4.3 and from this analytic model. It is actually surprising, how well the experiment and analytical result coincide. First, note that the curves for all ensemble sizes collapse to a universal relation between synchronization index and ratio of natural frequency difference and intensity of fluctuations. Second see that little statistics is involved in the numerical analysis: For each ensemble size, merely one ensemble with one natural frequency sample was analyzed. Further investigations should test the robustness to changes, e.g. of the threshold below which γ was actually averaged.

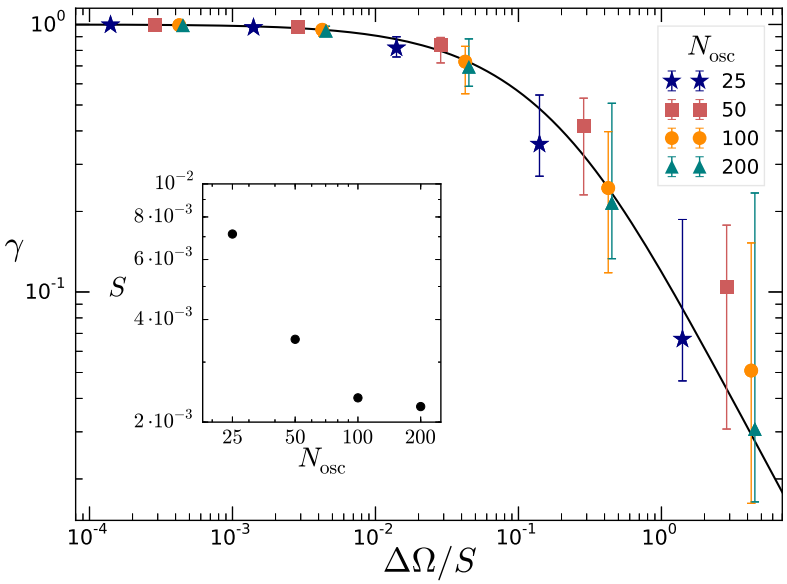

FIG. 4.14: Direct comparison of synchronization index γ between Fig. 4.8 and Fig. 4.13, see respective description. S in the inset is the variance of the active order parameter after cutting a transient. S in the main figure is either the same as in in the inset (for the comparison of ensemble sizes in the numerical experiments in Sect. 4.3), corresponding to all colored lines or it is the noise intensity in the analytical model, corresponding to the black line. The inset shows the scaling of the variance of the order parameter fluctuations with ensemble size. A deviation from the known $1/N$ law is due to having only one data point for each ensemble size.

4.5 Conclusion

In this chapter, we investigated the effect of finite-size fluctuations of the complex order parameter on Kuramoto oscillators.

In the first two sections, we compared the synchronizing effect of a) an ensemble with random Gaussian natural frequencies and b) an ensemble with equidistant natural frequencies at sub-critical coupling. In the letter case, fluctuations are considerably stronger. Especially in case a), fluctuations are weak compared to the typical natural frequency difference between asynchronous oscillators. We therefore let the fluctuating mean field act on passive Kuramoto oscillators that are mutually uncoupled. This principle allows for an arbitrary choice of natural frequency differences between the oscillators.

In the first section, we took snapshots of the phases of a large number of passive oscillators (with small natural frequency difference) against their natural frequency. In the Gaussian case, fluctuations are weak, so that only phases of oscillators with very small natural frequency difference are correlated and their phase difference is small for a comparably long time. In the equidistant ensemble, fluctuations are strong enough to generate correlation among oscillators with natural frequency differences of the order of about half of the maximal frequency difference in the active sample. While in the Gaussian case correlation is microscopic, in the equidistant case it turns out to be a macroscopic effect.

We quantified this correlation by a pairwise synchronization index. An additional transformation before applying this measure was necessary to stretch the phase distribution of the individual oscillators to an approximately uniform distribution. This transformation

accounts for the bias that occurs because all passive oscillators pass the same major bottleneck. The passive oscillators allowed us to measure correlation between oscillators with arbitrary natural frequency difference. We observe that the correlation decreases both with increasing natural frequency difference and with increasing frequency difference to the active mean field frequency. Furthermore, passive oscillators with natural frequencies in the vicinity of one of the active natural frequencies lock their frequency to the latter.

In the last section, we modeled the mean field fluctuations of the active ensemble by Gaussian white noise. We let this noise force act on a pair of passive oscillators with a small frequency difference. For this system, the Fokker-Planck equation of the difference and the sum of the two phases can be considerably simplified by applying multiple scale analysis. The static flux of the probability density of the phase difference then allows for an analytic expression of the synchronization index via trigonometric integrals. We found that the scaling of correlations with the pairwise ratio of natural frequency difference to noise intensity (or variance of order parameter fluctuations) coincides very well with our numerical results for the deterministic finite-size Kuramoto model.

Chapter 5

Discussion & Outlook

We here summarize and discuss the results of Chaps. 3 and 4 and comment on possibly viable lines of future research.

The main research question of this thesis was: How does the finite-size Kuramoto model relate to its infinite counterpart? Which additional effects emerge in the finite model that are absent in the infinite? And can some of the finite-size effects be translated to the infinite limit? We answered the first and the third question in Chap. 3, where we compared numerical results from finite ensembles to analytic results in the thermodynamic limit. The second question was discussed in Chap. 4, were we observed an unanticipated genuine finite-size effect, namely the ordering effect of the finite-size fluctuations of the Kuramoto order parameter.

In Chap. 3, we discussed the dynamics of the global mean field for Kuramoto ensembles of intermediate size ($\sim$ 25-200 oscillators). We revealed the connection between characteristics of the natural frequency sample and the resulting order parameter dynamics.

Like the Kuramoto ensemble in the thermodynamic limit, the finite system transitions from an incoherent to a partially synchronized state with increasing coupling strength. (Eventually, a fully synchronized state is always reached in the finite system, as is known from the infinite limit for frequency distributions with bounded support). The Kuramoto order parameter (that in infinite ensembles indicates this transition) fluctuates in finite ensembles and the transition is smeared out. Inspired by [TZT$^+$12], we defined an alternative indicator for the transition to a collective mode: the timely minimum of the order parameter after a transient. The new indicator allows to detect the critical coupling strength for the onset of a collective mode with arbitrary precision.

Our main result in this chapter was a generalization of some former publications that linked different natural frequency distributions to the corresponding order parameter dynamics.

First, we linked the shape of the natural frequency distribution to the curve progression of the order parameter with coupling strength. This result incorporates the former finding of a first-order transition for the uniform frequency distribution [Paz05] and puts it into relation with the long-known result for the Lorentz distribution [Kur75]. Extensive numerical experiments with finite Kuramoto ensembles of sizes between 25 and 200 oscillators uncovered the role of kurtosis of the natural frequency sample in the synchronization transition. In ensembles with negative excess kurtosis, i.e. platykurtic distributions like

the uniform distribution, some first portion of the oscillators synchronizes to a central synchronized cluster only at comparably strong coupling – and typically only slightly stronger coupling is necessary for synchronizing the entire ensemble. In contrast, in ensembles with leptokurtic natural frequency distribution, i.e. with positive excess kurtosis like the Laplace distribution, that have a central peak and fatter tails than the Gaussian distribution, oscillators close to the maximum of the distribution synchronize at comparably low coupling strength, but then all much stronger is required to synchronize oscillators in the tails.

A recent publication [Ska18] pronounced the importance of a generalization to a wider class of natural frequency distributions. They applied the Ott-Antonsen ansatz to a family of rational frequency distributions: $g_n(\omega) = n \sin(\pi/2n)\Delta^{2n-1}/\pi(\omega^{2n} + \Delta^{2n})$. The latter have poles, just as the Lorentz distribution, and therefore allow for closure of the mean field equations in the Ott-Antonsen framework [OA08]. Though the focus of that publication is different, their results confirm our findings on the effect of shape once again.

An open question at this point is the extension of this analysis to multimodal natural frequency distributions in the infinite case. The literature on this topic is restricted to combinations of Lorentz distributions, but reports on interesting results such as traveling waves and hysteresis [PM09, TIAY17]. A deeper understanding of the synchronization transition in ensembles with multimodal natural frequency distributions might also illuminate some questions in the finite model. Any finite sample can be considered as a multimodal distribution of equally weighted delta peaks. One question that remained unanswered in our analysis is the varying spread of the minimum of the order parameter at certain coupling strengths that could probably be explained by multistability due to the multimodality of the finite distribution.

As a second important result of Chap. 3, we linked the asymmetry of the natural frequency distribution to the mean frequency of the super-critical global phase. This is important, because almost all finite ensembles are asymmetric and the resulting drift of the mean field could not be explained otherwise. We found that the global phase ensembles with positively skewed natural frequency distribution rotate in mathematically negative direction, and vice versa. The absolute value of this rotation frequency is roughly proportional to the absolute value of the skewness of the sample. In perfectly symmetric samples, where for each natural frequency there exists exactly one natural frequency with the same absolute value but opposite sign, we observed that the super-critical global phase converges to a constant. A mathematical proof is still pending, but we here give the following heuristic explanation:

Let us suppose that for symmetry reasons, phases of pairs of oscillators i, j in such symmetric frequency samples with symmetric frequencies $\omega_i = -\omega_j$ are attracted to a dynamical state with a reflection symmetry of the individual phases with respect to the mean phase. (A reason for such attraction could lie the fluctuations of the forcing mean field as we discussed them in Chap. 4.) Apparently due to this attraction, the fluctuations in φ decay, also because on the attractor of partial synchrony, all pairs of oscillators have perfect reflection symmetry with respect to φ, and therefore $\varphi_2 \to 2\varphi$. Combining the model Eq. (2.3) and the definition for the order parameter in Eq. (2.4), the exact evolution equation for the global phase reads

$$\dot{\varphi} = \frac{1}{NR} \sum_i \omega_i \cos(\varphi - \theta_i) + \frac{\epsilon R_2}{2} \sin(2\varphi - \varphi_2) \tag{5.1}$$

The first term of the latter equation decays for pairs with $\omega_i = -\omega_j$ as $\varphi - \theta_i \to \theta_j - \varphi$. The second term vanishes because if $\theta_i = \varphi + \Delta\theta_i$ and $\theta_j = \varphi - \Delta\theta_i$ (i.e. if reflection symmetry of corresponding phases with respect to φ is fulfilled), then $\varphi_2 = \arg\left(\frac{1}{N}\sum_{i:\omega_i>0} \mathrm{e}^{\imath(2\varphi+2\theta_i)} + \mathrm{e}^{\imath(2\varphi-2\theta_i)}\right) = 2\varphi$. We see in the experiment that $2\varphi - \varphi_2 \to 0$ and that fluctuations of φ decay. The value the global phase φ converges to depends on the initial condition, due to the zero Lyapunov exponent corresponding to invariance to constant global phase shifts. A rigorous proof of this convergence to a constant super-critical global phase in perfectly symmetric samples should show that such a state is stable and attractive.

An open riddle that might be connected to such proof was posed in [CGP17]. The scaling of the largest Lyapunov exponent (LLE) with ensemble size (at sub-critical coupling strength) is $\sim \ln N/N$ or $\sim 1/N$ for regular or random samples, respectively (and the LLE is typically larger in random than in regular systems). The explanation might lie in the high symmetry of regular samples that might reduce the dynamics to a lower dimension in phase space.

Thinking the above discussions further, it seems quite plausible that kurtosis and asymmetry should have an effect on the size of the fluctuations of the global phase as well. To estimate the influence of kurtosis, take a small natural frequency sample with large kurtosis and therefore few extreme outliers. The latter will hardly be influenced by the central cluster of comparably small frequencies. Consequently, the motion is more regular and fluctuations are weaker, compare top and bottom panel in Fig. 3.2. The effect of skewness can be estimated under consideration of the convergence of the super-critical global phase in perfectly symmetric samples: when phase fluctuations vanish for samples with perfect symmetry they should stay small for a sample with tiny asymmetry.

In Chap. 4, we investigated the effect of finite-size fluctuations in the Kuramoto model. From former publications, we knew of the effect of noise-induced synchronization. We chose two types of ensembles: one with random Gaussian natural frequency sample at super-critical coupling strength and one with equidistant natural frequencies at sub-critical coupling strength. Especially in the former case, fluctuations are weak compared to the typical natural frequency difference among the asynchronous oscillators. We therefore let the fluctuating mean-field of few such oscillators act on uncoupled *passive* Kuramoto oscillators with freely eligible natural frequency difference.

The main work in this chapter consisted of observing and quantifying the correlations among pairs of such passive oscillators. We also modeled the fluctuating mean field as Gaussian white noise and again quantified the correlation among the noise driven passive oscillators, and found very good agreement with the numerical experiment. In both the deterministic and the stochastic model, the degree of correlation depends mostly on the ratio of the natural frequency difference of the passive oscillators and the variance of fluctuations (or the noise intensity). Prior to the application of the correlation measure, we needed to stretch the phase distributions of passive oscillators with a given natural frequency to a uniform phase distribution. We did so using the Möbius transform – a technique applied in time series analysis to obtain the phase from the protophase [KCR+08].

We first discuss the deterministic case of an active Kuramoto ensemble with Gaussian distributed frequencies at super-critical coupling, where a central cluster is already formed. Other than in the stochastic case, the behavior of the passive oscillators depends not only on pairwise frequency difference but also from the frequencies themselves. Passive oscillators with natural frequency close to the natural frequency of one of the active oscillators lock their observed frequency to the observed frequency of this active oscillator. This also means that the passive oscillators lock to the central cluster of the active ensemble. We therefore only consider a range of natural frequencies in which the active oscillators rotate asynchronously. Passive oscillators with natural frequency sufficiently (depending on the coupling strength) different from any of the active natural frequencies are predominantly influenced by the chaotic (or noisy) components of the driving. This fluctuating forcing joins phases, as we see directly in the phase versus natural frequency plane for the passive oscillators. Our synchronization index measures finite correlation among pairs of passive oscillators. It increases with decreasing natural frequency difference and decreases with increasing frequency detuning to the active mean field frequency.

Let us compare these observations to the traditional picture of the Kuramoto model which stems from the solutions in the thermodynamic limit. There, the complex Kuramoto order parameter assumes a constant absolute value and rotates at constant speed. The oscillators in this ensemble are effectively decoupled. They separate in two groups – synchronous and asynchronous. The synchronous oscillators lock to the global phase and are immobile in the corresponding reference frame – a perfectly ordered state. The asynchronous oscillators slow down close to the mean field phase but periodically perform phase slips that get more frequent with larger natural frequency difference to the global mean field frequency. Asynchronous oscillators with different natural frequencies therefore also have different observed frequencies and pairwise correlation among them (again, after a transformation that smooths the phase evolution to uniform rotation) averages to zero – reflecting perfect disorder.

In the finite model, in contrast, this clear distinction between ordered and disordered state does not hold. Finite-size fluctuations generate correlations among otherwise uncoupled oscillators (in the range of natural frequencies where active oscillators rotate asynchronously), thereby creating order. Also, the synchronous oscillators are not perfectly ordered. As long as the order parameter fluctuates, a varying number of oscillators fulfills the synchronization condition and the phase differences between the locked oscillators fluctuates. The traditional picture of order and disorder in the Kuramoto model (for synchronous and asynchronous oscillators, respectively) does consequently not hold in the finite case. We expect that such an ordering effect of inherent fluctuations is not restricted to mean field models.

As a consequence, questions that are already hard to answer in the infinite case, all the more elude analytical comprehension in the finite case. This is true for statements about the stability of the partially synchronized state, and thereby the question of the existence of a finite minimum of the order parameter(see Sect. 3.1) or the related question of the exact value of critical coupling in the $R_{\min}$-sense. In Sect. 3.6, we gave an analytic expression for the volume contraction in phase space that might hint to solutions for these questions.

In Fig. 4.5, we juxtaposed the observed frequencies of the active and passive oscillators with the power spectrum of the active complex mean field. It seems that the noise intensity decays with increasing frequency. We conjecture as an idea for future investigations that

the decay of the power spectrum of the active mean fields' order parameter with increasing frequency (which might correspond to pink noise) acts stronger on smaller frequencies – which is a possible explanation for the decay of the synchronization index with distance to the central synchronized cluster.

We now discuss the the deterministic case of an active ensemble with equidistant natural frequencies at sub-critical coupling. Prior to the critical transition, which in the thermodynamic limit corresponds to a first order phase transition, fluctuations are particularly strong – much stronger than in the super-critical Gaussian ensemble of the same size. The resulting correlation is macroscopic: it spans approximately half of the natural frequency range of the active oscillators. We plan to carry out further investigations in the equidistant case:

- We want to discuss the scaling of the synchronizing effect with $(\epsilon_c - \epsilon)$. An imminent problem is the failing of the Möbius transform as a suitable transform to a uniform density of phases close to ϵ_c – here we need to find an alternative.
- A white noise approximation might have oversimplified important details of the order parameter dynamics in the equidistant model. Fig. 4.9 (bottom panel) shows that the order parameter time series has a sizeable autocorrelation. It would therefore be interesting to test the stochastic model with more realistic noise spectra.

Finally, we tentatively suggest that the results of this thesis could also be interpreted as a contribution to the modeling of opinion dynamics. In [HS11], the public discourse was modeled by a mixture of troublemakers who want to prevent consensus by all means (with negative coupling) and others that strive for nothing but harmony (with positive coupling) – otherwise identical townsmen. We propose that more realistic (and still analytically tractable) social models could be achieved by including passive oscillators: Our non-identical passive oscillators could represent individuals of a broader mass in which the public discourse is led by few active oscillators, be it media owners, influencers on social media, or influential organizations whose purview exceeds the number of its actual memberships.

As a final conclusion we state that answering scientific questions is like pruning a plant: the cutting back encourages the growth of new vines.

Appendix A

Analytical Calculations

A.1 The asynchronous integral

Using symmetry arguments and applying the Weierstrass substitution solves the asynchronous integral over ψ in (3.19).

$$\frac{1}{2\pi}\int_{-\pi}^{\pi} \mathrm{e}^{\imath\psi}\frac{1}{|\omega-\Omega-a\sin\psi|}\,\mathrm{d}\psi = \frac{1}{2\pi a}\int_{-\pi}^{\pi} \mathrm{e}^{\imath\psi}\frac{1}{|A-\sin\psi|}\,\mathrm{d}\psi \tag{A.1}$$

where $A=(\omega-\Omega)/a$ and $|A|>1$. The integral over the cosine vanishes due to symmetry. For the integral over the sine, we treat case $A>1$ first, to then conclude on case $A<-1$. We have

$$\int_{-\pi}^{\pi}\frac{\sin\psi}{A-\sin\psi}\,d\psi = -\int_{-\pi}^{\pi}\frac{A-\sin\psi-A}{A-\sin\psi}\,\mathrm{d}\psi = -2\pi + A\int_{-\pi}^{\pi}\frac{1}{A-\sin\psi}\,\mathrm{d}\psi = \dots \tag{A.2}$$

Substitution now the tangent half-angle

$$t=\tan\left(\frac{\psi}{2}\right),\quad \frac{\mathrm{d}t}{\mathrm{d}\psi}=\frac{1+t^2}{2},\quad \sin\psi=\frac{2t}{1+t^2} \tag{A.3}$$

we get

$$\dots = -2\pi + 2A\int_{-\infty}^{\infty}\frac{1}{A(1+t^2)-2t}\,dt = -2\pi + 2\int_{-\infty}^{\infty}\frac{1}{1+t^2-2t/A}\,dt \tag{A.4}$$

$$= -2\pi + \frac{2A}{2i\sqrt{A^2-1}}\int_{-\infty}^{\infty}\left(\frac{1}{t-t_o^+}-\frac{1}{t-t_o^-}\right)dt \quad \text{where} \quad t_o^{\pm}=\frac{1\pm i\sqrt{A^2-1}}{A} \tag{A.5}$$

Complex integration over, e.g., the upper half plane with the isolated singular pole t_o^+ gives $2\pi i$ and we end up with

$$\int_{-\pi}^{\pi}\frac{\sin\psi}{A-\sin\psi}\,d\psi = -2\pi + \frac{A}{i\sqrt{A^2-1}}2\pi i = 2\pi\left(-1+\frac{A}{\sqrt{A^2-1}}\right) \tag{A.6}$$

Equivalently, for $A<-1$ we obtain

$$\int_{-\pi}^{\pi}\frac{\sin\psi}{|A|+\sin\psi}\,d\psi = 2\pi\left(1-\frac{|A|}{\sqrt{|A|^2-1}}\right) \tag{A.7}$$

and the full SCE - integral for the asynchronous oscillators is purely imaginary:

$$\begin{aligned} I_{\text{as}} &= \frac{1}{2\pi}\int_{-\pi}^{\pi} \mathrm{e}^{\imath\psi}\left(\int_{|\omega-\Omega|>a} \mathrm{d}\omega\, g(\omega)\,\frac{\sqrt{(\omega-\Omega)^2-a^2}}{|\omega-\Omega-a\sin\psi|}\right) d\psi \\ &= \frac{i}{a}\int_{a+\Omega}^{\infty} \mathrm{d}\omega\, g(\omega)\,\left((\omega-\Omega)-\sqrt{(\omega-\Omega)^2-a^2}\right) \\ &\quad + \frac{i}{a}\int_{-\infty}^{-a+\Omega} \mathrm{d}\omega\, g(\omega)\,\left((\omega-\Omega)+\sqrt{(\omega-\Omega)^2-a^2}\right) \end{aligned} \tag{A.8}$$

A.2 Moments of the Subbotin family of distributions

We here calculate the relation between parameters of the Subbotin family to central (not standardized) moments μ_i for $i = 0, ...4$. We will often make use of the gamma function relation

$$\Gamma(z+1) = z\cdot\Gamma(z) \tag{A.9}$$

First, we check the normalization. We integrate the un-normalized symmetric frequency distribution

$$\int_{-\infty}^{\infty} p(x)\mathrm{d}x = 2\int_{0}^{\infty} p(x)\mathrm{d}x = 2\int_{0}^{\infty} \mathrm{e}^{-\frac{|x-\mu|^p}{p\,\sigma_p^p}}\,\mathrm{dx}. \tag{A.10}$$

In the following, we set mean $\mu = \underline{\underline{\mu_1 = 0}}$. With the help of a transformation of the exponent to a new variable

$$y = \frac{x^p}{p\,\sigma_p^p}, \tag{A.11}$$

over which we perform the integration, converts the integral to a Gamma function.

$$y' = \frac{x^{p-1}}{\sigma_p^p} = \frac{(y\cdot p\cdot\sigma_p^p)^{\frac{p-1}{p}}}{\sigma_p^p} = \frac{y^{\frac{p-1}{p}}\cdot p^{\frac{p-1}{p}}}{\sigma_p} \tag{A.12}$$

Such that we finally obtain

$$\underline{\underline{\mu_0}} = \int_{-\infty}^{\infty} p(x)\mathrm{d}x = 2\,\sigma_p\,p^{\frac{1}{p}-1}\underbrace{\int_0^{\infty} y^{\frac{1}{p}-1}\,\mathrm{e}^{-y}dy}_{\Gamma\left(\frac{1}{p}\right)=p\cdot\Gamma\left(1+\frac{1}{p}\right)} = \frac{2\sigma_p}{p^{1-1/p}}\Gamma(1/p) = \underline{\underline{2\,\sigma_p p^{\frac{1}{p}}\Gamma\left(1+\frac{1}{p}\right)}} \tag{A.13}$$

The variance is given by the second moment integral, for which we can again use the reflection symmetry w.r.t. $x = 0$.

$$\int_{-\infty}^{\infty} x^2\,p(|x|)\,\mathrm{d}x = 2\int_{0}^{\infty} x^2\,p(x)\,\mathrm{d}x \tag{A.14}$$

in our case

$$\mu_2 = \sigma^2 = \frac{1}{\sigma_p p^{1/p}\Gamma(1+\frac{1}{p})}\int_0^{\infty} x^2\,\mathrm{e}^{-\frac{x^p}{p\,\sigma_p^p}}\,\mathrm{d}x \tag{A.15}$$

We substitute

$$y(x) = \frac{x^p}{p\,\sigma_p^p} \quad \rightarrow \quad \frac{\mathrm{d}y}{\mathrm{d}x} = \frac{x^{p-1}}{\sigma_p^p}, \quad y(0) = 0, \quad y(x \to \infty) \to \infty \tag{A.16}$$

by which the second central moment reads

$$\underline{\underline{\mu_2}} = \frac{1}{\sigma_p p^{1/p} \Gamma(1+\frac{1}{p})} \int_0^\infty \frac{x^2\,\sigma_p^p}{x^{p-1}}\,\mathrm{e}^{-y}\,\mathrm{d}y \qquad \left| \quad \frac{x^2\,\sigma_p^p}{x^{p-1}} = \frac{\sigma_p^p}{x^{p-3}} = \frac{\sigma_p^p}{(y\,p\,\sigma_p^p)^{-3}} = (yp)^{\frac{3}{p}-1}\,\sigma_p^3 \right. \tag{A.17}$$

$$= \frac{p^{\frac{2}{p}-1}\,\sigma_p^2}{\Gamma(1+\frac{1}{p})} \int_0^\infty y^{\frac{3}{p}-1}\,\mathrm{e}^{-y}\,\mathrm{d}y \Bigg| \quad \Gamma(z+1) = \int_0^\infty y^z\,\mathrm{e}^{-y}\,\mathrm{d}y \overset{z+1=3/p}{=} \Gamma(\frac{3}{p}) \tag{A.18}$$

$$= \frac{p^{\frac{2}{p}-1}\,\sigma_p^2}{\Gamma(1+\frac{1}{p})}\Gamma(\frac{3}{p}) = \underline{\underline{\frac{p^{\frac{2}{p}}\,\sigma_p^2}{\Gamma(1+\frac{1}{p})}\Gamma(1+\frac{3}{p}) \cdot \frac{1}{3}}} \tag{A.19}$$

In our model, a non-unity variance is a redundant parameter, which we can get rid of by rescaling time and coupling strength. To obtain $\sigma^2 \equiv 1$, we have to force

$$\underline{\underline{\sigma_p^2}} = \frac{\Gamma(1+\frac{1}{p})}{\Gamma(1+\frac{3}{p})} p^{-2/p} \cdot 3 \quad \Rightarrow \quad \sigma_p = \sqrt{3\frac{\Gamma(1+\frac{1}{p})}{\Gamma(1+\frac{3}{p})}} \cdot p^{-1/p}. \tag{A.20}$$

The third moment obviously vanishes, as the distribution is symmetric, $\underline{\underline{\mu_3 = 0}}$. The fourth moment is

$$\mu_4 = \frac{1}{\sigma_p p^{1/p} \Gamma(1+\frac{1}{p})} \int_0^\infty x^4\,\mathrm{e}^{-\frac{x^p}{p\,\sigma_p^p}}\,\mathrm{d}x \tag{A.21}$$

with the transformation

$$y(x) = \frac{x^p}{p\,\sigma_p^p} \quad \rightarrow \quad \frac{\mathrm{d}y}{\mathrm{d}x} = \frac{x^{p-1}}{\sigma_p^p} = x^4 \cdot \frac{x^{p-5}}{\sigma_p^p} = (yp)^{1-\frac{5}{p}}\,\sigma_p^5 \cdot x^4 \tag{A.22}$$

gives

$$\underline{\underline{\mu_4}} = \frac{\sigma_p^4\,p^{\frac{4}{p}-1}}{\Gamma(1+\frac{1}{p})} \cdot \Gamma(\frac{5}{p}) \tag{A.23}$$

from which, inserting σ_p as above, we can derive kurtosis and excess kurtosis

$$\beta_2 = \frac{\mu_4}{\mu_2^2} = \frac{\Gamma\left(\frac{1}{p}\right)\Gamma\left(\frac{5}{p}\right)}{\left(\Gamma\left(\frac{3}{p}\right)\right)^2} \quad \text{and} \quad \gamma_2 = \beta_2 - 3. \tag{A.24}$$

A.3 Evolution of Möbius transformed phase

Starting from Eq. (4.11), we first shift phases ψ_i such that the drift term depends on the cosine of the phase instead of sine:

$$\tilde{\psi}_i = \psi_i - \frac{\pi}{2}, \tag{A.25}$$

such that

$$\dot{\tilde{\psi}}_i = \Omega_i + h\,\cos\tilde{\psi}_i + \frac{a}{2}\,\cos\tilde{\psi}_i\,\xi_1 - \frac{b}{2}\,\sin\tilde{\psi}_i\,\xi_2 + \chi \tag{A.26}$$

We apply the Möbius transform in the form

$$\tan\frac{\varphi_i}{2} = \sqrt{\frac{\Omega_i - h}{\Omega_i + h}}\,\tan\frac{\tilde{\psi}_i}{2}. \tag{A.27}$$

Thee transformed phases evolve according to

$$\frac{\mathrm{d}}{\mathrm{d}t}\left(\tan\frac{\varphi}{2}\right) = \left(1+\tan^2\frac{\varphi}{2}\right)\,\frac{\dot{\varphi}}{2} = \sqrt{\frac{\Omega-h}{\Omega+h}}\frac{\mathrm{d}}{\mathrm{d}t}\left(\tan\frac{\tilde{\psi}}{2}\right) = \sqrt{\frac{\Omega-h}{\Omega+h}}\left(1+\tan^2\frac{\tilde{\psi}}{2}\right)\,\frac{\dot{\tilde{\psi}}}{2}$$

where we dropped indeces i.

$$\dot{\varphi} = \sqrt{\frac{\Omega-h}{\Omega+h}}\,\frac{1+\tan^2\frac{\tilde{\psi}}{2}}{1+\tan^2\frac{\varphi}{2}}\,\dot{\tilde{\psi}}.$$

Now, inserting time evolution of $\tilde{\psi}$ yields

$$\dot{\varphi} = \sqrt{\frac{\Omega-h}{\Omega+h}}\,\frac{1+\tan^2\frac{\tilde{\psi}}{2}}{1+\tan^2\frac{\varphi}{2}}\,\left(\Omega + h\,\cos\tilde{\psi} + \frac{a}{2}\,\cos\tilde{\psi}\,\xi_1 - \frac{b}{2}\,\sin\tilde{\psi}\,\xi_2 + \chi\right) \tag{A.28}$$

Then, using half tangent relations

$$\cos\alpha = \frac{1-\tan^2\frac{\alpha}{2}}{1+\tan^2\frac{\alpha}{2}} \quad \text{and} \quad \sin\alpha = \frac{2\tan\frac{\alpha}{2}}{1+\tan^2\frac{\alpha}{2}} \tag{A.29}$$

and inserting the Möbius transform we get

$$\dot{\varphi} = \sqrt{\frac{\Omega-h}{\Omega+h}}\,\frac{1+\frac{\Omega+h}{\Omega-h}\tan^2\frac{\varphi}{2}}{1+\tan^2\frac{\varphi}{2}}\,\left(\Omega + (h\,+\frac{a}{2}\xi_1)\frac{1-\frac{\Omega+h}{\Omega-h}\tan^2\frac{\varphi}{2}}{1+\frac{\Omega+h}{\Omega-h}\tan^2\frac{\varphi}{2}}\,-\frac{b}{2}\frac{2\sqrt{\frac{\Omega+h}{\Omega-h}}\tan\frac{\varphi}{2}}{1+\sqrt{\frac{\Omega+h}{\Omega-h}}\tan^2\frac{\varphi}{2}}\,\xi_2 + \chi\right)$$

canceling terms and multiplying out

$$\begin{aligned}\dot{\varphi} = \sqrt{\frac{\Omega-h}{\Omega+h}}\,\frac{1}{1+\tan^2\frac{\varphi}{2}}\Bigg(&\Omega + \Omega\frac{\Omega+h}{\Omega-h}\tan^2\frac{\varphi}{2} + h\left[1-\frac{\Omega+h}{\Omega-h}\tan^2\frac{\varphi}{2}\right]\\ &+\frac{a}{2}\left[1-\frac{\Omega+h}{\Omega-h}\tan^2\frac{\varphi}{2}\right]\xi_1 - \frac{b}{2}2\sqrt{\frac{\Omega+h}{\Omega-h}}\,\tan\frac{\varphi}{2}\,\xi_2 + \chi\Bigg)\end{aligned}$$

The terms in the first line simplify considerably, and also the a, b terms in the second line can be expressed much simpler by $\cos\varphi$, $\sin\varphi$:

$$\begin{aligned}\dot{\varphi} &= \sqrt{\frac{\Omega-h}{\Omega+h}}\,\frac{1}{1+\tan^2\frac{\varphi}{2}}\left(\Omega + h + (\Omega-h)\frac{\Omega+h}{\Omega-h}\tan^2\frac{\varphi}{2}\right)\\ &\quad + \frac{a}{2}\frac{1}{\sqrt{\Omega^2-h^2}}\,\frac{\Omega-h-(\Omega+h)\tan^2\frac{\varphi}{2}}{1+\tan^2\frac{\varphi}{2}}\xi_1 - \frac{b}{2}\sin\varphi\,\xi_2 + \sqrt{\frac{\Omega-h}{\Omega+h}}\,\frac{1}{1+\tan^2\frac{\varphi}{2}}\chi\\ &= \sqrt{\Omega^2-h^2} + \frac{a}{2}\frac{1}{\sqrt{\Omega^2-h^2}}\,(\Omega\,\cos\varphi - h)\,\xi_1 - \frac{b}{2}\sin\varphi\,\xi_2 + \sqrt{\frac{\Omega-h}{\Omega+h}}\,\frac{1}{1+\tan^2\frac{\varphi}{2}}\chi\end{aligned} \tag{A.30}$$

Finally the χ term has the same cosine form as the a-term:

$$\boxed{\dot{\varphi}_i = \sqrt{\Omega_i^2 - h^2} + \frac{1}{\sqrt{\Omega_i^2 - h^2}} \left(\Omega_i \cos\varphi_i - h\right) \left[\frac{a}{2}\xi_1 + \chi\right] - \frac{b}{2} \sin\varphi_i \, \xi_2} \tag{A.31}$$

Appendix B

Protocols of numerical experiments

B.1 Standard deviation of $\epsilon(R_{\min} = 0.2)$ with error

The inset of Fig. 3.7 shows the scaling of the spread of the coupling strengths at which different samples of a Gaussian natural frequency distribution reach a certain degree of synchronization ($R_{\min} = 0.2$) with ensemble size. The data analysis strategies in preparation for Fig. 3.5 differs between data for $N = 25, 50, 100, 200$ and higher N. This has practical reasons. For the smaller ensembles, we already scanned the whole ϵ-range to get a general picture. For the larger ensembles, we are only interested in the scaling with N for certain observed effects:

1. How does the critical coupling for the $R_{\min}$-parameter depend on different properties of the natural frequency distribution? – We saw the connection to the kurtosis of the sample and we also discuss it in the infinite case.

2. How does the standard deviation of $R_{\min}$ at the horizontal cut depend on the system size (and does that fit to how the spread of the kurtosis in a Gaussian sample depends on the sample size?)

To save computational power, we use for $N = 25$, 50, 100, 200 the time series that we generated for Fig. 3.5, see following Sect. B.1.1, and for $N = 400$, 800, 1600 a bisection method, see following Sect. B.1.2.

B.1.1 Standard deviation and error for $N = 25$, 50, 100, 200

We use the same $R_{\min}$'s as in Fig. 3.5 to quantify the spread of coupling strengths at which $R_{\min} \approx 0.2$ for $N = 25$, 50, 100, and 200. For each natural frequency sample, i.e. for each curve $R_{\min}(\epsilon)$, we first check, how often the horizontal line at 0.2 is crossed; which is necessary because $R_{\min}(\epsilon)$ is in general not monotonous, especially for smaller ensembles. For all samples, and all N's, it was only crossed once. In the grid of coupling strengths, we search for the first change in sign of $(R_{\min} - 0.2)$ (let us call the preceding minimum of order parameter R_{low} and the first above the threshold R_{up}), for each of the $N_{g(\omega)}$ natural frequency samples. Between that and the preceding ϵ in the grid, we interpolate $R_{\min}(\epsilon)$ linearly and save the coupling strength at which the resulting line crosses $R_{\min} = 0.2$. The error of this method is largest when the slope of this line is smallest. We estimate the error of each of $N_{g(\omega)}$ crossing coupling strengths (label i) by the error of $R_{\min}$, $\Delta R^i_{\min} \sim (R_{\text{up}} - R_{\text{low}})/2$ by following standard error analysis $\Delta\epsilon_i = |\partial\epsilon_i/\partial R^i_{\min}|\,\Delta R^i_{\min}$ and thereby the four standard errors for the four different ensemble sizes are estimated as $\Delta\sigma = \sum_i |\partial\sigma/\partial\epsilon_i|\,\Delta\epsilon_i = \sum_i |\epsilon_i - \bar{\epsilon}|/(N_{g(\omega)} \cdot \sigma)\,\Delta\epsilon_i$.

B.1.2 Standard deviation and error for $N = 400, 800, 1600$

For larger sample sizes, two reasons motivate us to change the scheme by which we obtain $\epsilon(R_{\min} = 0.2)$ for different natural frequency samples for larger sample sizes. First, the

computational power of the RK4-integration of the globally coupled Kuramoto model scales linearly with ensemble size, but the computational power needed for 10^7 time steps is already high for only 25 oscillators. Second, $R_{\min}$ grows more likely monotonously (perhaps because multi-modality occurs more unlikely?). We can therefore apply a bisection method. From Fig. 3.5, we estimate an interval of coupling strengths in which the $R_{\min}(\epsilon)$-curves likely cross the arbitrary threshold of $R_{\min} = 0.2$. For 400 oscillators, we expect crossings in $[1.1, 1.9]$, for 800 in $[1.46, 1.82]$, and for 1600 in $[1.4, 1.8]$. The bisection starts at the self-consistent value in the infinite case $\epsilon = 1.5957$. For each frequency sample, at each step, the program generates a time series of 10^7 RK4 time steps of size 0.01 and measures $R_{\min}$ after a transient of 10^4 time steps. If $R_{\min}$ falls below 0.19, we save additional computation time by aborting the time series. Then, we choose a new ϵ value between the current and either the upper or the lower value, depending on whether $R_{\min}$ was smaller or larger than 0.2. All time evolutions start from the same initial condition This process loops until either the algorithm gets stuck – in which case we asymmetrically shift upper and lower bound by $+0.03$ and -0.02, respectively – or until $|R_{\min} - 0.2| < 0.01$. This procedure results in a statistic of $(R_{\min} = 0.2)$-coupling strengths for 100 frequency distribution samples $\{\omega\}$ for each of $N = 400$, 800, 1600 (i.e. in a set of pairs $\epsilon_i, \{\omega\}_i$). The inset contains both the standard deviation of these 100 values and the corresponding error bars, estimated again by means of standard error analysis. From $\sigma^2 = \sum_i (\epsilon_i - \bar{\epsilon})^2 / N_{g(\omega)}$ with $N_{g(\omega)}$ natural frequency samples and therefore the standard error of the standard deviation can be approximated as $\Delta\sigma = \sum_i |\partial\sigma/\partial\epsilon_i| \, \Delta\epsilon_i = \sum_i |\epsilon_i - \bar{\epsilon}| / (N_{g(\omega)} \cdot \sigma) \, \Delta\epsilon$ where we approximate $\Delta\epsilon$ to be 0.001 from the difference of coupling strengths between the penultimate and the ultimate step before reaching $R_{\min} = 0.2$.

B.2 Synchronization index γ in active-passive system

Active natural frequencies are a) randomly sampled from a Gaussian distribution with variance one and mean zero and b) equidistant in $[-1, 1]$. Around 110 natural frequencies equidistant in a) $[0.8, 3.]$ and b) $[-1, 1]$, we symmetrically place pairs of passive oscillators whose natural frequencies have differences a) $\Delta\Omega = 10^{-2}$ to 10^{-6} an b)$\Delta\Omega = 1$ to 10^{-3}, respectively. The coupling strength of a) 1.85 b) 1.25 is a) super- b) sub-critical for the respective natural frequency samples. A transient of 10^4 is omitted. We use a Runge-Kutta scheme of order 4 with step size 0.01. Over an averaging time a) $2 \cdot 10^7$ and b) 10^6, we use every hundredth step to average the timely order parameter $z_i = \langle \mathrm{e}^{\imath(\varphi_i(t) - \phi_{\mathrm{act}}(t))} \rangle_t$ for each individual passive oscillator, where we subtract the active mean field in each time step. The resulting complex value is the parameter in transform Eq. (4.4), again after subtracting the mean field phase $\varphi_i(t) - \phi_{\mathrm{act}}(t)$. Finally, we evaluate synchronization index γ, see Eq. (4.5) for pairs of transformed passive phases. We display $|z_i|$ before and after transformation, see Fig. 4.6 to illustrate the success of the transformation, i.e. to show that phases indeed rotate approximately uniformly after transformation.

Acknowledgements

In the first place, I thank Prof. Arkady Pikovsky for taking me in his group and for his supervision. He is an exceptional researcher, not only by his admirable work and his intellectual power. He is also extremely quick in revising and answers questions the next day (latest!) with a complete analytical calculation and numerical evidence. He finds the key points in a haystack of questions and ideas. I am thankful for this lucky twist of fate that transferred me into the abandoned Golmer Luch. I thank Prof. Pikovsky for the evermore interesting topic. Also for opening doors to the community of biological rhythms on a conference already in the second week of my PhD and for including me in the COSMOS activities.

I thank Prof. Pikovsky, Dr. Michael Zaks and Prof. Andrzejak for their evaluation.

I want to thank Prof. Elbert Einstein Nehrer Macau and Jürgen Kurths for the organization of the graduate school IRTG 1740, and Prof. Arkady Pikovsky for granting me six additional months that resulted in a beautiful paper.

Prof. Macau and his department LAC in São José dos Campos, Brazil, gave me an incredibly warm welcome in their round. The stay there, in which I could freely use their computer cluster and in which I had several opportunities to give talks raised my confidence as a scientist. But more than that, it makes me still happy that I met all these wonderful people.

A bit delayed, I want to thank my maths teacher Prof. Werner Timmermann again for teaching me this beautiful language in an elegant and rigorous way and for being an example in many ways. He would be surprised how often I think back to this four-semester journey – I am deeply grateful.

Thanks to my group, especially Ralf Tönjes for all the scientific coffee sessions, and all of you for being so pleasant fellows. I did very much enjoy the time with you.

Meiner geliebten Familie danke ich aufs herzlichste für die Unterstützung, etwaige Mini-Rosinenbomben und ein rotes Telefon in der heißen Phase.

Auch Friedrichs Familie danke froh ich für ihre Unterstützung, für die schöne Zeit, für den Arbeitsplatz im Garten, und ihre vielen Fragen zu meiner Forschung.

Danke A.-S. R., T. D., M. S., T. K., C. B., J. S., F. A., C. S., und H. R., A. N., C. N., und C. H. dafür dass es euch gibt und ihr mich so froh macht.

Friedrich, Du bist die wunderbarste Freude; – das Glück das ich mit Dir habe ist eine Quelle der Energie «die nie verströmt» – quasi Kernfusion. Danke für's Gegenlesen und dafür, dass ich mich am Ende wirklich ganz auf die Arbeit konzentrieren konnte.

Bibliography

[ABV+05] Juan A. Acebrón, L. L. Bonilla, Conrad J Pérez Vicente, Félix Ritort, and Renato Spigler. The Kuramoto model: A simple paradigm for synchronization phenomena. *Reviews of Modern Physics*, 77(1):137–185, 2005.

[Adl46] R. Adler. A study of locking phenomena in oscillators. *Proceedings of the IRE*, 34(6):351–357, June 1946.

[AKM+08] Alex Arenas, Jürgen Kurths, Yamir Moreno, Albert Díaz-Guilera, and Changsong Zhou. Synchronization in complex networks. *Physics Reports*, 469(3):1–56, 2008.

[AS65] M. Abramowitz and I. Stegun. *Handbook of Mathematical Functions*. Dover Publications, 1965.

[AS04] Daniel M. Abrams and Steven H. Strogatz. Chimera states for coupled oscillators. *Phys. Rev. Lett.*, 93:174102, Oct 2004.

[Azz13] Adelchi Azzalini. *The Skew-Normal and Related Families*. Cambridge University Press, Part of Institute of Mathematical Statistics Monographs edition, 2013.

[Bar13] Gilad Barlev. *Synchronization of Network Coupled Chaotic and Oscillatory Dynamical Systems*. PhD thesis, University of Maryland, 2013.

[BBH+81] John Buck, Elisabeth Buck, Frank E. Hanson, James F. Case, Laurens Mets, and George J. Atta. Control of flashing in fireflies. *Journal of comparative physiology*, 144(3):277–286, Sep 1981.

[BBW00] Martin Bier, Barbara M. Bakker, and Hans V. Westerhoff. How yeast cells synchronize their glycolytic oscillations: A perturbation analytic treatment. *Biophysical Journal*, 78(3):1087 – 1093, 2000.

[BCC01] James Blowey, John P. Coleman, and Alan W. Craig. *Theory and Numerics of Differential Equations*. Durham 2000, Universitext, Springer-Verlag Berlin Heidelberg, 1. edition, 2001.

[BM88] Kevin P. Balanda and H. L. MacGillivray. Kurtosis: A critical review. *The American Statistician*, 42(2):111–119, 1988.

[BPM18] C. Bick, M. J. Pannaggio, and E. A. Martens. Chaos in Kuramoto oscillator networks. *Chaos*, 28:071102, 2018.

[BU07] Lasko Basnarkov and Viktor Urumov. Phase transitions in the Kuramoto model. *Phys. Rev. E*, 76(5):1–4, 2007.

[BU08] Lasko Basnarkov and Viktor Urumov. Kuramoto model with asymmetric distribution of natural frequencies. *Phys. Rev. E*, 78:011113, Jul 2008.

[BUTN13] Sz Boda, Sz Ujvári, A Tunyagi, and Z Néda. Kuramoto-type phase transition with metronomes. *European Journal of Physics*, 34(6):1451, 2013.

[CDJ17] Tommaso Coletta, Robin Delabays, and Philippe Jacquod. Finite-size scaling in the Kuramoto model. *Phys. Rev. E*, 95:042207, Apr 2017.

[CGP17] Mallory Carlu, Francesco Ginelli, and Antonio Politi. Origin and scaling of chaos in weakly coupled phase oscillators. *Phys. Rev. E*, 97, 10 2017.

[CHB12] P. M. R. Clarke, S. P. Henzi, and L. Barrett. Estrous synchrony in a nonseasonal breeder: adaptive strategy or population process? *Behavioral Ecology*, 23(3):573–581, 2012.

[Chi00] M. Chiodi. Le curve normali di ordine p come distribuzioni di errori accidentali: una rassegna dei risultati e problemi aperti per il caso univariato e per quello multivariato. pages 289–300, Firenze, 2000. In "Atti della XL Riunione Scientifica della SIS".

[Chi15] Hayato Chiba. A proof of the Kuramoto conjecture for a bifurcation structure of the infinite-dimensional Kuramoto model. *Ergodic Theory and Dynamical Systems*, 35(3):762–834, 2015.

[CHK13] Chulho Choi, Meesoon Ha, and Byungnam Kahng. Extended finite-size scaling of synchronized coupled oscillators. *Phys. Rev. E*, 88(3):1–8, 2013.

[CPR16] Pau Clusella, Antonio Politi, and Michael Rosenblum. A minimal model of self-consistent partial synchrony. *New Journal of Physics*, 18(9):093037, 2016.

[Cra94] John David Crawford. Amplitude expansions for instabilities in populations of globally-coupled oscillators. *Journal of Statistical Physics*, 74(5):1047–1084, Mar 1994.

[Dai86] Hiroaki Daido. Discrete-time population dynamics of interacting self-oscillators. *Progress of Theoretical Physics*, 75(6):1460–1463, 1986.

[Dai87] Hiroaki Daido. Scaling behaviour at the onset of mutual entrainment in a population of interacting oscillators. *Journal of Physics A: Mathematical and General*, 20(10):L629–L636, 1987.

[Dai90] Hiroaki Daido. Intrinsic fluctuation and a phase transition in a class of large population of interacting oscillators. *Journal of Statistical Physics*, 60:753, 1990.

[Erm85] G. Bard Ermentrout. Synchronization in a pool of mutually coupled oscillators with random frequencies. *Journal of Mathematical Biology*, 22(1):1–9, Jun 1985.

[Fau10] Lynn Frierson Faust. Natural History and Flash Repertoire of the Synchronous Firefly Photinus carolinus (Coleoptera: Lampyridae) in the Great Smoky Mountains National Park. *Florida Entomologist*, 93(2):208–217, 2010.

[FNP08] G. Filatrella, A. H. Nielsen, and N. F. Pedersen. Analysis of a power grid using a Kuramoto-like model. *The European Physical Journal B*, 61(4):485–491, Feb 2008.

[FSL+12] Karin Fisch, Tilo Schwalger, Benjamin Lindner, Andreas V. M. Herz, and Jan Benda. Channel noise from both slow adaptation currents and fast currents is required to explain spike-response variability in a sensory neuron. *Journal of Neuroscience*, 32(48):17332–17344, 2012.

[GGnGAM11] Jesús Gómez-Gardeñes, Sergio Gómez, Alex Arenas, and Yamir Moreno. Explosive synchronization transitions in scale-free networks. *Phys. Rev. Lett.*, 106:128701, Mar 2011.

[GMP17] Rafael Gallego, Ernest Montbrió, and Diego Pazó. Synchronization scenarios in the winfree model of coupled oscillators. *Phys. Rev. E*, 96:042208, Oct 2017.

[GP85] D. L. González and O. Piro. Symmetric kicked self-oscillators: Iterated maps, strange attractors, and symmetry of the phase-locking Farey hierarchy. *Phys. Rev. Lett.*, 55:17–20, 1985.

[GP04] D. S. Goldobin and A. S. Pikovsky. Synchronization of periodic self-oscillations by common noise. *Radiophysics and Quantum Electronics*, 47(10):910–915, Oct 2004.

[GP05a] Denis S. Goldobin and Arkady Pikovsky. Synchronization and desynchronization of self-sustained oscillators by common noise. *Phys. Rev. E*, 71:045201, Apr 2005.

[GP05b] D.S. Goldobin and A.S. Pikovsky. Synchronization of self-sustained oscillators by common white noise. *Physica A: Statistical Mechanics and its Applications*, 351(1):126 – 132, 2005.

[GPRP17] Denis S. Goldobin, Anastasiya V. Pimenova, Michael Rosenblum, and Arkady Pikovsky. Competing influence of common noise and desynchronizing coupling on synchronization in the Kuramoto-Sakaguchi ensemble. *The European Physical Journal Special Topics*, 226(9):1921–1937, Jun 2017.

[GR80] I.S. Gradsteyn and I.M. Ryzhik. *Tables of Integrals, Series and Products*. Academic Press, New York, 1980.

[GRD12] Valentina Gumenyuk, Thomas Roth, and Christopher L. Drake. Circadian Phase, Sleepiness, and Light Exposure Assessment in Night Workers With and Without Shift Work Disorder. *Chronobiology International*, 29(7):928–936, 2012.

[GWF+98] B. T. Grenfell, K. Wilson, B. F. Finkenstädt, T. N. Coulson, S. Murray, S. D. Albon, J. M. Pemberton, T. H. Clutton-Brock, and M. J. Crawley. Noise and determinism in synchronized sheep dynamics. *Nature*, 394:674, 1998.

[HBH+14] Xin Hu, S. Boccaletti, Wenwen Huang, Xiyun Zhang, Zonghua Liu, Shuguang Guan, and Choy-Heng Lai. Exact solution for first-order synchronization transition in a generalized Kuramoto model. *Scientific Reports*, 4(8):7262, 2014.

[HCPT07] Hyunsuk Hong, Hugues Chaté, Hyunggyu Park, and Lei Han Tang. Entrainment transition in populations of random frequency oscillators. *Phys. Rev. Lett.*, 99(18):1–4, 2007.

[HCTP15] Hyunsuk Hong, Hugues Chaté, Lei Han Tang, and Hyunggyu Park. Finite-size scaling, dynamic fluctuations, and hyperscaling relation in the Kuramoto model. *Phys. Rev. E*, 92(2):1–9, 2015.

[HF96] Rob J. Hyndman and Yanan Fan. Sample quantiles in statistical packages. *The American Statistician*, 50(4):361–365, 1996.

[HPT07] Hyunsuk Hong, Hyunggyu Park, and Lei Han Tang. Finite-size scaling of synchronized oscillation on complex networks. *Phys. Rev. E*, 76(6):1–7, 2007.

[HS11] Hyunsuk Hong and Steven H. Strogatz. Kuramoto model of coupled oscillators with positive and negative coupling parameters: An example of conformist and contrarian oscillators. *Phys. Rev. Lett.*, 106(5):1–4, 2011.

[HS16] Hyunsuk Hong and Steven H Strogatz. Correlated disorder in the Kuramoto model: Effects on phase coherence, finite-size scaling, and dynamic fluctuations. *Chaos*, (26):10, 2016.

[IK06] E.M. Izhikevich and Y. Kuramoto. *Weakly Coupled Oscillators*. In: Encyclopedia of Mathematical Physics. Academic Press, Oxford, 2006.

[Izh07] E.M. Izhikevich. *Dynamical Systems in Neuroscience*. Computational Neuroscience Dynamical Systems in Neuroscience. MIT Press, 2007.

[KB02] Y. Kuramoto and D. Battogtokh. Coexistence of Coherence and Incoherence in Nonlocally Coupled Phase Oscillators. *Nonlinear Phenomena in Complex Systems*, 5(4):380–385, 2002. This special issue is dedicated to the 75th anniversary of Professor Hermann Haken.

[KCR+08] Björn Kralemann, Laura Cimponeriu, Michael Rosenblum, Arkady Pikovsky, and Ralf Mrowka. Phase dynamics of coupled oscillators reconstructed from data. *Phys. Rev. E*, 77:066205, Jun 2008.

[KK15] Hiroshi Kori and Yoshiki Kuramoto. Kuramoto talks about the Kuramoto model. `https://www.youtube.com/watch?v=lac4TxWyBOg`, 2015. Video speech from Tokyo to Dresden prepared for a conference dedicated to the 40th anniversary of the Kuramoto model.

[KKJ+14] Hiroshi Kori, Yoshiki Kuramoto, Swati Jain, István Z. Kiss, and John L. Hudson. Clustering in globally coupled oscillators near a hopf bifurcation: Theory and experiments. *Phys. Rev. E*, 89:062906, Jun 2014.

[KN87] Yoshiki Kuramoto and Ikuko Nishikawa. Statistical macrodynamics of large dynamical systems. Case of a phase transition in oscillator communities. *Journal of Statistical Physics*, 49(3):569–605, Nov 1987.

[KP13] Maxim Komarov and Arkady Pikovsky. Multiplicity of Singular Synchronous States in the Kuramoto Model of Coupled Oscillators. *Phys. Rev. Lett.*, 111:204101, Nov 2013.

[KP14] M. Komarov and A. Pikovsky. The Kuramoto model of coupled oscillators with a bi-harmonic coupling function. *Physica D: Nonlinear Phenomena*, 289:18–31, 2014.

[KPW13] M Kochmański, T Paszkiewicz, and S Wolski. Curie–Weiss magnet—a simple model of phase transition. *European Journal of Physics*, 34(6):1555, 2013.

[KSYHS98] M K. Stephen Yeung and Steven H. Strogatz. Time Delay in the Kuramoto Model of Coupled Oscillators. *Phys. Rev. Lett.*, 82, 07 1998.

[Kur75] Y Kuramoto. Self-entrainment of a population of coupled non-linear oscillators. *Conference Proceedings: International Symposium on Mathematical Problems in Theoretical Physics*, 39:420–422, 1975.

[Kur84] Y. Kuramoto. *Chemical Oscillations, Waves, and Turbulence*, volume 19. Springer Berlin Heidelberg, Springer Series in Synergetics edition, 1984.

[LFCP18] Maxime Lucas, Duccio Fanelli, Timoteo Carletti, and Julien Petit. Desynchronization induced by time-varying network. *EPL (Europhysics Letters)*, 121(5):50008, 2018.

[LYK14] Mi Jin Lee, Su Do Yi, and Beom Jun Kim. Finite-time and finite-size scaling of the Kuramoto oscillators. *Phys. Rev. Lett.*, 112(7):6–9, 2014.

[MBS+09a] E. A. Martens, E. Barreto, S. H. Strogatz, E. Ott, P. So, and T. M. Antonsen. Exact results for the Kuramoto model with a bimodal frequency distribution. *Phys. Rev. E*, 79(2):1–11, 2009.

[MBS+09b] E. A. Martens, E. Barreto, S. H. Strogatz, E. Ott, P. So, and T. M. Antonsen. Exact results for the Kuramoto model with a bimodal frequency distribution. *Phys. Rev. E*, 79:026204, Feb 2009.

[MJ00] K.V. Mardia and P.E. Jupp. *Directional Statistics*. Wiley Series in Probability and Statistics. Wiley, 2000.

[MMS09] Seth A. Marvel, Renato E. Mirollo, and Steven H. Strogatz. Identical phase oscillators with global sinusoidal coupling evolve by Möbius group action. *Chaos*, 19(4), 2009.

[Moo88] J. J. A. Moors. A quantile alternative for kurtosis. *Journal of the Royal Statistical Society. Series D (The Statistician)*, 37(1):25–32, 1988.

[MP06] P K Mohanty and Antonio Politi. A new approach to partial synchronization in globally coupled rotators. *Journal of Physics A: Mathematical and General*, 39(26):L415, 2006.

[MS95] ZF Mainen and TJ Sejnowski. Reliability of spike timing in neocortical neurons. *Science*, 268(5216):1503–1506, 1995.

[Nay81] A.H. Nayfeh. *Introduction to Perturbation Techniques*. Wiley classics library. Wiley, 1981.

[NDL+16] Ido Nitsan, Stavit Drori, Yair E. Lewis, Shlomi Cohen, and Shelly Tzlil. Mechanical communication in cardiac cell synchronized beating. *Nature Physics*, 12:472 EP –, Jan 2016.

[NIT+14] Isao Nishikawa, Koji Iwayama, Gouhei Tanaka, Takehiko Horita, and Kazuyuki Aihara. Finite-size scaling in globally coupled phase oscillators with a general coupling scheme. *Progress of Theoretical and Experimental Physics*, 2014(2):1–8, 2014.

[NK10] Ken H. Nagai and Hiroshi Kori. Noise-induced synchronization of a large population of globally coupled nonidentical oscillators. *Phys. Rev. E*, 81:065202, 2010.

[NTA13] Isao Nishikawa, Gouhei Tanaka, and Kazuyuki Aihara. Nonstandard scaling law of fluctuations in finite-size systems of globally coupled oscillators. *Phys. Rev. E*, 88(2):1–5, 2013.

[NTHA12] Isao Nishikawa, Gouhei Tanaka, Takehiko Horita, and Kazuyuki Aihara. Long-term fluctuations in globally coupled phase oscillators with general coupling: Finite size effects. *Chaos*, 22(1), 2012.

[OA08] Edward Ott and Thomas M. Antonsen. Low dimensional behavior of large systems of globally coupled oscillators. *Chaos*, 18(3), 2008.

[OA09] Edward Ott and Thomas M. Antonsen. Long time evolution of phase oscillator systems. *Chaos: An Interdisciplinary Journal of Nonlinear Science*, 19(2):023117, 2009.

[OLS16] Bertrand Ottino-Löffler and Steven H. Strogatz. Kuramoto model with uniformly spaced frequencies: Finite-n asymptotics of the locking threshold. *Phys. Rev. E*, 93:062220, Jun 2016.

[OW12] Oleh E. Omel'chenko and Matthias Wolfrum. Nonuniversal transitions to synchrony in the Sakaguchi-Kuramoto model. *Phys. Rev. Lett.*, 109:164101, 2012.

[OW13] Oleh E. Omel'chenko and Matthias Wolfrum. Bifurcations in the Sakaguchi-Kuramoto model. *Physica D*, 263:74, 2013.

[PA15] Mark J Panaggio and Daniel M Abrams. Chimera states: coexistence of coherence and incoherence in networks of coupled oscillators. *Nonlinearity*, 28(3):R67, 2015.

[Paz05] Diego Pazó. Thermodynamic limit of the first-order phase transition in the Kuramoto model. *Phys. Rev. E*, 72(4):1–6, 2005.

[Pet18a] Franziska Peter. Playlist: Bars and stripes at the onset to synchronization. `https://www.youtube.com/watch?v=-wzO_VeqfMI&list=PL08zEjqXjgUQU3NS8EdNINdbSEmR7eMjH`, 2018.

[Pet18b] Franziska Peter. Quasiperiodic signal mimics mean field of 50 coupled oscillators. `https://www.youtube.com/watch?v=lKKWudHEaEk`, 2018.

[Pet18c] Franziska Peter. Striped pattern in subcritical Kuramoto oscillators – equidistant frequencies. `https://www.youtube.com/watch?v=ti8_AMG20DM`, 2018.

[Pet18d] Franziska Peter. The undecided form the bars. `https://www.youtube.com/watch?v=RrUy8bfg43A`, 2018.

[PGRP16] Anastasiya V. Pimenova, Denis S. Goldobin, Michael Rosenblum, and Arkady Pikovsky. Interplay of coupling and common noise at the transition to synchrony in oscillator populations. *Scientific Reports*, 6:38518, 2016.

[Pik84] A.S. Pikovskii. *Synchronization and stochastization of nonlinear oscillations by external noise*. Number Bd. 3 in Nonlinear and Turbulent Processes in Physics: Proceedings of the Second International Workshop on Nonlinear and Turbulent Processes in Physics, Kiev, USSR, 10-25 October 1983. Harwood Academic Publishers, 1984.

[PM09] Diego Pazó and Ernest Montbrió. Existence of hysteresis in the Kuramoto model with bimodal frequency distributions. *Phys. Rev. E*, 80:046215, Oct 2009.

[PMT05] Oleksandr V. Popovych, Yuri L. Maistrenko, and Peter A. Tass. Phase chaos in coupled oscillators. *Phys. Rev. E*, 71(6):3–6, 2005.

[PP16] A. Pikovsky and A. Politi. *Lyapunov Exponents: A Tool to Explore Complex Dynamics*. Cambridge University Press, 2016.

[PP18] Franziska Peter and Arkady Pikovsky. Transition to collective oscillations in finite Kuramoto ensembles. *Phys. Rev. E*, 97:032310, Mar 2018.

[PR99] Arkady Pikovsky and Stefano Ruffo. Finite-size effects in a population of interacting oscillators. *Phys. Rev. E*, 59(2):1633–1636, 1999.

[PR08] Arkady Pikovsky and Michael Rosenblum. Partially integrable dynamics of hierarchical populations of coupled oscillators. *Phys. Rev. Lett.*, 101(26):1–4, 2008.

[PR15] Arkady Pikovsky and Michael Rosenblum. Dynamics of globally coupled oscillators: Progress and perspectives. *Chaos (Woodbury, N.Y.)*, 25(9):097616, 2015.

[PRK03] A. Pikovsky, M. Rosenblum, and J. Kurths. *Synchronization: A Universal Concept in Nonlinear Sciences*. Cambridge Nonlinear Science Series. Cambridge University Press, 2003.

[RP15] Michael Rosenblum and Arkady Pikovsky. Two types of quasiperiodic partial synchrony in oscillator ensembles. *Phys. Rev. E*, 92:012919, Jul 2015.

[RPJK16] Francisco A. Rodrigues, Thomas K. DM. Peron, Peng Ji, and Jürgen Kurths. The Kuramoto model in complex networks. *Physics Reports*, 610:1 – 98, 2016.

[RPK+02] Michael G. Rosenblum, Arkady S. Pikovsky, Jürgen Kurths, Grigory V. Osipov, István Z. Kiss, and John L. Hudson. Locking-based frequency measurement and synchronization of chaotic oscillators with complex dynamics. *Phys. Rev. Lett.*, 89:264102, Dec 2002.

[RSTA95] Nikolai F. Rulkov, Mikhail M. Sushchik, Lev S. Tsimring, and Henry D. I. Abarbanel. Generalized synchronization of chaos in directionally coupled chaotic systems. *Phys. Rev. E*, 51:980–994, Feb 1995.

[SH10] Seung Woo Son and Hyunsuk Hong. Thermal fluctuation effects on finite-size scaling of synchronization. *Phys. Rev. E*, 81(6):1–7, 2010.

[SK86] Hidetsugu Sakaguchi and Yoshiki Kuramoto. A soluble active rotater model showing phase transitions via mutual entertainment. *Progress of Theoretical Physics*, 76(3):576–581, 1986.

[Ska18] Per Sebastian Skardal. Low-dimensional dynamics of the Kuramoto model with rational frequency distributions. *Phys. Rev. E*, 98:022207, Aug 2018.

[SS07] Christoph Schorl and John M. Sedivy. Analysis of cell cycle phases and progression in cultured mammalian cells. *Methods*, 41(2):143 – 150, 2007. Methods in Cell Cycle Research.

[SSW92] James W. Swift, Steven H. Strogatz, and Kurt Wiesenfeld. Averaging of globally coupled oscillators. *Physica D: Nonlinear Phenomena*, 55(3):239 – 250, 1992.

[Str00] Steven H. Strogatz. From Kuramoto to Crawford: exploring the onset of synchronization in populations of coupled oscillators. *Physica D: Nonlinear Phenomena*, 143(1-4):1–20, 2000.

[Str15] S. H. Strogatz. *Nonlinear Dynamics and Chaos: With Applications to Physics, Biology, Chemistry, and Engineering*, volume 1. Westview Press, 2. edition, 2015.

[Stu27] Student. Errors of routine analysis. *Biometrika*, 19(1-2):151–164, 1927.

[Tan11] Lei-Han Tang. To synchronize or not to synchronize, that is the question: finite-size scaling and fluctuation effects in the Kuramoto model. *Journal of Statistical Mechanics: Theory and Experiment*, 2011(01):P01034, 2011.

[TIAY17] Yu Terada, Keigo Ito, Toshio Aoyagi, and Yoshiyuki Y Yamaguchi. Nonstandard transitions in the Kuramoto model: a role of asymmetry in natural frequency distributions. *Journal of Statistical Mechanics: Theory and Experiment*, 2017(1):013403, 2017.

[Tön08] Ralf Tönjes. *Pattern formation through synchronization in systems of nonidentical autonomous oscillators*. Phd thesis, Universität Potsdam, 2008.

[Tou14] Jonathan Touboul. The hipster effect: When anticonformists all look the same. *arxiv preprint*, 10 2014.

[TT04] Jun-nosuke Teramae and Dan Tanaka. Robustness of the noise-induced phase synchronization in a general class of limit cycle oscillators. *Phys. Rev. Lett.*, 93:204103, Nov 2004.

[TZT+12] Amirkhan A. Temirbayev, Zeinulla Zh. Zhanabaev, Stanislav B. Tarasov, Vladimir I. Ponomarenko, and Michael Rosenblum. Experiments on oscillator ensembles with global nonlinear coupling. *Phys. Rev. E*, 85:015204, Jan 2012.

[VM07] Mark Verwoerd and Oliver Mason. Global phase-locking in finite populations of phase-coupled oscillators. *SIAM Journal on Applied Dynamical Systems*, 7(1):31, 2007.

[WHS+10] Christopher P. Warren, Sanqing Hu, Matt Stead, Benjamin H. Brinkmann, Mark R. Bower, and Gregory A. Worrell. Synchrony in Normal and Focal Epileptic Brain: The Seizure Onset Zone is Functionally Disconnected. *Journal of Neurophysiology*, 104(6):3530–3539, 2010.

[Win67] Arthur T. Winfree. Biological rhythms and the behavior of populations of coupled oscillators. *Journal of Theoretical Biology*, 16(1):15 – 42, 1967.

[Win80] Arthur T. Winfree. *The Geometry of Biological Time*. Springer Study Edition, 1. edition, 1980.

[WPZH12] André Weber, Yury Prokazov, Werner Zuschratter, and Marcus J. B. Hauser. Desynchronisation of glycolytic oscillations in yeast cell populations. *PLOS ONE*, 7(9):1–8, 09 2012.

[WRGB15] Chengwei Wang, Nicolás Rubido, Celso Grebogi, and Murilo S. Baptista. Approximate solution for frequency synchronization in a finite-size Kuramoto model. *Phys. Rev. E*, 92(6):1–5, 2015.

[WS94] Shinya Watanabe and Steven H. Strogatz. Constants of motion for superconducting Josephson arrays. *Physica D: Nonlinear Phenomena*, 74(3-4):197–253, 1994.

[ZPL17] Xiyun Zhang, Arkady Pikovsky, and Zonghua Liu. Dynamics of oscillators globally coupled via two mean fields. *Nature Scientific Reports*, 7, 01 2017.